Investigating the Interactions between Free Radicals and Supported Noble Metal Nanoparticles in Oxidation Reactions

Charles-Oneil Crites

Thesis submitted to the
Faculty of Graduate and Postdoctoral Studies
In partial fulfillment of the requirements for the
Doctor of Philosophy degree
In the Ottawa-Carleton Chemistry Institute
Department of Chemistry and Biomolecular Sciences, University of Ottawa

Université d'Ottawa • University of Ottawa

Candidate	Supervisor
Charles-Oneil Crites	Professor J.C. Scaiano

À mes parents

Pour leur amour and leurs encouragements

&

To my mentors

Tito Scaiano, Gerardo Diaz and J.C. Netto-Ferreira

for their help and patience

Who Dares Wins

Fais ce que dois (H. Bourassa)

Abstract

This thesis studies the interaction between free radical species and supported noble metal nanoparticles (silver and gold) in the context of oxidation reactions. The peroxidation of cumene is the first reaction to be discussed and the difference in peroxidation product distribution using silver nanoparticles (AgNP) *versus* gold nanoparticles (AuNP) is examined. Specifically, cumyl alcohol is obtained as the major product obtained when using supported AuNP, whereas cumene hydroperoxide is favoured for AgNP. Such variations in product distribution are partially explained by the differences in the nanoparticle Fenton activity, where the TiO_2 support was proposed to enhance such activity due to possible electron shuttling capabilities with the nanoparticle surface. Use of hydrotalcite as a support was found to minimize this characteristic, due to its insulating properties. The stability of hydroperoxide was tested in the presence of various others supports (activated carbon, Al_2O_3, ZnO, SiO_2 and clays) with little success, with hydroperoxide exhibiting stability in the presence of HT. Using an oxygen uptake apparatus, the interaction of the cumyl peroxyl radical with the AuNP surface was demonstrated. Furthermore, this interaction promotes decomposition leading to the corresponding alkoxyl radical and subsequent hydrogen abstraction to form the observed cumyl alcohol product. The radical interaction with supported

nanoparticles, and its reversibility appear different for gold and silver and accounts for a large part of the product distribution differences observed between AuNP and AgNP, as illustrated below.

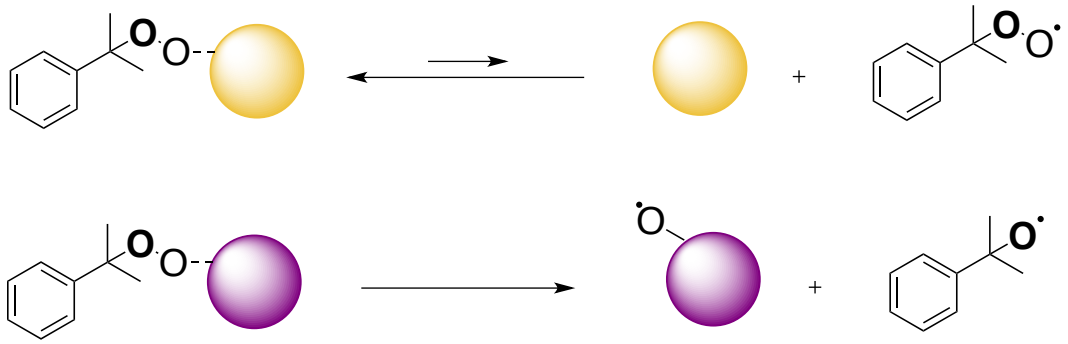

The peroxidation of ethylbenzene and propylbenzene was studied and revealed the participation of a reactive surface oxygen species due to the decomposition of peroxyl radicals on the nanoparticle surface. This intermediate was found to be transient in nature in the case of AuNP . Furthermore, this surface species was found to be an important participant in hydrogen abstraction leading to peroxide product formation. Finally, supported nanoparticle catalyzed tetralin peroxidation was investigated to determine the influence of temperature on the peroxidation product distribution and how changes in the reaction temperature can effect the radical-nanoparticle surface interactions.

Acknowledgements

I would like to thank my PhD advisor, Dr. Tito Scaiano, for welcoming me in his group. I was very fortunate to study under the guidance of one of the best chemists in the country. In addition to be a top scientist, Tito is a very kind and patient person. I will always remember him checking on me at 3 in the morning after I had an allergic reaction at his cottage.

Thanks is also due to Dr. Gerardo Diaz, who gave me my first chance in doing research when I was an undergraduate. Since then, I have known that research is what I want to do. I also would like to thank Dr. José Carlos Netto-Ferreira for all his help and patience, I would not be where I am today without his help. A special thank you is also due to Dr. Geniece Hallett-Tapley for all her help with the science, but especially with correcting my English grammar and listening to numerous practice talks. I would also like to thank Dr. Maria Gonzalez-Béjar for her help at the beginning of my PhD studies, Dr. Emilio Alarcon for his encouragement, advice and friendship, Dr. Mathieu Frenette for his help with the oxygen uptake, Mrs. Betty Yakimenko for her help with all administrative issues and Michel Grenier for his help with all sorts of technical issues, such as the EPR, and his friendship.

Everybody in the group has played an important role and helped me at one point or another in my graduate studies. The people present in the

group when I started: Matthew Decan, Matthew York, Dr. Paul Billione, Dr. Jessie Blake, Dr. Laetitia Réné-Boisneuf, Dr. Maria Gonzalez-Béjar, Dr. Geniece Hallett-Tapley, Dr. Erika Wee, Dr. Carlos Bueno Alejo , Dr. Kevin Stamplecoskie, Dr. Natalia Pacioni, Vasillisa Filippenko, Dr. Emilio Alarcon, Dr. Katherine McGilvray. Also thanks goes to the other who joined after I began: Chris McTiernan, Dimitry Malyshev, Spencer Pitre, Daniela Marquez-Soto, Chiara Fasciani, Dr. Luciana Schmidt, Dr. Adela Carrilo-Gomez, Greg Hodgson, Dr. Anabel Lanterna, Dr. Marco Mazzona, Dr. Stefania Impellizzeri and Dr. Hossein Ismaili. =

A very special thanks you goes to the people who helped me with the correction of this thesis starting with my mother, Chris McTiernan, Dr. Emilio Alarcon, Daniela Marquez-Soto and, especially Dr. Geniece Hallett-Tapley and Dr. José Carlos Netto-Ferreira.

J'aimerais aussi remercier ma famille pour leur soutient tout au long de mes études au doctorat. Un merci tout spécial à ma mère qui m'a aidé en corrigeant mes textes depuis toujours.

Table of Contents

7.0. The role of AuNP-Radical Interactions in the Peroxidation of Tetralin 167

List of Figures

List of Schemes

List of Tables

List of Abbreviations

μ_β = Bohr magneton

μL = Microliter

τ = Inhibition period

υ = Chain length

α– tetralone 3,4-Dihydro-1(2H)-naphthalenone

Ag = Silver

Ag(I) = Silver+ (Ag^+)

Ag_2O = Silver oxide

AgNP = Silver nanoparticle

AgNP@HT = Silver nanoparticle on Hydrotalcite

Al_2O_3 = Aluminum oxide

Au = Gold

AuNP = Gold nanoparticle

AuNP@CeO_2 = Gold nanoparticle on Cerium(IV) Oxide

AuNP@nanoCeO_2 = Gold nanoparticle on nano Cerium(IV) Oxide

AuNP@graphite = Gold nanoparticle on graphite

AuNP@HT = Gold nanoparticle on hydrotalcite

AuNP@TiO_2 = Gold nanoparticle on Titanium Dioxide

cAuNP@TiO_2 = Commercial Gold nanoparticle on Titanium Dioxide

hAuNP@TiO_2 = Home Made Gold nanoparticle on Titanium Dioxide

AuNP@Support = Supported gold nanoparticle

AuPd@TiO_2 = Gold/Palladium alloys on Titanium Dioxide

AIBN = Azobis(isobutyronitrile)

B_0 = Magnetic field

β-scission = beta scission

CHP = Cumene hydroperoxide

[CHP]/[cumyl alcohol] = Concentration of Cumene hydroperoxide/ concentration of cumyl alcohol

CO = Carbon monoxide

Cumyl Alcohol = 2-phenyl-2-propanol

Cu_2O = Copper Oxide

CW = Continuous wave

DBHA = 2,6-di-*tert*-butyl-4-methoxyphenol

DCP = Dicumyl peroxide

DMPO = 5,5-Dimethyl-1-Pyrrroline-N-Oxide

EPR = Electron paramagnetic resonance

eV = Electron Volts

$HAuCl_4$ = Tetrachloroauric acid

In_2O_3 = Indium(III) oxide

HT = Hydrotalcite

HO^- = Hydroxide

H_2O_2 =Hydrogen peroxide

$h\upsilon$ = Electromagnetic radiation

k_{GB} = Constant of Gold binding

k_{GB} = Reverse Gold binding constant

K_H = Constant for hydrogen abstraction

K_{SD} = Constant for peroxyl radical surface decomposition

MΩ = Megaohm

m-CPBA = Met-chloroperbenzoic acid

mg = Milligramme

MgO = Magnesium oxide

Mmol = milimolar

Mol = Mole

M/s= Mole/seconds

$M^{-1}s^{-1}$ = 1/(Mole *second)

MnO_2 = Manganese dioxide

N_2 = Nitrogen gas

$NaBH_4$ = Sodium Borohydride

NH_4OH = Ammonium hydroxide

nmol = nanomolar

NMR = Nuclear Magnetic Resonance

HPLC = High Performance Liquid Chromatography

O_2 = Molecular oxygen

R· = Carbon center radical

R_i = Rate of initiation

RO· = Alkoxyl radical

ROH = Alcohol

ROO· = Peroxyl radical

ROOH = Hydroperoxide

ROOR = Peroxide

R_p = Rate of propagation

RT = Room temperature

TBHP = Tert-butyl hydroperoxide

TEM = Transmission Electron microscopy

TEMPO= 2,2,6,6-tetramethylpiperidin-1-yl)oxidanyl Free radical

α–Tetralone = 3,4-Dihydro-1(2H)-naphthalenone

Ti-MCM41 = Titanium Mobil Composition of Matter #41

TiO_2 = Titanium Dioxide

TiO_2 P25 = Titanium Dioxide P25 (note a specific type)

$SrTiO_2$ = Strontium Titanate

XPS = X-Ray photoelectron spectroscopy

WO_3 = Tungsten Trioxide

1. Introduction to silver and gold catalysis and free radical chemistry

1.0. Table of contents

1.1. Opening remarks

The work in this thesis can be viewed as being at the intersection between free-radical chemistry and catalysis. The main objective is to examine the influence that supported gold (AuNP) and silver nanoparticles (AgNP) have on reactions involving free-radical species. This thesis is divided into 8 chapters. Chapter 1 provides a basic introduction to free-radical species and their role in both gold and silver catalysis. Chapter 2 examines the peroxidation of cumene in the presence of both AgNP and AuNP catalysts. Chapter 3 explores the role of the catalyst support in the supported AuNP mediated peroxidation of cumene. Chapter 4 and 5 examine the peroxidation of ethylbenzene and n-propylbenzene with particular emphasis on the role of reactive surface oxygen species on the heterogeneous, AuNP@TiO_2 catalyst. Furthermore, Chapter 5 more closely examines the specific differences in the reactivity of AgNP and AuNP with regards to the surface mediated decomposition of peroxyl radicals formed throughout the aforementioned peroxidation processes. Chapter 6 delves into the epoxidation of *cis*-stilbene and the role that the surface of AuNP may play in this transformation. Lastly, Chapter 7 will focus on the product distribution obtained upon peroxidation of tetralin, specifically looking at the dependence of temperature on the products obtained when using AuNP@TiO_2 as catalyst.

In order to be able to discuss the results presented in this thesis, the fundamental basics with regards to free-radical chemistry, noble metal nanoparticle catalysis and also the interaction between free-radicals and the nanoparticle surface must be considered. Interestingly, a large diversity of oxidative reactions in the presence of AuNP and AgNP can be rationalized by the interation of oxygen centered radicals with the nanoparticle surface.

1.2. Free-radicals

1.2.1. What is a radical species?

Radical species are molecules that have an open shell configuration. Therefore, free-radicals are molecules that contain one unpaired valence electron.[1] The unpaired electrons can be centered on different atoms; with the most common organic entities being carbon, oxygen, nitrogen and sulphur centered radicals. Scheme 1.1 shows the different radicals that will be encontered in this thesis: the first being a carbon-centered cumyl radical, whereas the second and third are oxygen-centered alkoxyl and peroxyl radicals, respectively. All of these species play an important role in the free-radical peroxidation of solvents, such as cumene, to be discussed in the coming chapters.

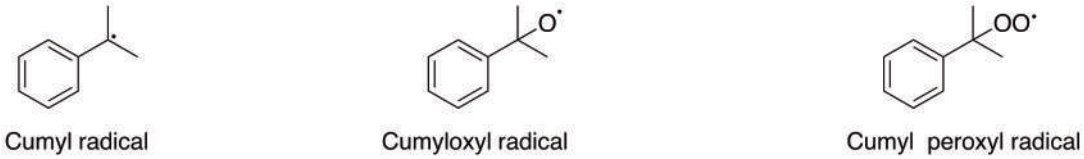

Scheme 1.1. Typical radical species to be encountered in this thesis.

1.2.2. Free-radical oxidation of a solvent

Solvent peroxidation involves oxidation of molecules where an atmospheric source of oxygen is a key participant.[2] Taking the peroxidation of cumene as an example, the two main products obtained are cumene hydroperoxide and cumyl alcohol. These oxidation products are illustrated in Scheme 1.2.

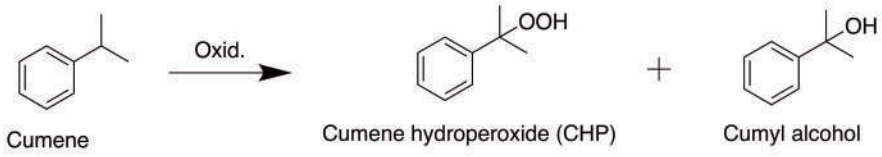

Scheme 1.2. Major products obtained in the oxidation of cumene.

The ability to obtain the two products shown above is due to the participation of the free-radical intermediates depicted in Scheme 1.1.[3] Prior to a more detailed discussion on cumene peroxidation, one must first understand the types of reactions involved in free-radical processes. Every peroxidation (that involves a free-radical chain reaction) is constituted of four different pathways. The first pathway is initiation (eq. 1), where molecules form free-radical species. One

example of such a reaction would be the homolytic decomposition of a hydroperoxide into alkoxyl and hydroxyl radicals.

Initiation:	production of R• , ROO• or RO•	(1)
Chain Transfer:	RO• + RH → ROH + R•	(2)
Propagation:	R• + O_2 → ROO•	(3)
	ROO• + HR → ROOH + R•	(4)
Termination	ROO• + ROO• →non-radical products	(5)

Initiaition is then proceeded by a chain transfer reaction (eq. 2), as radical species produced in the initiation step are converted to those that can start a chain reaction. The third type of reaction involved in the free-radical chain reaction, the propagation steps, is a continual source of various radical species (eq. 3 and 4). The termination step comprises the last family of reactions, where non-radical molecules are formed from radical precursors (eq. 5). In Scheme 1.3 the various chain reaction steps and species involved in cumene peroxidation are presented as each step of the free-radical chain, with the equation numbering coinciding with the individual steps presented above.

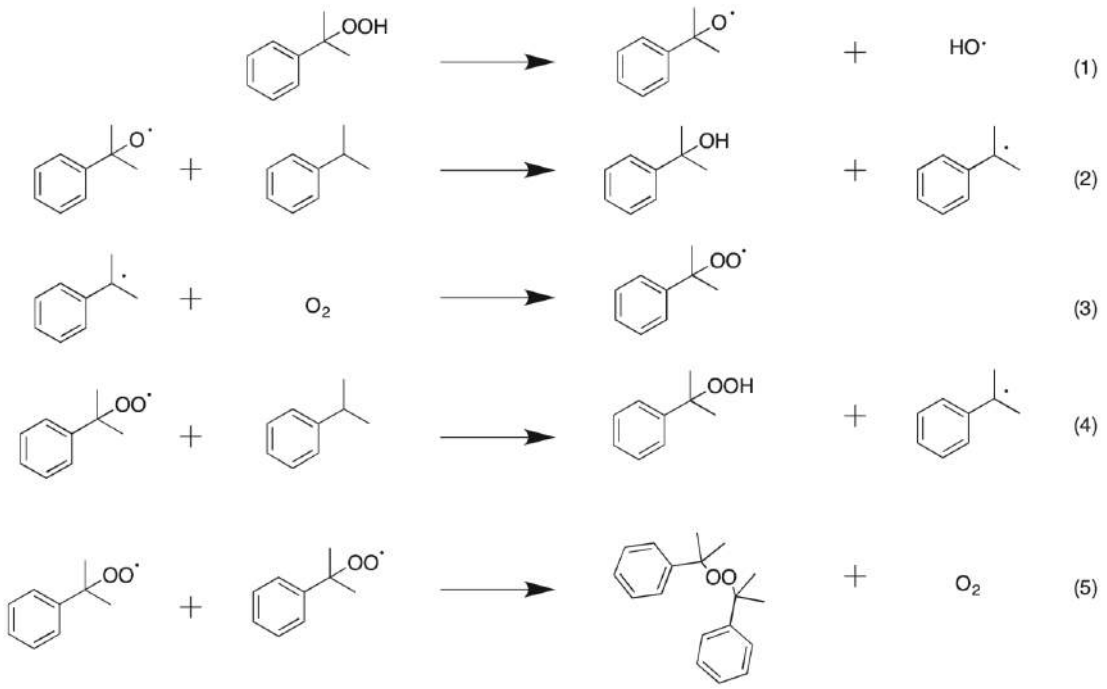

Scheme 1.3. Free-radical chain reactions involved in the cumene peroxidation process.

In the example above, it is assumed that the initiator is cumene hydroperoxide (CHP) and that the initiation step results from thermal cleavage of the hydroperoxide into its corresponding alkoxyl and hydroxyl radicals, as shown in Scheme 1.3, eq. 1. The resulting cumyloxyl radical can then abstract a hydrogen from cumene (Scheme 1.3, eq. 2) to form cumyl alcohol and a cumyl alkyl radical, in a chain transfer reaction. The other radical formed in this homolytic cleavage is the very reactive hydroxyl radical. The cumyl alkyl radical can then react with oxygen to form the cumyl peroxyl radical shown in Scheme 1.3, eq. 3. The resulting peroxyl radical will abstract hydrogen from cumene in order to form cumene hydroperoxide and a cumyl alkyl radical (Scheme 1.3, eq. 4). Scheme 1.3, eq. 5 illustrates the most likely termination reaction between two

peroxyl radicals. This reaction would ultimately lead to the formation of dicumyl peroxide and oxygen.

Scheme 1.4 presents the reactions discussed in Scheme1.3 in an alternative manner. Here, the reactions are arranged in a circular fashion, in which the propogation steps of Scheme 1.3 (red) are shown within the cycle and the initiation (blue) and termination steps (black) (Scheme 1.3, eq 1 and 5) are illustrated to the right of the scheme.

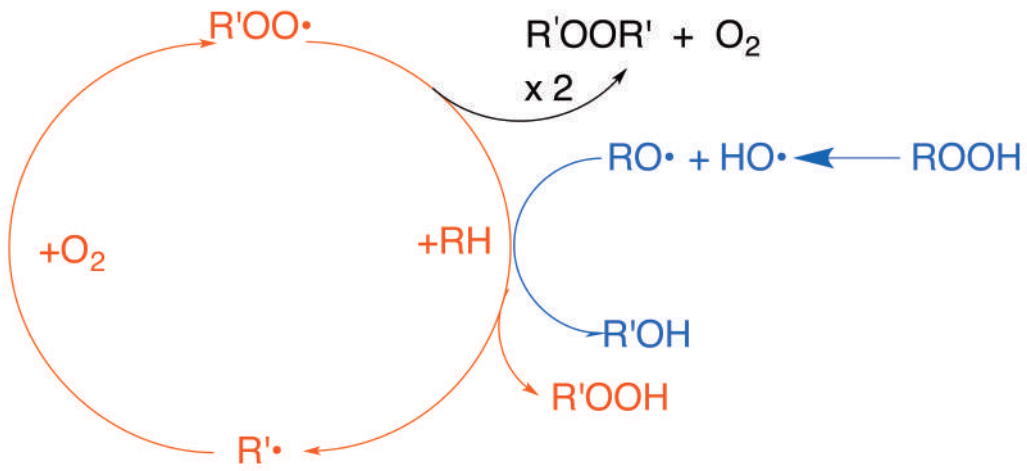

Scheme1.4. Reactions involved in the peroxidation of cumene

1.2.3. Fenton chemsitry

Fenton chemisty is one process that can be used to initiate free radical chemistry processes. Fenton chemistry consists of Fenton and Fenton-like reactions (Scheme 1.5). The typical Fenton reaction begins when Fe^{2+} transfers an electron to a hydroperoxide to form an akoxyl radical and a hydroxyl anion,

shown in red. In the Fenton-like reaction, the hydroperoxide transfers an electron to Fe^{3+} to regrenatate the Fe^{2+} and formed a peroxyl radical and a proton, depicted in black.

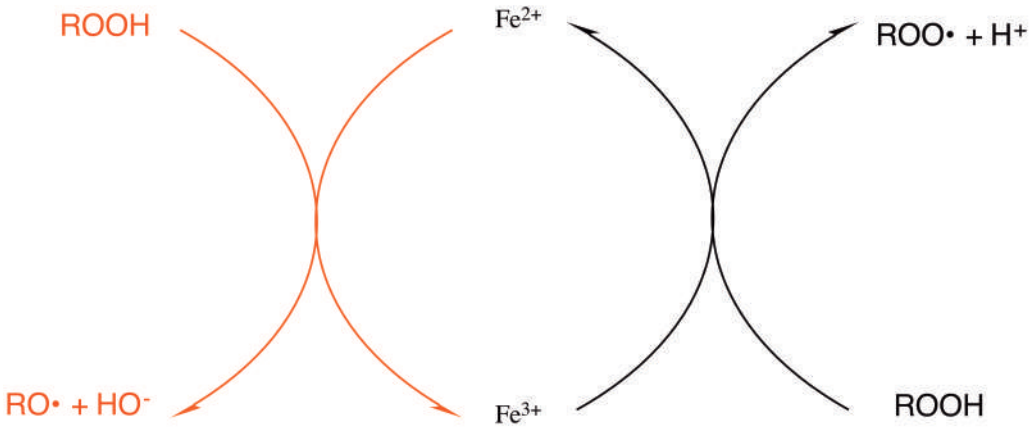

Scheme1.5. Fenton chemistry of hydroperoxide

1.3. Gold catalysis

Gold was originally thought to be an inert material in the context of catalysis. However, this changed with the pioneering paper from Haruta in 1989, which showed that gold nanoparticles (AuNP) supported on metal oxides were very active in the catalytic oxidation of carbon monoxide into carbon dioxide at low temperature.[4] Following this discovery, the interest in catalysis using supported AuNP has significantly increased. The high catalytic activity of AuNP has been attributed to the high surface area and unique electronic properties, a direct consequence of their small size.[5] The interaction between AuNP and the support may also play an important role in the catalytic abilities of these

heterogeneous materials. For example, some reactions, such as CO oxidation, are believed to occur at the interface between the AuNP and the support surface. The manner in which the nanoparticles are synthesized can influence this interaction and, by extension, the catalytic activity of the material.[6] The presence of ionic gold, which is believed to play a role in the catalytic activity of supported AuNP, has been shown to be present at the interface between the AuNP and the support itself. These interfacial ionic gold species have been observed in AuNP@TiO_2 made using a deposition-precipitation method and confirmed using time-of-flight secondary-ion mass spectrometry.[7] The presence of ionic gold was also demonstrated for AuNP@CeO_2.[8] There are numerous reactions in the literature that involve the use of AuNP as catalysts; notably, reduction[9], oxidation[10-12] and C-C coupling[13,14] reactions. In addition, there are countless reviews on the applications of AuNP catalysis in the literature.[5,15-18] As this thesis only involves oxidation reactions employing supported AuNP, background discussion on the catalytic abilities of AuNP will be limited to this reaction. A 2008 review by Rossi and co-workers offers a more in-depth overview on AuNP mediated oxidation reactions.[16]

1.3.2. Oxidation of alkenes and alkanes using AuNP

The oxidation of alkenes using *tert*-butylhydroperoxide (TBHP) as a chain initiator has been widely demonstrated.[16] Scheme 1.6 shows the product distribution obtained when TBHP was used as an initiator in the oxidation of cyclohexene.[19]

The selectivity of the reaction was found to be largely influenced by the solvent, with the highest selectivity (50 %) toward the epoxide being obtained when hexafluorobenzene was used as the solvent.[19] A similar neat reaction was also performed using AuNP@CeO_2 in the presence of azobis(isobutyronitrile) (AIBN) as a radical initiator, in which a yield of 20% and a selectivity of 57 % toward the epoxide was observed.[20]

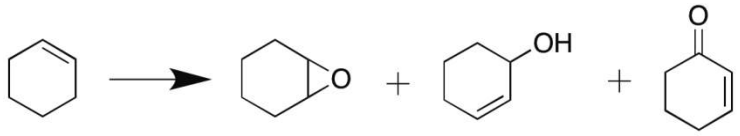

Scheme 1.6. Possible products obtained from of the oxidation of cyclohexene.[16]

The oxidation of styrene has also been attempted (Figure 1.7). When TBHP was used as the radical initiator, styrene oxide was found to be selectively formed (69 %) with an overall conversion of 84% using AuNP supported on mesoporous Al_2O_3.[21] Furthermore, a study by Choudhary *et al.*[22] discussed the influence of the support and the nanomaterial preparation methods on catalyst performance in styrene oxidations.

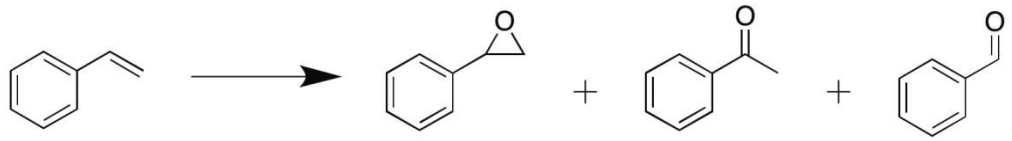

Figure 1.7. Products of styrene oxidation.[16]

The epoxidation of stilbene has also been explored using supported AuNP and a peroxidizable solvent, such as cumene[19] or methylcyclohexane.[23] The mechanism of this transformation is believed to be free-radical based, with this mechanism being revisited and rediscussed in Chapter 6. Au_{55} clusters have shown promise in styrene oxidation using O_2. Here, the formation of reactive surface oxygen species *via* O_2 dissociation on the AuNP surface was found to yield benzaldehyde as the major product.[24]

The oxidation of alkanes has also been explored. The oxidation of cyclohexane into cyclohexanol and cyclohexanone is important as both products (cyclohexanol and cyclohexanone) are useful intermediates in the formation of caprolactam and adipic acid, key precursors in the synthesis of Nylon 6 and Nylon 6,6, respectively.[16] However, the oxidation of cyclohexane is usually carried out in the absence of radical initiators and at elevated temperatures (~150°C).[11,12,19] The mechanism for cyclohexane peroxidation is proposed to involve the participation of radical intermediates, where the resulting hydroperoxide is decomposed into a corresponding alkoxyl radical, that could account for the isolation of the aforementioned products. However, the exact route leading to the formation of these products has not been studied or described in detail.[12]

The oxidation of decane has also been investigated by Lloyd and co-workers in the presence of AuNP@nanoCeO_2[25] and they found that the presence of either

AIBN or CHP as a radical initiator was required for the reaction to proceed. Lastly, the oxidation of toluene has also been performed in the presence of supported AuNP (Au-Pd@TiO_2) and required the use of TBHP as a radical initiator.[26]

1.4. Silver catalysis

Literature precedence as it pertains to the usage of supported silver nanoparticles (AgNP) in oxidation reactions is not as abundant as for AuNP, with one of the few examples being the oxidation of ethylene to ethylene oxide.[27] This thesis will expand on the underdeveloped usage of supported AgNP in the oxidation reactions to be discussed in more detail in the following chapters.

1.4.1 Oxidation of alkanes using silver nanoparticles

Supported AgNP have also been employed in the oxidation of cyclohexane with the selectivity of this reaction determined to be 83% cyclohexanol at 11% conversion of cyclohexane. [28]Examples also exist from the 1970's, demonstrating the ability of supported AgNP to catalyze the oxidation of cumene into cumene hydroperoxide.[29,30]

1.5. The interaction between AuNP or AgNP and free radical species

The interaction between free radicals and AuNP or AgNP plays an important role in the mechanisms to be proposed within this thesis. For this reason, we will

introduce literature precedent for interaction between these species. Work by Meyerstein and co-workers[31] employed methyl radicals formed by the reaction between hydroxyl radicals and DMSO to determine the rate constant of reaction between AgNP or AuNP and methyl radicals, determined to be 3.7 x 10^9 M^{-1} s^{-1} and 1.4 x 10^8 M^{-1} s^{-1}, respectively. These results demonstrated that AuNP and AgNP are good scavengers of free radical species.[31] The same group has also shown that the interaction between methyl peroxyl radicals and AuNP or AgNP leads to the formation of methanol via a suggested heterolytic cleavage of the O-O bond on the nanoparticle surface.[32] In the EPR work of Meyerstein *et al.*,[31] TEMPO derived molecules were used as probes in order to examine the interaction between a nitrone radical and the AuNP surface. A complete disappearance of the EPR signal was observed upon addition of AuNP, demonstrating that the nitrone radical is indeed interacting with the nanoparticle surface. While the authors described the interaction as being strong, it was demonstrated that one can displace the nitrone radical from the surface through addition of ethanolamine which leads to the restoration of the EPR signal. This indicates that the interaction between the free-radical and the nanoparticle surface seems to be reversible. The formation of an adduct between carbon-centered radicals and Au species has also been demonstrated by Garcia *et al.*[33] In examining the formation of organo-gold intermediates *via* the reaction of benzyl radicals with gold chloride, the authors could observe the formation of an adduct between the benzyl radical and gold

chloride ($PhCH_2AuClOH$). In an analogous experiment performed by the same group, AIBN was used as the carbon-centered radical source with similar results being observed.[20] The authors proposed that the carbon-centered radical, formed *via* the decomposition of AIBN, interacts with the AuNP@CeO_2 and plays an important role in the peroxidation of cyclohexene. The role of the formation of organo-gold species *via* the decomposition of AIBN was also proposed to play an important part in the formation of cumene hydroperoxide, which is used as a peroxidising agent for the epoxidation of 1-octene in the presence of Ti-MCM-41 catalyst.[34]

1.6. Conclusions

The work in this thesis examines the interaction between radical species and the surface of AgNP and AuNP in the context of catalysis. The fundamental aspect of solvent peroxidation, which is a free-radical chain reaction, will be presented. The use of AgNP and AuNP in the context of alkene oxidations was also explored.

1.7. References

(1) Lefort, D.; Fossey, J.; Sorba, J. Free Radical in Organic Chemistry; Wiley, 1995.

(2) Denisoe, E. T.; Afanas'ev, I. B. Oxidation and Antioxidant in Organic Chemistry and Biology 2005.

(3) Ingold, K. U. Acc. Chem. Res. 1969, 2, 1.

(4) Haruta, M.; Yamada, N.; Kobayashi, T.; Iijma, S. J. Catal. 1989, 115, 301.

(5) Haruta, M. CatTech 2002, 6, 101.

(6) Tsubota, S.; Nakamura, T.; Tanaka, K.; Haruta, M. Cat. Lett. 1998, 56, 131.

(7) Celliera, C.; Lambert, S.; Gaigneauxa, E. M.; Poleunisb, C.; Ruauxa, V.; Eloy, P.; Lahousse, C.; Bertrand, P.; Pirard, J.-P.; Grang, P. Appl. Catal. B 2007, 70, 406.

(8) Abad, A.; Concepción, P.; Corma, A.; García, H. Angew. Chem. Int. Ed. 2005, 44, 4066.

(9) Hallett-Tapley, G. L.; Crites, C.-O. L.; McGilvray, K. L.; González-Béjar, M.; Netto-Ferreira, J. C.; Scaiano, J. C. J. Photochem. Photobiol., A 2011, 224, 8.

(10) Noujim, T. A.; Mizugaki, T.; Jitsukawa, K.; Kaneda, K. Adv. Synth. Catal. 2009, 351, 1890.

(11) Liu, Y.; Tsunoyama, H.; Akita, T.; Xie, S.; Tsukuda, T. ACS Catal. 2011, 1, 2.

(12) Hereijgers, B. P. C.; Weckhuysen, B. M. J. Catal. 2010, 210, 16.

(13) González-Arellano, C.; Abad, A.; Corma, A.; García, H.; Iglesias, M.; Sánchez, F. Angew. Chem. Int. Ed. 2007, 46, 1536.

(14) Carrettin, S.; Guzman, J.; Corma, A. Angew. Chem. Int. Ed. 2005, 117, 2282.

(15) Corma, A.; Garcia, H. Chem. Soc. Rev 2008, 37, 2096.

(16) Pina, C. D.; Falletta, E.; Prati, L.; Rossi, M. Chem. Soc. Rev. 2008, 37, 2077.

(17) Stephen K, H.; Hutchings, G. J. Angew. Chem. Int. Ed. 2006, 45, 7896.

(18) Choudhary, V. R.; Dumbre, D. K. Ind. Eng. Chem. Res. 2009, 48, 9471.

(19) Hughes, M. D.; Xu, Y.-J.; Jenkins, P.; McMorn, P.; Landon, P.; Enache, D. I.; Carley, A. F.; Attard, G. A.; Hutchings, G. J.; King, F.; Stitt, E. H.; Johnston, P.; Griffin, K.; Kiely, C. J. Nature 2005, 437, 1132.

(20) Álvaro, M.; Aprile, C.; Corma, A.; Ferrer, B.; García, H. J. Catal. 2007, 245, 249.

(21) Yin, D.; Qin, L.; Liu, J.; Li, C.; Jin, Y. J. Mol. Catal. A: Chem 2005, 240, 40.

(22) Patil, N. S.; Uphade, B. S.; McCulloh, D. G.; Bhargava, S. K.; Choudhary, V. R. Cat. Comm. 2004, 5, 681.

(23) Lignier, P.; Morfin, F.; Mangematin, S.; Massin, L.; Rousset, J.-L.; Caps, V. Chem. Commun. 2007, 186.

(24) Turner, M.; Golovko, V. B.; Vaughan, O. P. H.; Abdulkin, P.; Berenguer-Murcia, A.; Tikhov, M. S.; Johnson, B. F. G.; Lambert, R. M. Nature 2008, 454, 981.

(25) Lloyd, R.; Jenkins, R. L.; Piccinini, M.; He, Q.; Kiely, C. J.; Carley, A. F.; Golunski, S. E.; Bethell, D.; Bartley, J. K.; Hutchings, G. J. J. Catal. 2011, 283, 161.

(26) bin Saiman, M. I.; Brett, G. L.; Tiruvalam, R.; Forde, M. M.; Sharples, K.; hetford, A.; Jenkins, R. L.; Dimitratos, N.; Lopez-Sanchez, J. A.; Murphy, D. M.; Bethell, D.; Willock, D. J.; Taylor, S. W.; Knight, D. W.; Kiely, C. J.; Hutchings, G. J. Angew. Chem. Int. Ed. 2012, 51, 5981.

(27) Verykios, X. E.; Stein, F. P.; Coughlin, R. W. Catal. Rev.-Sci. Eng. 1980, 22, 197.

(28) Zhaoa, H.; Zhoua, J.; Luoa, H.; Zenga, C.; Lia, D.; Liu, Y. Cat. Lett. 2006, 108, 49.

(29) Casemier, J. H. R.; Nieuwenhuys, B. E.; Sachlter, W. M. H. J. Catal. 1973, 29, 367.

(30) Ham, N. H. A. V.; Nieuwenhuys, B. E.; Sachtler, W. M. H. J. Catal. 1971, 20, 408.

(31) Zidki, T.; Cohen, H.; Meyerstein, D. Phys. Chem. Chem. Phys. 2006, 8, 3552.

(32) Bar-Ziv, R.; Zilbermann, I.; Zidki, T.; Cohen, H.; Meyerstein, D. J. Phys. Chem. C. 2009, 113, 3281.

(33) Aprile, C.; Boronat, M.; Belen, F.; Corma, A.; Garcia, H. J. Am . Chem . Soc. 2006, 128, 8388.

(34) Aprile, C.; Corma, A.; Domine, M. E.; Garcia, H.; Mitchell, C. J. Catal. 2009, 264, 44

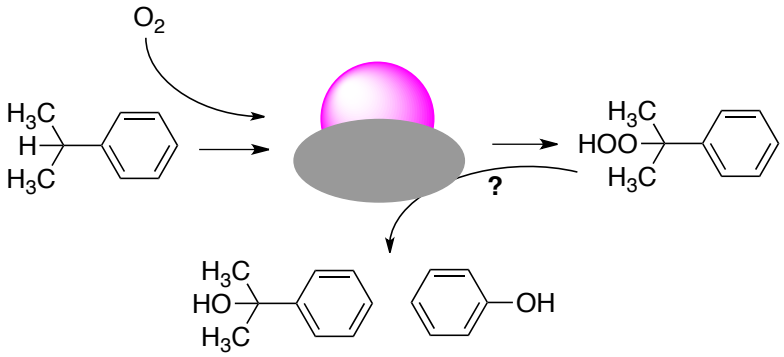

2. Insights into the Mechanism of Cumene Peroxidation using Supported Gold and Silver Nanoparticles

2.0. Table of contents

2.1. Introduction

Hydroperoxides are important precursors in industry.[1] Ethylbenzene hydroperoxide is used as part of the Halcon process and in the oxidation of cyclohexane into cyclohexanol,[2-5] which is a precursor to the formation of caprolactam used in the synthesis of Nylon-6. However, the most important industrial process involving hydroperoxide is the formation of cumene hydroperoxide (CHP). CHP is the precursor to the formation of phenol and acetone, both obtained via the Hock rearrangement.[6] More importantly, to date, CHP formation is not catalyzed in industry.[7] The formation of CHP is achieved by the free-radical chain oxidation of cumene. Like every free-radical chain reaction, this oxidation is comprised of 4 different types of elemental steps that constitute the free-radical process as shown in the introduction.

In the 1950's and 1960's, the influence of metal salt catalysts on free-radical processes was examined in the peroxidation of tetralin.[8,9] Later, heterogeneous materials, such as MnO_2 and CuO_2,[10] were used as catalysts in the study of cumene peroxidation. The stability of the resultant cumene hydroperoxide in the presence of catalysts poses a major problem due to the rapid hydroperoxide decomposition into the corresponding alcohol.[11] Several literature precedents have shown that the stability of CHP is problematic in the presence of a variety of heterogeneous catalysts, including silver nanoparticles (AgNP) on Al_2O_3,[12] copper oxide nanoparticles,[13] and copper oxide on MgO.[7] . On the other hand,

Casemier *et al.*[14] have demonstrated that AgNP catalyze the peroxidation of cumene with minimal decomposition of the desired CHP to cumyl alcohol. Furthermore, studies using AuNP@CeO_2 as a catalyst for cumene peroxidation have shown that the support was partially responsible for some of hydroperoxide decomposition to cumyl alcohol.[15] Given these results from the literature, it is evident that the nature of the support can considerably influence the stability of CHP. The objectives of this chapter are two-fold. First, this study aims to gain some insight into the impact of AuNP and AgNP on the free-radical oxidation process by way of cumene peroxidation. Secondly, the influence of AgNP and AuNP, as well as the support constituting the heterogeneous catalyst, on the nature of the peroxidation product will also be discussed. Three catalysts will be used to investigate the role of supported nanoparticle catalysts in free radical processes: gold nanoparticles supported on TiO_2 (AuNP@TiO_2), gold nanoparticles supported on hydrotalcite (AuNP@HT) and silver nanoparticles supported on hydrotalcite (AgNP@HT).

2.2. Results

2.2.1. TEM of catalysts used in this study

AuNP@TiO_2 is a commercial sample purchased from Strem Chemicals. The average particle size of AuNP was determined to be 2.3 ± 0.6 nm (Figure 2.1). AuNP@HT and AgNP@HT were synthesized following the published method of Mitsudome *et al*[16,17] with detailed experimental procedures being found in

Sections 2.5.3 and 2.5.4, respectively. The average particle size was determined to be 5.8 ± 2.7 nm for AuNP@HT (Figure 2.2) and 10 ± 3.2 nm for AgNP@HT (Figure 2.3).

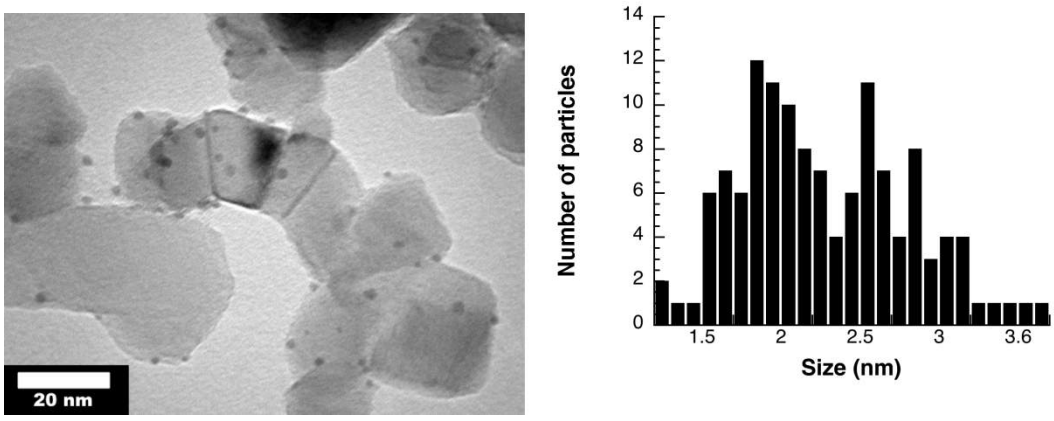

Figure 2.1. TEM (left) and size distribution histogram (right) of commercial AuNP@TiO_2.
Reprint with permission from ACS Catal., 2013, 3 (9), 2062. Copyright 2013 American Chemical Society

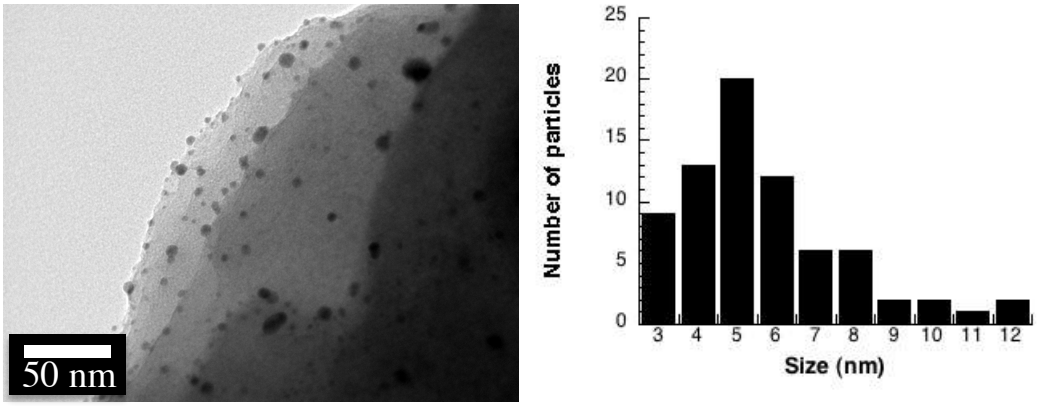

Figure 2.2. TEM (left) and size distribution histogram (right) of AuNP@HT. Reprint with permission from ACS Catal., 2013, 3 (9), 2062. Copyright 2013 American Chemical Society

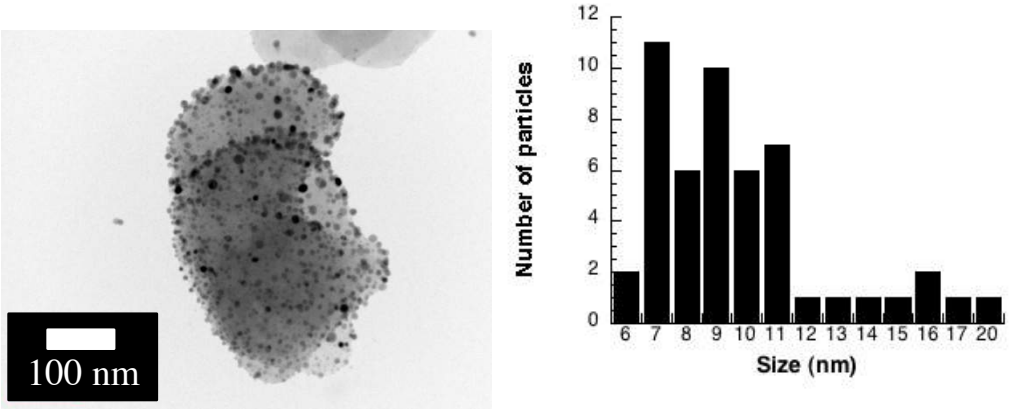

Figure 2.3. TEM (left) and size distribution histogram (right) of AgNP@HT. Reprint with permission from ACS Catal., 2013, 3 (9), 2062. Copyright 2013 American Chemical Society

2.3.2. Commercial AuNP@TiO_2 as a catalyst for cumene peroxidation

Commercial AuNP@TiO_2 was the initial material tested as a heterogeneous catalyst for cumene peroxidation. Scheme 2.1 presents the general reaction conditions used throughout the peroxidation experiments. More details of the experimental conditions can be found in Section 2.5.5.

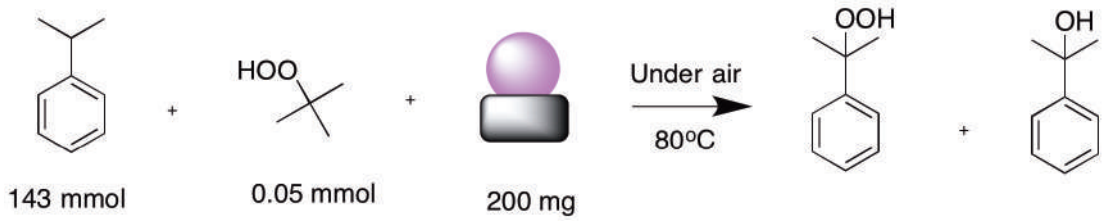

Scheme 2.1. General reaction conditions of the peroxidation of cumene using supported nanoparticle catalysts.

Figure 2.4 illustrates the products obtained for the peroxidation of cumene using AuNP@TiO_2 after 24 hours. In the absence of catalyst, the only product obtained

was CHP in a 1.0% yield. However, in the presence of AuNP@TiO_2, both CHP and cumyl alcohol are obtained in yields of 1.0% and 3.8 %, respectively, indicating that the selectivity of the reaction is influenced by the presence of AuNP. When TiO_2 itself is used as a catalyst, 0.4% of CHP is obtained as the sole product, demonstrating that TiO_2 alone is not a good catalyst.

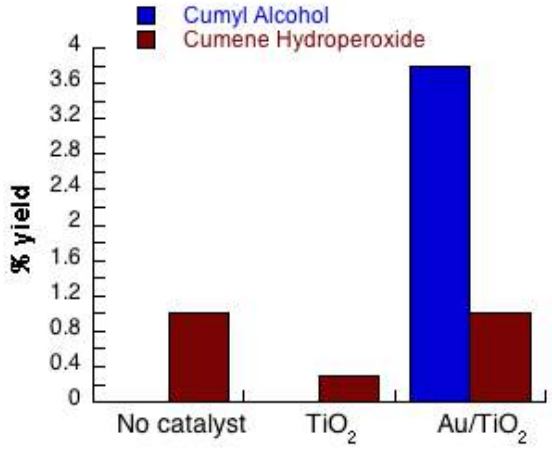

Figure 2.4. Bar graph illustrating the yield of cumyl alcohol and CHP after 24 hours when using no catalyst, TiO_2 and commercial AuNP@TiO_2 at 80°C and *tert*-butyl hydroperoxide as an initiator. Reprint with permission from ACS Catal., 2013, 3 (9), 2062. Copyright 2013 American Chemical Society

The reaction kinetics of AuNP@TiO_2 catalyzed cumene peroxidation was monitored over an 8 hours period and is presented in Figure 2.5. As can be seen, the major product obtained is cumyl alcohol. Importantly, no CHP could be detected in the first 3 hours of the reaction. Other products, namely acetophenone and dicumyl peroxide, were also observed. Acetophenone was

formed by way of the β-scission of the cumyloxyl radicals (Scheme 2.2a) and dicumyl peroxide (DCP) is obtained following the radical recombination of two cumyloxyl radicals (Scheme 2.2b) or the radical recombination of two cumyl peroxyl radicals (Scheme 2.2c). In fact, radical recombination of two cumyloxyl radicals is unlikely due to the fact that this radical readily abstracts hydrogen from cumene. The corresponding control reactions are also presented in Figures 2.6 and 2.7. The control reaction using either TiO_2 (CHP=0.03%; Figure 2.6) or in absence of any catalyst (Figure 2.7) showed only trace amounts of CHP.

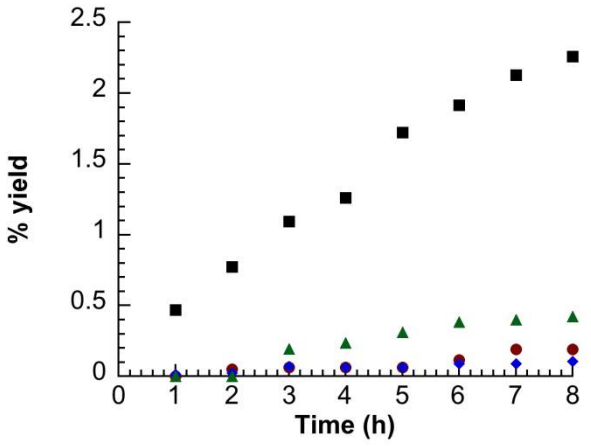

Figure 2.5. Percent yield of cumyl alcohol (■), CHP (●), acetophenone (◆) and DCP (▲) obtained for the peroxidation of cumene using commercial AuNP@TiO_2 at 80°C, over 8 hours. Reprint with permission from ACS Catal., 2013, 3 (9), 2062. Copyright 2013 American Chemical Society

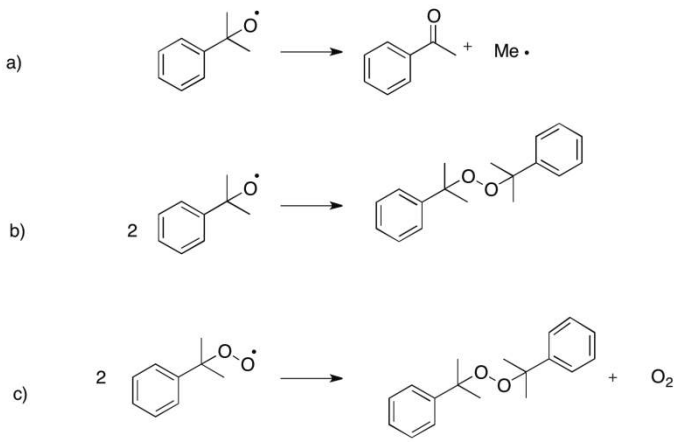

Scheme 2.2. Formation of secondary products for cumene peroxidation using commercial AuNP@TiO_2: a) formation of acetophenone *via* β-scission of the cumyloxyl radical, b) formation of dicumylperoxide (DCP) *via* radical recombination of two cumyloxyl radicals and c) formation of DCP *via* recombination of two cumyl peroxyl radicals. Reprint with permission from ACS Catal., 2013, 3 (9), 2062. Copyright 2013 American Chemical Society

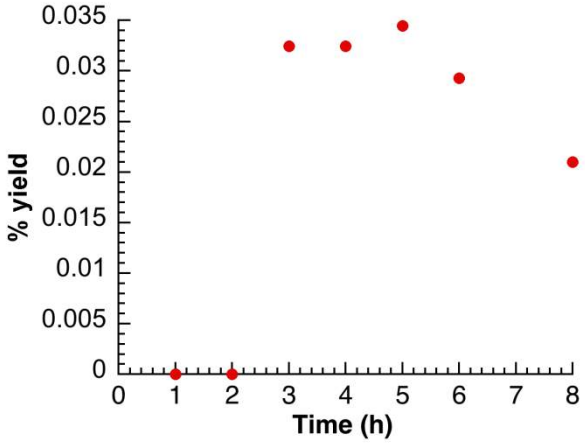

Figure 2.6. Percent yield of CHP using TiO_2 only (with *tert*-butyl hydroperoxide as initiator) for cumene peroxidation at 80°C. Note the extremely small yields. Reprint with permission from ACS Catal., 2013, 3 (9), 2062. Copyright 2013 American Chemical Society

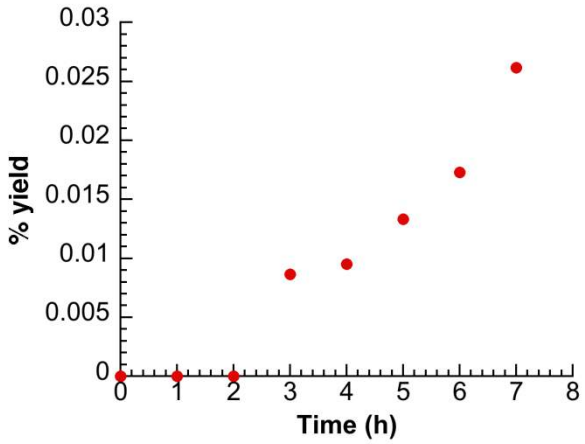

Figure 2.7. Percent yield of CHP in absence of catalyst (with *tert*-butyl hydroperoxide as initiator) for cumene peroxidation at 80°C. Note the extremely small yields. Reprint with permission from ACS Catal., 2013, 3 (9), 2062. Copyright 2013 American Chemical Society

As the stability of CHP was largely influenced by the presence of the catalyst, this process warranted closer examination. The experiment consisted of adding a known amount of CHP to a solvent that was relatively inert toward radical processes (*n*-dodecane)[18] and monitoring the degradation of CHP as a function of time(see Section 2.5.8 for experimental details). As shown in Figure 2.8, CHP is stable in the absence of catalyst, which is expected given the stability of CHP at the reaction temperature of 80°C considering the half-life is 29 hours at 130°C.[19] However, in the presence of both TiO_2 and AuNP@TiO_2, CHP is decomposed, with the nature of the product distribution being unique in the two cases. In the case of the AuNP@TiO_2, the major decomposition product is cumyl alcohol by way of a radical pathway.[20] On the other hand, the major decomposition

product obtained when using TiO_2 was phenol, formed by a non-radical pathway and the acidic nature of the TiO_2 support.[21]

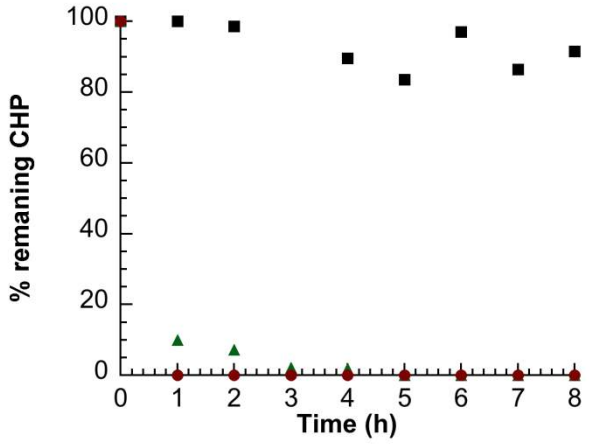

Figure 2.8. Decomposition of CHP using no catalyst (■), TiO_2 only (▲) and commercial AuNP@TiO_2 (●) at 80°C. Reprint with permission from ACS Catal., 2013, 3 (9), 2062. Copyright 2013 American Chemical Society

The formation of phenol from CHP in the presence of TiO_2 was shown to be dependent on the acidity of the TiO_2.[22] Literature precedents employing both dry and hydrated clay show that CHP is decomposed into phenol only when the water content of the clay is below 6 %.[23] As such, hydration of the TiO_2 was examined as a possible influence in the observed CHP degradation illustrated in Figure 2.8. The TiO_2 P25 used for the control reaction was dried in a furnace under atmospheric conditions for 72 hours at 400°C. As expected, the dry TiO_2 increased the efficiency of CHP into phenol, where this is not the case for the hydrated TiO_2 as shown in Figure 2.9.

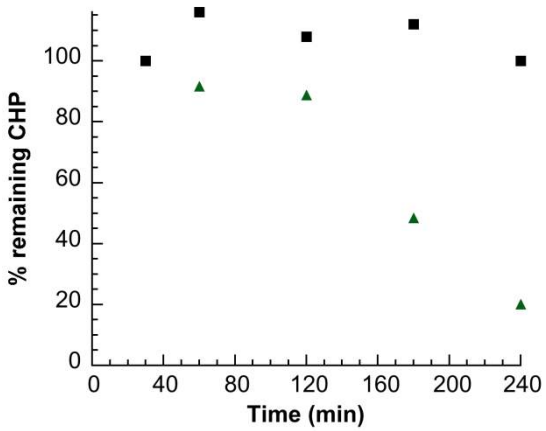

Figure 2.9. CHP decomposition using calcined TiO_2 (▲ ; 400°C, 72 hours) and hydrated TiO_2 (■) at 80°C. The major decomposition product obtained when using the hydrated support was phenol. Reprint with permission from ACS Catal., 2013, 3 (9), 2062. Copyright 2013 American Chemical Society

2.3.3. Using AuNP@HT as a catalyst

As shown above, the radical nature of cumene hydroperoxidation requires that the hydroperoxide be stable in the presence of the support that one chooses to use. In order to gain a better understanding of the influence of the support on this process, the stability of CHP was examined in the presence of a variety of supports in order to determine one that would be relatively unreactive towards the CHP degradation pathway. A number of supports were tried, including Al_2O_3, ZnO, clays, and hydrotalcite (HT; magnesium aluminum anionic clays). Hydrotalcite was found to meet the inertness criteria towards radical reactions,[24] and, as such, was chosen to continue the cumene peroxidation study. As was observed in the case of AuNP@TiO_2, cumyl alcohol was the major product

obtained when AuNP@HT was used as a catalyst in the peroxidation reaction (Figure 2.10). However, the amount of CHP obtained was significantly increased as compared to when AuNP@TiO_2 was employed as the catalytic material.

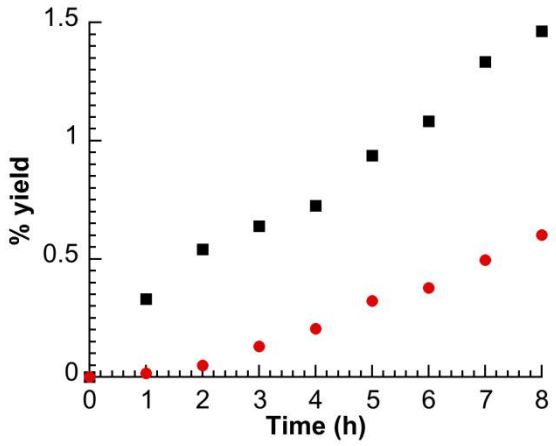

Figure 2.10. Percent yield of cumyl alcohol (■) and CHP (●) for AuNP@HT catalyzed cumene peroxidation at 80°C Reprint with permission from ACS Catal., 2013, 3 (9), 2062. Copyright 2013 American Chemical Society

The control experiment using HT as the catalyst (Figure 2.11) demonstrates that only traces amounts of CHP are present and validates that this support does not decompose CHP by radical or acidic pathways. The low percentage of conversion is due to the fact that the initiator at this temperature is not decomposed either thermally or by the catalyst.

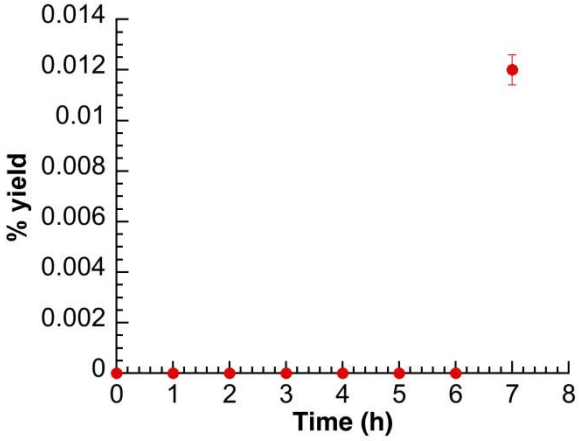

Figure 2.11. Percent yield of CHP using HT only (with *tert*-butyl hydroperoxide as initiator) for cumene peroxidation at 80°C. Note the extremely small yields even after 7 hours reaction. Reprint with permission from ACS Catal., 2013, 3 (9), 2062. Copyright 2013 American Chemical Society

The stability of CHP was assessed in the presence of HT and AuNP@HT (Figure 2.12). In the absence of catalyst or in the presence of HT alone, CHP is remarkably stable. On the other hand, when AuNP@HT was used as a catalyst, CHP was decomposed into cumyl alcohol and reached a plateau after 2 hours. This plateau can be attributed to the establishment of a steady-state between the degradation of the CHP and the formation of CHP due to the presence of cumene as an impurity (~20%) in the commercial CHP solution used for this experiment. Furthermore, when this reaction is performed under inert atmosphere (N_2), complete degradation is oberved (Figure 2.13), as the formation of CHP from cumene is not possible due to the absence of oxygen.

The observed plateau may also be partially attributed to catalyst fatigue or to change in the properties of the catalyst.

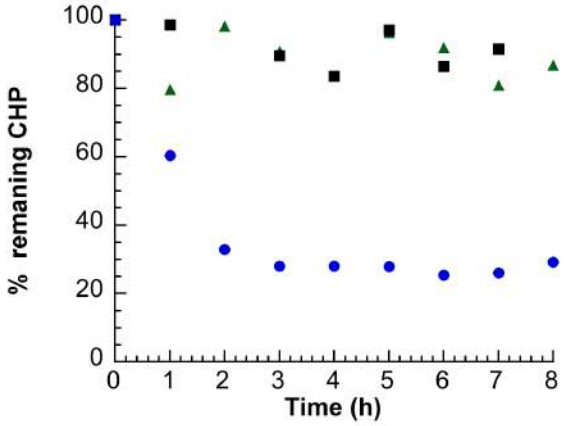

Figure 2.12. Decomposition of CHP into cumyl alcohol using no catalyst (■), HT (▲) and AuNP@HT (●), at 80°C. Reprint with permission from ACS Catal., 2013, 3 (9), 2062. Copyright 2013 American Chemical Society

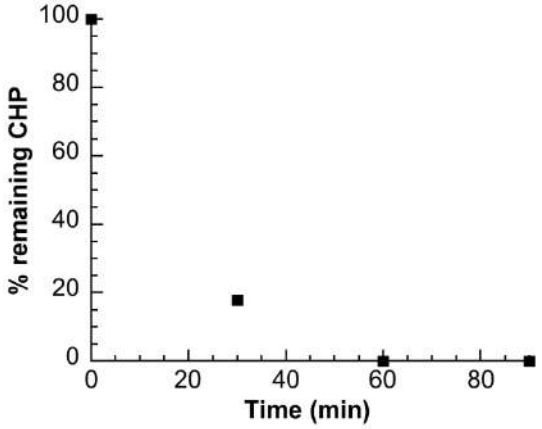

Figure 2.13. CHP decomposition using AuNP@HT under N_2 saturated conditions at 80°C. Reprint with permission from ACS Catal., 2013, 3 (9), 2062. Copyright 2013 American Chemical Society

A comparison of the results obtained when employing AuNP@TiO_2 and AuNP@HT as the peroxidation catalyst shows that AuNP@TiO_2 was clearly more active towards the formation of cumyl alcohol. On the other hand, if the target product were CHP (the desired industrial precursor for the formation of phenol and acetone), then AuNP@HT would be the best choice. The difference in catalyst activity will be more closely addressed in Chapter 3. In brief, two hypotheses can be considered to account for the difference in activity between AuNP supported on TiO_2 or HT. The first suggestion focuses on the difference in size of the AuNP on the two composites (5.8 nm for AuNP@HT *versus* 2.3 nm for Au@TiO_2) which could be responsible for the difference in activities.[25] The second hypothesis centers on the nature of the support and the intrinsic differences in the interaction between the support and the AuNP.[26]

2.3.4. Using AgNP@HT as a catalyst

As mentioned in the Introduction, the work of Casemier *et al.*[14] discusses the possibility that AgNP are capable of catalyzing cumene peroxidation with minimal decomposition of CHP into cumyl alcohol. Considering this, along with the inertness of HT toward free-radical processes, supported AgNP on HT (AgNP@HT) were synthesized following the published procedure by Mitsudome and co-workers.[17] (see Section 2.5.4). The results obtained using AgNP@HT for the peroxidation of cumene (Figure 2.14) show that CHP is the major product

obtained (1.0% of CHP *versus* 0.08% of cumyl alcohol) after 8 hours. These results represent an inversion of product selectivity as compared to those obtained when AuNP@HT was used.

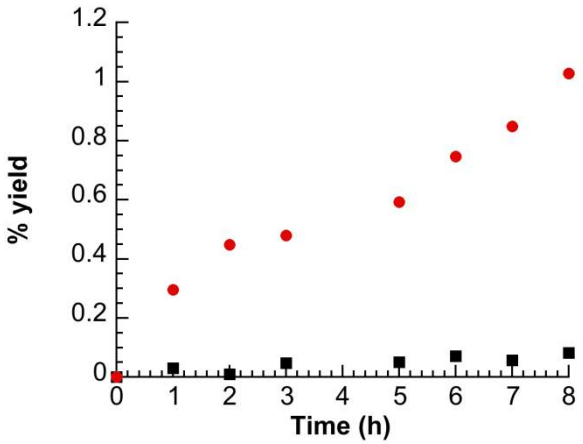

Figure 2.14. Percent yield of cumyl alcohol (■) and CHP (●) for AgNP@HT catalyzed cumene peroxidation, at 80°C. Reprint with permission from ACS Catal., 2013, 3 (9), 2062. Copyright 2013 American Chemical Society

Figure 2.15 illustrates the limited ability of AgNP@HT to degrade CHP into cumyl alcohol, as little difference in CHP decomposition can be seen when HT alone or AgNP@HT is used as the catalyst.

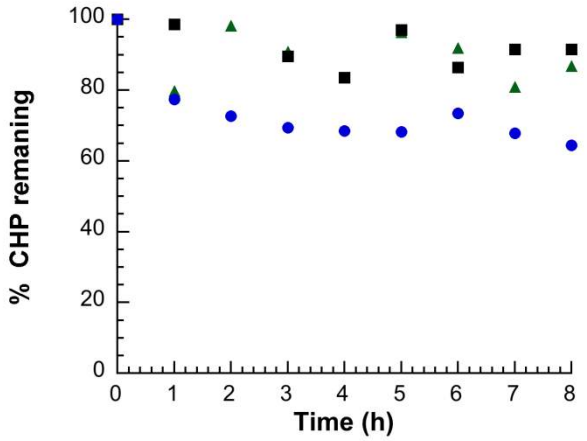

Figure 2.15. Decomposition of CHP into cumyl alcohol using no catalyst (■), HT (▲) and AgNP@HT (●), at 80°C. Reprint with permission from ACS Catal., 2013, 3 (9), 2062. Copyright 2013 American Chemical Society

In order to increase the yield of CHP in the reaction mixture, the reaction was carried out under oxygen-saturated conditions through bubbling oxygen in the solution at a rate of 5 mL/min (Figure 2.16). The formation of CHP was enhanced from 1% to 9.4% under O_2, while the % yield of cumyl alcohol increased from 0.1% to 2.4 %, as compared to the % yield obtained under atmospheric conditions.

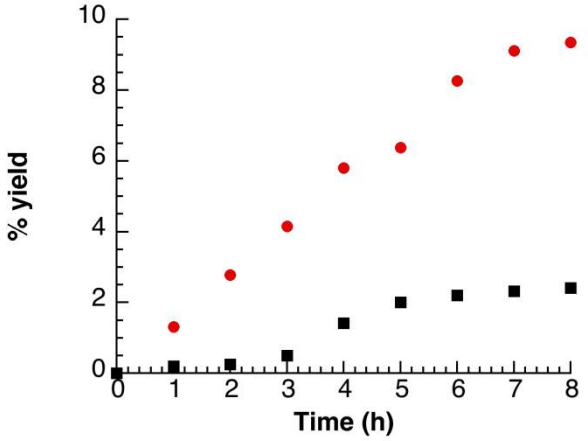

Figure 2.16. Percent yield of cumyl alcohol (■) and CHP (●) for AgNP@HT catalyzed cumene peroxidation at 80°C under oxygen saturated conditions. Reprint with permission from ACS Catal., 2013, 3 (9), 2062. Copyright 2013 American Chemical Society

A summary of the results obtained using supported HT materials over 8 hours reaction is presented in Table 1. Some interesting conclusions can be drawn from this table. Firstly, the selectivity toward the formation of CHP is clearly influenced by the nature of the metal nanoparticle in the material, with AgNP favouring formation of CHP over cumyl alcohol. Secondly, oxygen flow tends to have a major influence on the overall yield of CHP. Specifically, when AgNP@HT was used as a catalyst, the % yield of CHP is shown to increase considerably in the presence of oxygen.

Table 2.1. Product distribution and selectivity of supported AuNP and AgNP catalyzed cumene peroxidation after 8 hours reaction at 80°C under atmospheric condition (no flow) or under oxygen saturated condition (O_2 flow) .Reprint with permission from ACS Catal., 2013, 3 (9), 2062. Copyright 2013 American Chemical Society

Catalyst	O_2 Flow/No flow	*% Yield Cumyl Alcohol*	*% Yield CHP*	*Selectivity CHP (%)*
AuNP@HT	No flow	0.9	0.3	25 %
AgNP@HT	No flow	0.1	1.0	92 %
No catalyst	No flow	ND	0.03	-
HT	No flow	ND	0.01	-
AgNP@HT	*O_2 flow*	2.4	9.4	80%
No catalyst	*O_2 flow*	ND	0.1	-
HT	*O_2 flow*	0.2	1.8	80%

(ND= not detected)

2.3.5. Recyclability study

The recyclability of AuNP@HT and AgNP@HT under atmospheric and oxygen saturated conditions was also investigated and is presented as relative yield in Figure 2.17. The activity of the AuNP@HT catalyst remains relatively stable for the first cycle and decreases by ~50% in the second cycle with respect to the amount of cumyl alcohol. However, a two-fold increase in the amount of CHP was observed between trials. This increase in CHP formation accompanied by less favourable cumyl alcohol formation (by way of CHP degradation) may also be used to explain the plateau in CHP decomposition previously observed in

Figure 2.12 (*vide supra*). When AgNP@HT was used under atmospheric conditions, the activity of the catalyst is maintained over two cycles, suggesting improved stability of this material as compared to supported AuNP. However, the results obtained using AgNP@HT under O_2 saturated conditions show that the catalyst is not as stable. This is apparent as the activity of the catalyst decreases more than 50% when monitoring the formation of CHP and 75% for cumyl alcohol in a subsequent use.

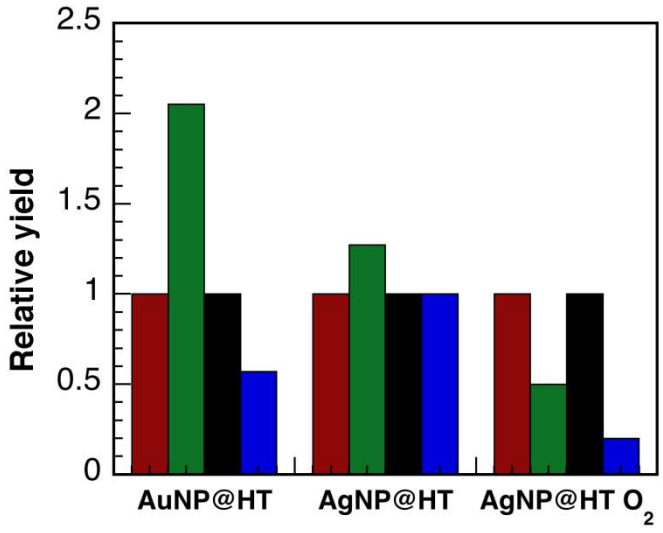

Figure 2.17. Recyclability experiments after one reuse of AuNP@HT and AgNP@HT (under atmospheric and oxygen saturated conditions): CHP first cycle (■), CHP second cycle (■), cumyl alcohol first cycle (■) cumyl alcohol second cycle (■). Please note that these data only within the same catalyst. Reprint with permission from ACS Catal., 2013, 3 (9), 2062. Copyright 2013 American Chemical Society

In order to explain the decreased catalytic activity of the AgNP@HT catalyst under oxygen saturated conditions, the material was thoroughly characterized before and after catalysis using TEM and XPS. As illustrated in Figure 2.18, TEM images taken before and after reaction show degradation of the layered

hydrotalcite structure and the formation of more three-dimensional domains. In addition, one important observation was the change in the visual aspect of the catalyst, which changed from yellow (before catalysis) to blue/black (after catalysis). The change in color, in combination with the change in the material structure suggest the formation of a tridimensional spinel phase of ($MgAlO_4$) after catalytic use.[27]

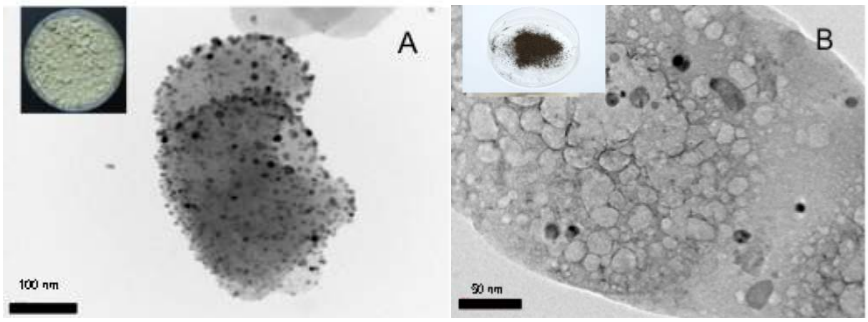

Figure 2.18. TEM images and photos (insert) of AgNP@HT (a) before and (b) after catalysis under 5mL/min oxygen flow. Reprint with permission from ACS Catal., 2013, 3 (9), 2062. Copyright 2013 American Chemical Society

XPS analysis was also carried out in order to gain additional information about the changes in the oxidation states of the supported AgNP. Considering the limitation in the minimal nominal loading required to obtain an acceptable signal in XPS analysis, the presented data were obtained using a catalyst made with 4% Ag . The XPS results illustrate that the supported AgNP are not stable under oxygen saturated conditions, as evidenced by the appearance of XPS peaks at 370.0 eV and 376.1 eV due to the formation of Ag(I) and the likely

presence of Ag_2O (Figure 2.19). The formation of Ag_2O may also partially explain the blue/black colour of the catalyst after reaction, given the similarity in colour with the oxide Figure 2.19 .

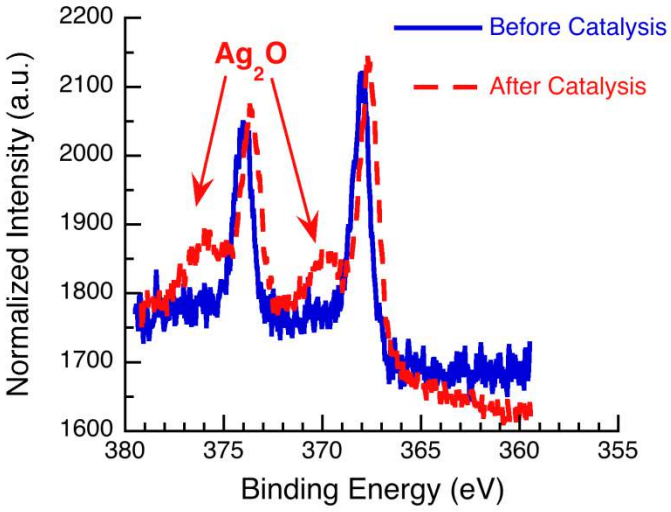

Figure 2.19. XPS of 4% AgNP@HT before and after catalysis under 5mL/min oxygen flow. Note the appearance of Ag(I) at 370.0 eV and 376.1 eV. Reprint with permission from ACS Catal., 2013, 3 (9), 2062. Copyright 2013 American Chemical Society

2.3.6. Oxygen Uptake Experiments

The oxygen uptake apparatus is useful for determining the rate at which a gas is produced or consumed over a determined period of time. This is a standard technique that has been used for decades when studying the mechanism of oxidation reactions by focusing on the rate of oxygen consumption.[28] A more detailed explanation of the apparatus can be found in Experimental Sections 2.5.9 and 2.5.10, as well as in Appendix 2. Two different experiments were carried out using oxygen uptake. The first focuses on the rate at which oxygen is

consumed and is used to determine the corresponding rate of propagation (R_p) of the free-radical chain reaction. The rate of oxygen uptake, or the rate of propagation, is given by the slope of the black traces found in Figure 2.20. The second experiment determined the rate of initiation, giving us information on the rate at which radical species are formed from non-radical precursors.

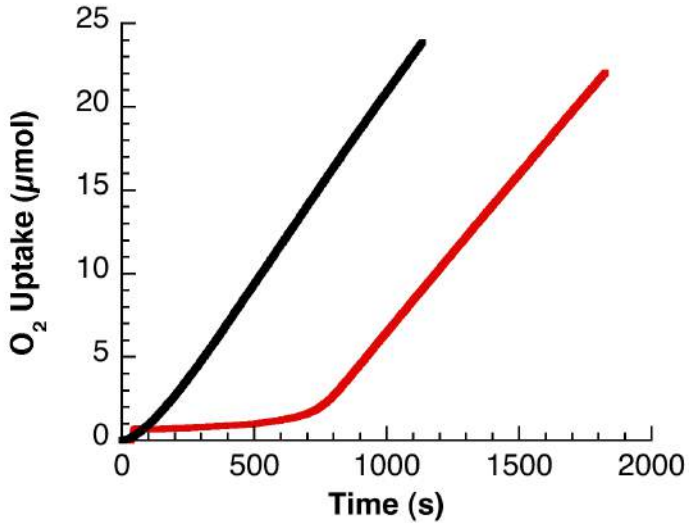

Figure 2.20. Typical oxygen uptake traces obtained for commercial AuNP@TiO_2-catalyzed cumene peroxidation using *tert*-butyl hydroperoxide as initiator. The black line represents actual experimental data obtained and was used to calculate the amount of O_2 consumed as a function of time and the red line represents actual experimental data using an antioxidant to calculate the rate of initiation. Reprint with permission from ACS Catal., 2013, 3 (9), 2062. Copyright 2013 American Chemical Society

Due to experimental limitations, it was only possible to use the oxygen uptake at 30°C and, at such temperature, only AuNP@TiO_2 showed some activity. The rate of propagation (R_p) for the commercial AuNP@TiO_2 was determined to be ~1.0 × 10^{-5} M/s and decreased as the reaction progressed.

Furthermore, we can determine the rate of initiation (R_i) by examining the length of the induction period that is present following the addition of an antioxidant, as the antioxidants can prevent the propagation step (see Appendix 2 for a more detailed explanation). The rate of initiation (R_i) was determined to be ~1.7×10^{-7} M/s through the use of 2,6-di-*tert*-butyl-4-methoxyphenol as an antioxidant.

The chain length, a value that relates to the number of propagation steps *versus* a single initiation step, was calculated by dividing R_p/R_i and is 58. This quantity should be proportional to [CHP]/[cumyl alcohol]. In order to check this affirmation, HPLC analysis was carried out in parallel with the oxygen uptake experiments and the amount of product obtained is presented in Figure 2.21 From the HPLC data, the ratio between [CHP]/[cumyl alcohol] was determined to be approximately 2, not 58 as was determined by oxygen uptake experiments.

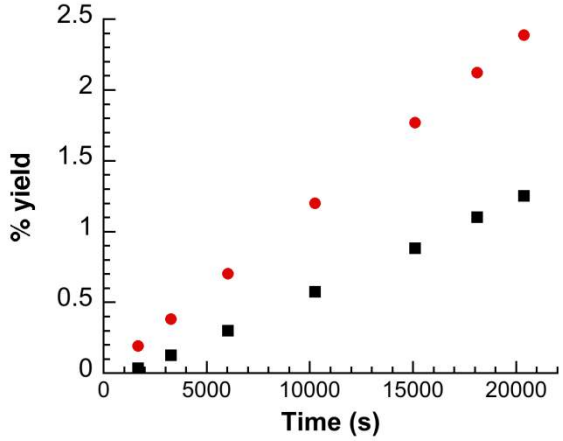

Figure 2.21. Percent yield of cumyl alcohol (■) and CHP (●) for cumene peroxidation using AuNP@TiO_2 at 30°C using the oxygen uptake technique. Reprint with permission from ACS Catal., 2013, 3 (9), 2062. Copyright 2013 American Chemical Society

2.3.7. Mechanistic investigation at 80°C

2.3.7.1. Control experiments using new batch of AuNP@HT, AgNP@HT and AuNP@TiO_2

Considering the limitation of the oxygen uptake experiments, we decided to get information on the nature of the mechanism at 80°C. In order to carry out these experiments, a new batch of catalyst was required. As batch to batch variations are observed when dealing with nanomaterials,[29] the peroxidation of cumene was also carried out using the new material to ensure the same trends were obtained as was previously observed. This will also allow for a direct comparison with the mechanistic insights reactions to be performed (Figures 2.22 to 2.24). One should also note that the results obtained within the same batch are quite reproducible.

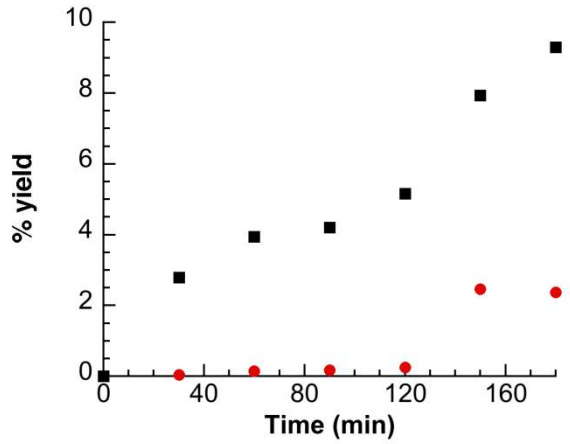

Figure 2.22 Percent yield of cumyl alcohol (■) and CHP (●) for AuNP@TiO_2 catalyzed cumene peroxidation at 80°C under atmospheric conditions using the new batch of catalyst. Reprint with permission from ACS Catal., 2013, 3 (9), 2062. Copyright 2013 American Chemical Society

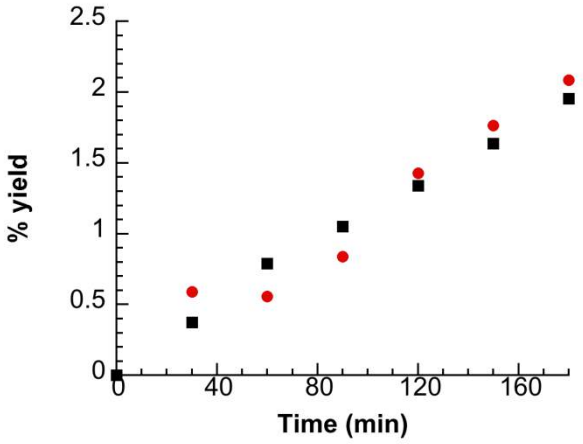

Figure 2.23. Percent yield of cumyl alcohol (■) and CHP (●) for AuNP@HT catalyzed cumene peroxidation at 80°C under atmospheric conditions using the new batch of catalyst. Reprint with permission from ACS Catal., 2013, 3 (9), 2062. Copyright 2013 American Chemical Society

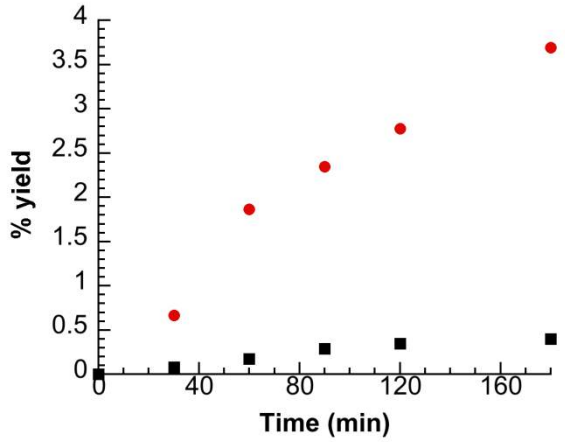

Figure 2.24. Percent yield of cumyl alcohol (■) and CHP (●) for AgNP@HT-catalyzed cumene peroxidation at 80°C under atmospheric conditions using the new batch of catalyst. Reprint with permission from ACS Catal., 2013, 3 (9), 2062. Copyright 2013 American Chemical Society

2.3.7.2. Experiments using 2,6-di-*tert*-butyl-4-methoxyphenol (DBHA) as an antioxidant.

In order to demonstrate the nature of the reaction at 80°C, DBHA was used as antioxidant for the 3 catalysts in this study. The mechanism by which DBHA inhibits the free-radical reaction is shown in Scheme 2.3

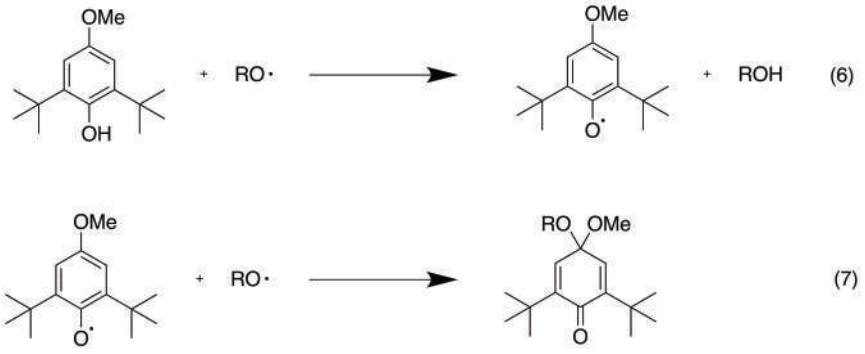

Scheme 2.3. Antioxidant activity of DBHA as illustrated using an alkoxyl radical.

Briefly, DBHA can terminate two equivalents of radical species per molecule, first *via* a phenolic hydrogen abstraction from the DBHA (Scheme 2.3, eq. 1) and second via the trapping of a radical species (Scheme 2.3, eq. 2). The experiment was carried out as follows: the reaction was allowed to proceed for one hour (in the presence of AuNP@HT, AgNP@HT or AgNP@HT under O_2 conditions) and then DBHA was added. The results, presented in Figures 2.25 to 2.27, show that the reaction is inhibited by the addition of DBHA for all three heterogeneous catalysts and no increase in the overall yield is observed after the first hour. The decrease in the amount of CHP observed in Figures 2.25 and 2.26 is most likely due to the catalyst-assisted decomposition of CHP into cumyl alcohol.

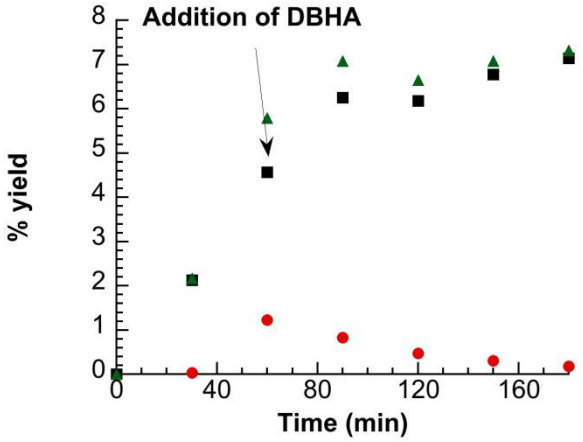

Figure 2.25. Percent yield of cumyl alcohol (■), CHP (●) and total products (▲) for AuNP@TiO_2-catalyzed cumene peroxidation at 80°C under atmospheric conditions following the addition of DBHA after 1 hour. Reprint with permission from ACS Catal., 2013, 3 (9), 2062. Copyright 2013 American Chemical Society

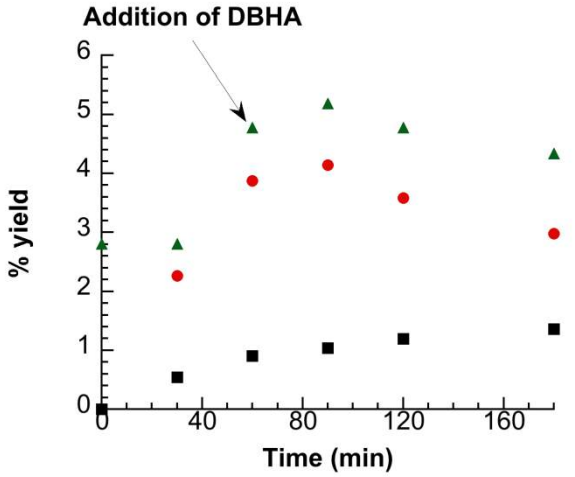

Figure 2.26. Percent yield of cumyl alcohol (■), CHP (●) and total products (▲) for AuNP@HT-catalyzed cumene peroxidation at 80°C under atmospheric conditions following the addition of DBHA after 1 hour. Reprint with permission from ACS Catal., 2013, 3 (9), 2062. Copyright 2013 American Chemical Society

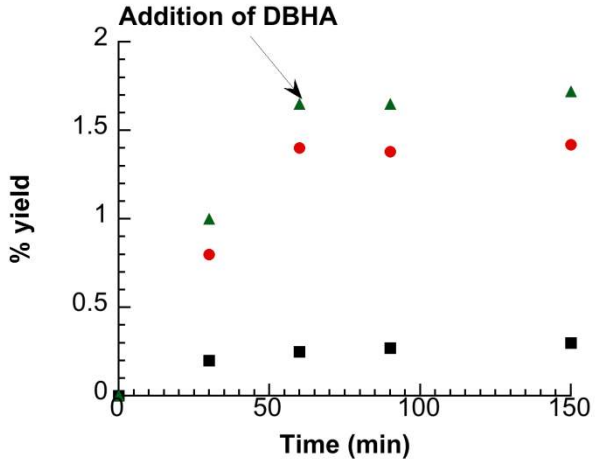

Figure 2.27. Percent yield of cumyl alcohol (■), CHP (●) and total products (▲) for AgNP@HT-catalyzed cumene peroxidation at 80°C under atmospheric conditions following the addition of DBHA after 1 hour. Reprint with permission from ACS Catal., 2013, 3 (9), 2062. Copyright 2013 American Chemical Society

2.3.7.3. Experiments using lipoic acid as a surface capping agent

Experiments using lipoic acid as a surface capping agent were carried out in order to gain additional information regarding the role of AuNP in the peroxidation mechanism and, in particular, the role of the interaction between free-radical species and the AuNP surface. Lipoic acid should interact with the nanoparticles by way of a strong Au-S bond (Scheme 2.4).[30] Literature precedent also suggests that it is possible for AgNP to undergo similar surface interactions with thiols.[31]

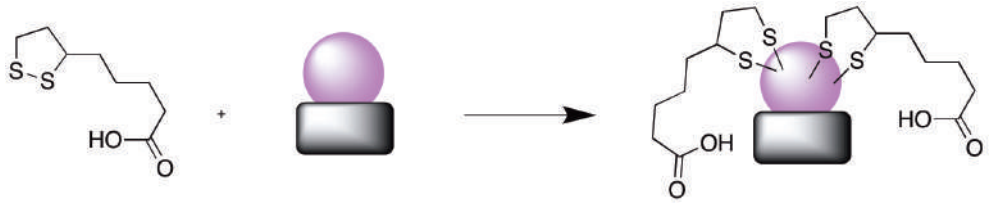

Scheme 2.4. Schematic illustration for the surface capping of metallic nanoparticles by lipoic acid.

The lipoic acid experiments were carried out in an analogous fashion to the DBHA trials (see above). The reaction in the presence of AuNP@HT, AgNP@HT or AgNP@HT under O_2 was allowed to stir for 1 hour and then 5 mg of lipoic acid were added (see Section 2.5). The effects of lipoic acid addition on the reaction kinetics are presented in Figures 2.28 to 2.30 and demonstrate a plateau for both product formation in the presence of the sulfur capping agent, suggesting that restricting access to the nanoparticle surface prohibits the cumene

peroxidation mechanism and strongly implicates participation of the nanoparticle surface on the reaction pathway.

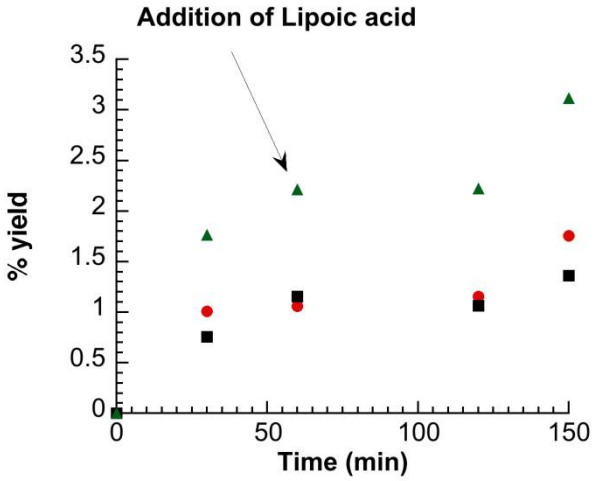

Figure 2.28. Percent yield of cumyl alcohol (■), CHP (●) and total products (▲) for AuNP@HT-catalyzed cumene peroxidation at 80°C under atmospheric conditions following the addition of lipoic acid. Reprint with permission from ACS Catal., 2013, 3 (9), 2062. Copyright 2013 American Chemical Society

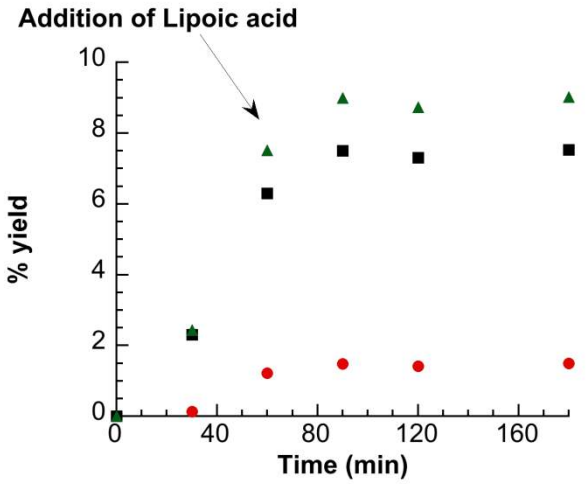

Figure 2.29. Percent yield of cumyl alcohol (■), CHP (●) and total products (▲) for AuNP@TiO_2-catalyzed cumene peroxidation at 80°C under atmospheric conditions following the addition of lipoic acid Reprint with permission from ACS Catal., 2013, 3 (9), 2062. Copyright 2013 American Chemical Society

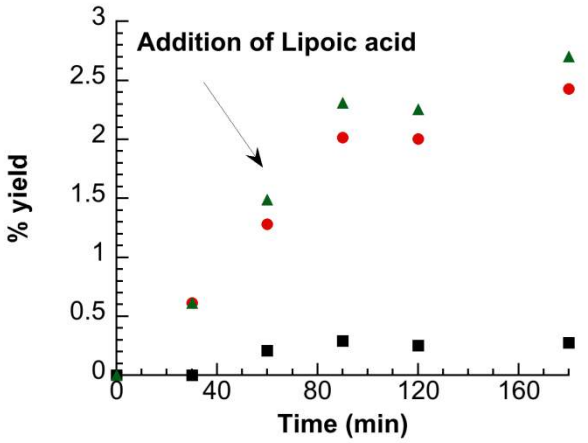

Figure 2.30. Percent yield of cumyl alcohol (■), CHP (●) and total products (▲) for AgNP@HT-catalyzed cumene peroxidation at 80°C under atmospheric conditions following the addition of lipoic acid. Reprint with permission from ACS Catal., 2013, 3 (9), 2062. Copyright 2013 American Chemical Society

2.4. Discussion

One of the main objectives of this chapter was to determine the catalytic activity of supported AuNP and AgNP on classical free-radical pathways, specifically on the elemental steps of initiation, propagation and termination. Clearly, from the CHP decomposition experiments (Figures 2.8, 2.12 and 2.15) using the 3 previously described catalysts, supported AuNP are able to decompose CHP into the corresponding alcohol, in this case cumyl alcohol. The ability of the 3 catalysts to decompose CHP was shown to be high in the case of the AuNP@TiO_2, followed by AuNP@HT. CHP was found to be the most stable when AgNP@HT was used as the catalyst. Previous work has shown that hydrogen peroxide is readily decomposed by way of Fenton-like chemistry through interaction with both AuNP[32] and AgNP,[33] most likely through adsorption of the resulting hydroperoxide onto the nanoparticle surface. Therefore, it is reasonable to suggest that the participation of Fenton chemistry is likely responsible for the initiation of the free-radical chain reactions in the case of the present reaction, nanoparticle-catalyzed cumene peroxidation, and is illustrated in the proposed mechanism presented in Scheme 2.5. Another possible reaction pathway would be the homolytic decomposition of CHP, but this is unlikely at 80°C, considering the relative stability of the hydroperoxide as illustrated when the decomposition of cumene hydroperoxide is examined in the absence of catalyst. The possibility of leaching of the catalyst and by

extension the possibility of a homogeneous reaction was dismissed by ICP measurements of the reaction mixture after removal of the catalyst, which showed no signs of any Au species.

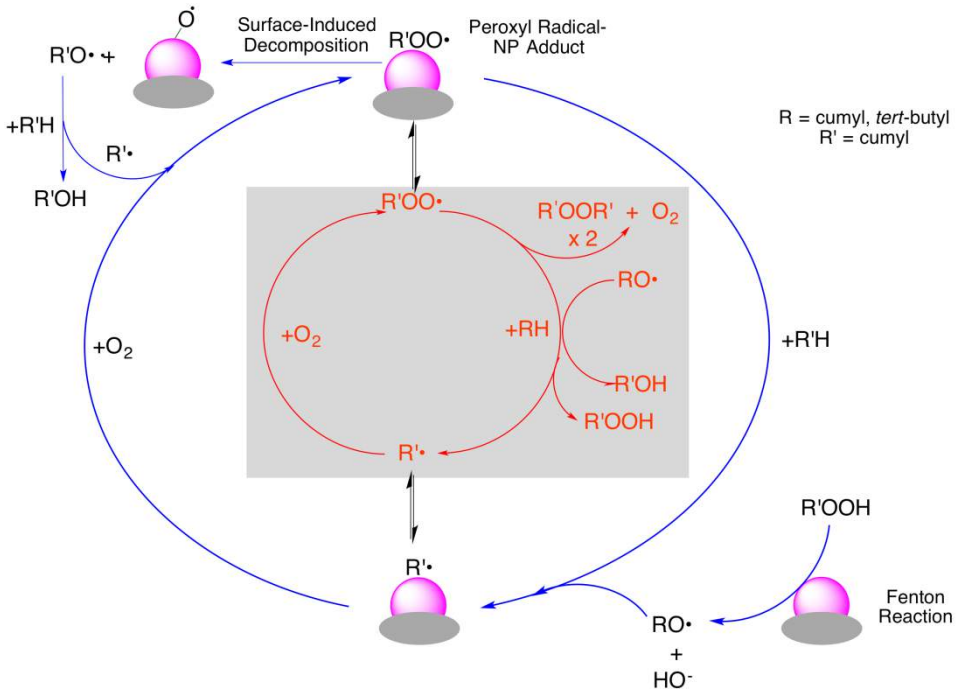

Scheme 2.5. Schematic representation of cumene peroxidation in the presence of metallic nanoparticles. Blue arrows are representative of reactions occurring on the nanoparticle surface, while red arrows indicate pathways within the bulk solution. The red pathway enclosed in a grey box is well established in solution; such homogeneous auto-oxidation is a slow process at the temperatures used in this work, but this may be largely due to inefficient homogeneous initiation. Reprint with permission from ACS Catal., 2013, 3 (9), 2062. Copyright 2013 American Chemical Society

Beginning in the lower right hand corner of Scheme 2.5, either *tert*-butyl hydroperoxide or CHP can be decomposed into the corresponding alkoxyl radical and HO^- *via* Fenton chemistry. However, one important question remains - do the nanoparticles play another role? Given the results obtained throughout this work, one possible explanation lies in the influence of the interaction

between free-radical species and the nanoparticle surface.[34] Following along the pathways presented above, once the alkoxyl radical is formed, it can proceed to abstract a hydrogen from a molecule of solvent and form a carbon-centered radical and the corresponding alcohol. Then, the carbon-centered radical can react with oxygen to form a peroxyl radical. In principle, all of these radical species (carbon-centered radicals and peroxyl radicals) could interact with the nanoparticle surface and/or simply remain in solution. The reaction between the carbon-centered radical and oxygen to form the peroxyl radical has been considered; however, considering that this reaction happens at a rate close to diffusion-controlled,[35] it is unlikely that the nanoparticles can help to improve its efficiency. Two, more likely possibilities can be envisioned for the role of the nanoparticle surface. The first proposed pathway is direct interaction between the peroxyl radical and the nanoparticle surface, represented within the surface process portion of Scheme 2.5. In addition, the fate of the peroxyl radical may also involve abstraction of a hydrogen from the solvent to form a hydroperoxide, presented within the solution process of Scheme 2.5. Considering the rapid rate at which peroxyl radicals interact with AuNP surfaces (3.5×10^8 M^{-1} s^{-1}),[36] the interaction between the peroxyl radical and the nanoparticle surface is more likely than the solution pathway. The resultant intermediate, defined as the peroxyl radical-nanoparticle adduct, would be the preferred route. Once this adduct is formed, it is possible that it will simply go back into solution in order to abstract a hydrogen from a molecule of cumene or undergo a termination

reaction by self-reaction to form DCP. This route accounts for the small yields of DCP observed when using AuNP@TiO_2 as the catalyst. The second possibility involves the peroxyl radical-nanoparticle adduct decomposing on the nanoparticle surface to form a reactive surface oxygen species and a cumyl alkoxyl radical (top-left hand corner; Scheme 2.5). The decomposition of the peroxyl radical-nanoparticle adduct has been proposed in the past.[36] The cumene alkoxyl radical formed *via* the surface decomposition will then abstract a hydrogen from the solvent and continue the radical chain reaction. In addition, oxygen uptake experiments support the formation of cumyl alcohol *via* a pathway other than the Fenton chemistry, as the chain length of 58 is significantly different than the ratio determined from HPLC analysis of 2. One possible explanation for the variation in the values obtained between oxygen uptake and HPLC analysis is the more likely surface decomposition of the peroxyl radical adduct on the nanoparticle surface. To confirm the participation of a free-radical mechanism, an antioxidant (in this case DBHA) was added to the solution to see the effect on product generation (Figures 2.25 and 2.26). As was observed, the reaction was halted in the presence of the antioxidant, confirming a free-radical process. Moreover, lipoic acid was also added to a separate peroxidation reaction in order to confirm participation of the nanoparticle surface in the free-radical mechanism. In such a case, capping of the nanoparticle surface by lipoic acid should limit access to the nanoparticle surface. From these results (Figures 2.28 and 2.29), it is evident that the reaction

did plateau and can be attributed to the inability of the peroxyl radical to be decomposed on the AuNP surface, thus demonstrating nanoparticle surface participation in the peroxidation mechanism.

The results obtained using the AgNP@HT suggest that it is a superior catalyst than AuNP@HT and AuNP@TiO_2 due to tis ability of this catalyst to favor the formation of CHP. Oxygen uptake experiments were not possible using AgNP@HT due to its inactivity at 30°C, therefore addition of both DBHA and lipoic acid to the reaction mixture at 80°C was used to gain information regarding the mechanism in such cases. The results obtained using DBHA (Figure 2.27) were similar to those obtained in the case of AuNP@TiO_2 and suggest the presence and involvement of radical species within the nanoparticle catalyzed peroxidation mechanism. The data obtained from the addition of lipoic acid (Figures 2.30) are closely similar to those obtained using the supported AuNP materials, where the kinetic profiles illustrate a plateau after introduction of the capping agent and demonstrate the involvement of the AgNP surface in the peroxidation of cumene. Considering that CHP is the major product obtained when AgNP are used as a catalyst, one possible hypothesis is the formation of a AgNP-peroxyl radical adduct, but that binding to the surface is a reversible process and, by extension, the decomposition of the adduct is not a favourable process. This behaviour will be discussed further in Chapter 5.

2.5. Conclusion

The peroxidation of cumene using both supported AuNP and AgNP as catalysts was examined and showed that the nature of the metal catalyst had a profound influence on the product obtained. When supported AuNP catalysts were used, the major product was cumyl alcohol. However, the formation of CHP dominated when AgNP were used. Due to the distinct differences between the two families of catalysts, the participation of the nanoparticle surface was proposed. The nanoparticle surface is believed to partake in the catalysis in two ways. First, via Fenton chemistry and, second, through the formation of a peroxyl radical-metal nanoparticle adduct. In the case of supported AuNP, the formation of the peroxyl radical-AuNP adduct is followed by its decomposition into the alkoxyl radical and a reactive surface oxygen species, whereas in the case of supported AgNP the formation of the peroxyl radical-AgNP adduct is thought to be reversible, with minimal decomposition of this intermediate occurring on the nanoparticle surface.

2.6. Experimental

2.6.1. Reagents.

Cumene, cumene hydroperoxide (CHP), (technical grade 80%, largely cumene impurity), cumyl alcohol (98 %; 2-phenyl-2-propanol), acetophenone (98 %), dicumyl peroxide (DCP) (97 %), 2,6-di-*tert*-butyl-4-methoxyphenol (95%, DBHA),

tert-butyl hydroperoxide solution in H_2O (80%) and dodecane (99%), chlorobenzene (99.5%), hydrotalcite (HT), sodium borohydride ($NaBH_4$), tetrachloroauric acid ($HAuCl_4 \bullet H_2O$), silver nitrate, phenol, lipoic acid (99%) and optima grade acetonitrile were purchased from Sigma-Aldrich and used as received. TiO_2 P25 was a gift from Evonik Degussa. AUROlite™ 1% AuNP@TiO_2 was purchased from Strem Chemicals and was ground using a mortar and pestle prior to use. Optima grade heptane, 2-propanol and ammonia (28% in H_2O) were purchased from Fisher Chemicals and used as received. Millipore H_2O was deionized in house (18.2 MΩ at 25°C) and used in the synthesis of supported metal nanoparticles.

2.6.2 Instruments.

The size of the metallic nanoparticles was determined using a JEM-2100F FETEM transmission electron microscope (TEM) from Jeol Ltd. Analysis of the reaction mixture (cumyl alcohol, acetophenone and CHP) was carried out using a normal phase Agilent 1100 HPLC (eluent 99:1 heptane:2-propanol). The amount of dicumyl peroxide was determined using a Waters HPLC fitted with a reverse phase C-18 silica column and employing an eluent mixture of 60:40 acetonitrile:water. Representative reverse and normal phase HPLC spectra are shown in Appendix 1.

2.6.3. Synthesis of supported gold nanoparticles on hydrotalcite (AuNP@HT).

The procedure was adapted from previous work by Mitsudome *et al.*[16] 2 g of hydrotalcite were added to 60 mL of an aqueous solution of 1.8 mM $HAuCl_4 \bullet H_2O$. 0.09 mL of a 10% solution of NH_4OH was added after several minutes and the mixture was allowed to stir overnight. The supported Au^{3+} composite was filtered, washed with water, re-suspended in water and 10 mL of a 200 mM solution of sodium borohydride was added and allowed to react for 2 h. Finally, the purple solid was filtered, washed with water and dried under ambient conditions. The theoretical loading was 1% and the average nanoparticle size was determined to be 5.8 nm by TEM (see Figure 2.2.)

2.6.4 Synthesis of supported silver nanoparticles on hydrotalcite (AgNP@HT).

The procedure was adapted from previous work from Mitsudome and co-workers.[17] 2 g of hydrotalcite were added to 60 mL of an aqueous solution of 2.9 mM silver nitrate. The solution was cooled using an ice bath and purged with nitrogen. After stirring for 4 hours, the Ag^+/hydrotalcite composite was filtered, washed and re-suspended in water. Under a nitrogen atmosphere, 10 mL of a 200 mM solution of sodium borohydride were added to the slurry. The yellow solid was then filtered and washed with water and dried at ambient temperature. The theoretical loading was calculated to be 1% and the average nanoparticle size was determined to be 10 nm by TEM (see Figure 2.3).

2.6.6 Peroxidation of cumene under atmospheric conditions.

In a 50 mL, two-neck round bottom flask, 200 mg of catalyst and 12 μL (0.05 mmol) of an aqueous solution of *tert*-butyl hydroperoxide were added to 20 mL of cumene and the reaction heated to 80°C. An aliquot was taken from the reaction mixture every hour, centrifuged and subsequently analyzed by HPLC. Control reactions were carried out using the support itself and in the absence of heterogeneous materials (*tert*-butyl hydroperoxide initiator only).

2.6.7 Peroxidation of cumene under oxygen saturated conditions.

The experimental protocol is the same as used for the reactions under atmospheric conditions. However, oxygen was continuously bubbled into the solution using a Teflon needle in order to prevent contamination by iron. The oxygen flow was controlled using a flow regulator. The typical experiment error that was obtained using HPLC analysis is around 10% of the reported values.

2.6.8 Decomposition of CHP in *n*-dodecane.

In a 50 mL, two-neck flask, 200 mg of catalyst and 500 μL of an 80% solution of CHP were added to 20 mL of *n*-dodecane and the reaction was heated to 80°C. An aliquot was taken from the reaction mixture every hour, centrifuged and then analyzed by HPLC. Control reactions were also carried out as indicated in the procedure for the peroxidation of cumene under O_2. The typical experiment error that was obtained using HPLC analysis is around 15% of the reported values.

2.6.9. Oxygen uptake experiments.

The oxygen uptake apparatus was a gift from Prof. Ross Barclay of Mount Allison University (Sackville, NB). This system, built in-house, monitors small pressure differences between two samples (sensitivity < 100 nmol O_2). Technical details of the design are presented elsewhere.[37,38] The amount of oxygen consumed was determined by measuring the change in the pressure between the reference and the reaction cell. Oxygen uptake experiments were carried out at 30°C due to technical limitations of the instrument.

The experiments were conducted as follows: 5 mL of cumene were added to the reference and reaction cells and then 12.6 mg of the catalyst of interest were added to the reaction cell. To initiate the reaction, 100 μL of a 176 mM aqueous solution of *tert*-butyl hydroperoxide were added to the reaction cell. The rate of propagation is determined by graphical measurements and corresponds to the first derivative of the amount of oxygen produced with time.

2.6.9.Oxygen uptake experiments: Determining the rate of initiation (R_i)

The same general procedure described in the preceding section was used; however after measuring the rate of propagation, 100 μL of 8.0 mM solution of 2,6-di-*tert*-butyl-4-methoxyphenol antioxidant were added in order to determine the inhibition period due to trapping of radical species. This inhibition period provides information about the rate of initiation, which corresponds to the rate at which free radicals are formed from non-radical precursors. [39]

2.6.10.Recyclability Experiments

In a 50 mL, two-neck round bottom flask, 200 mg of catalyst and 12 μL (0.05 mmol) of an aqueous solution of *tert*-butyl hydroperoxide were added to 20 mL of cumene and the reaction heated to 80°C for a period of 8 hours. After reaction, the slurry was transferred to glass centrifuge tubes and centrifuged at 3000 rpm for 15 minutes. The catalyst was separated from the reaction mixture and washed three times using CH_3CN to remove any adsorbed organics from the composite surface. The typical experiment error that was obtained using HPLC analysis is around 10% of the reported values.

2.6.11. Peroxidation Inhibition using 2,6-di-*tert*-butyl-4-methoxyphenol (DBHA) and AuNP Surface Functionalization using lipoic Acid

In a 50 mL, two-neck round bottom flask, 100 mg of catalyst and 7 μL (0.025 mmol) of an aqueous solution of *tert*-butyl hydroperoxide were added to 10 mL of cumene and the reaction heated to 80°C for a period of 3 hours. An aliquot was taken every 30 minutes, centrifuged and subsequently analyzed by HPLC. Either 100 mg of 2,6-di-*tert*-butyl-4-methoxyphenol or 5 mg of lipoic acid were added after 1 hour to observe the effects on the overall product yields. The typical experiment error that was obtained using HPLC analysis is around 10% of the reported values.

2.7.1. Appendix 1. Representative HPLC traces

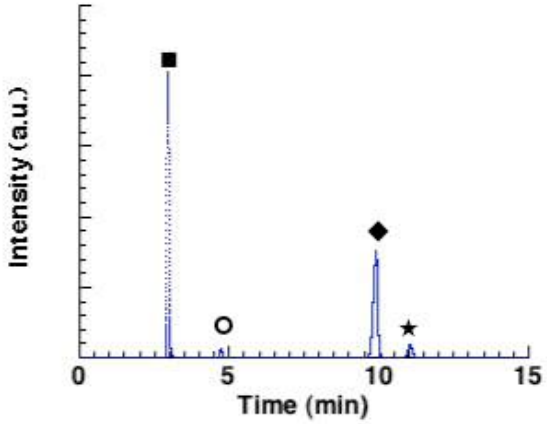

Figure 2.31. Representative normal phase HPLC trace of AgNP@HT-catalyzed cumene peroxidation. Peak identification: cumene and DCP (■), acetophenone (O), CHP, (◆) and cumyl alcohol (★). (99:1 Heptane/Isopropanol isocratic) Reprint with permission from ACS Catal., 2013, 3 (9), 2062. Copyright 2013 American Chemical Society

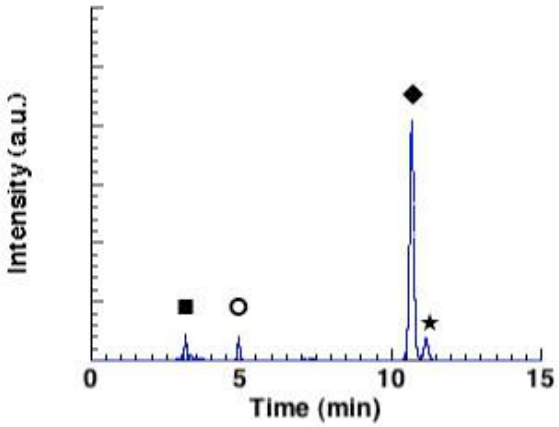

Figure 2.32. Representative normal phase HPLC trace of AgNP@HT-catalyzed CHP decomposition. Peak identification: cumene, DCP (not observed) (■), acetophenone (O), CHP, (◆) and cumyl alcohol (★).(99:1 Heptane/Isopropanol isocratic) Reprint with permission from ACS Catal., 2013, 3 (9), 2062. Copyright 2013 American Chemical Society

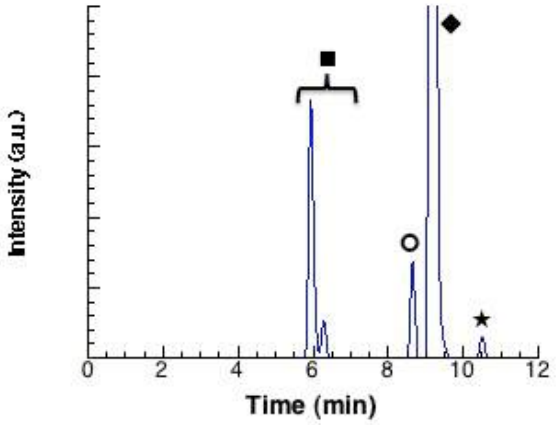

Figure 2.33. Representative reverse phase HPLC trace of the peroxidation of cumene using commercial AuNP@TiO_2. Peak identification: cumyl alcohol and CHP (■), unidentified yellow byproduct (**O**), cumene (◆) and DCP ( ) (acetonitrile/water. 60:40 isocratic) Reprint with permission from ACS Catal., 2013, 3 (9), 2062. Copyright 2013 American Chemical Society

2.7.2 Appendix 2. Description of Oxygen Uptake Apparatus and Experimental Interpretation.

The oxygen uptake is a home-made system and was a gift from Professor Ross Barclay from Mount Allision University. The apparatus monitors the change in pressure between a reference cell and a reaction cell. This is achieved by a gas transducer system where the change in the pressure affects the shape of a metallic membrane, which, in turn, changes the electric properties of this membrane. This variation is recorded as a change in the cell voltage. The

system is calibrated by adding a known amount of air and by using the calibration factor presented below in equation 8 In order to obtain this, one needs to consider the difference in voltage and the quantity of oxygen used to calibrate the system (equation 6). More details can be found in previously published references.[37,38,40]

$$\text{Calibration Factor} = \frac{\text{mol } O_2}{Volts} \tag{8}$$

$$\text{mol } O_2 = \frac{PV}{RT} \tag{9}$$

Once the calibration factor is determined, it is possible to convert the raw data into quantity of oxygen that was produced or consumed by the reaction of interest. Figure 2.36 illustrates how a typical experiment of oxygen uptake looks like when the reaction is consuming oxygen after the voltage was converted to moles of oxygen produced.

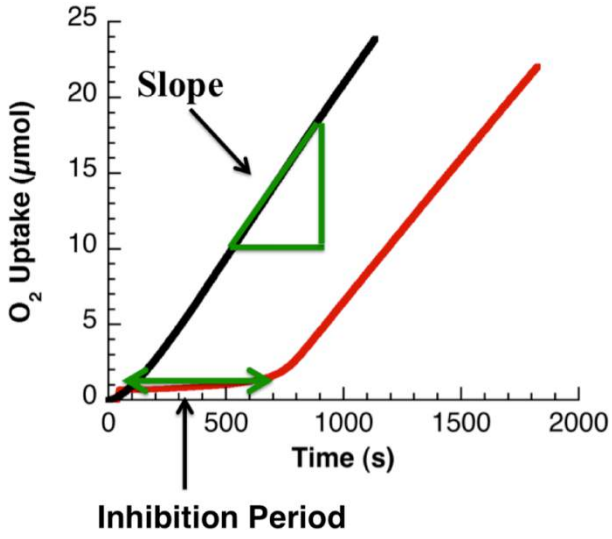

Figure 2.34. Typical oxygen uptake traces obtained for commercial AuNP@TiO_2-catalyzed cumene peroxidation using *tert*-butyl hydroperoxide as the initiator. The black line represents actual experimental data obtained and was used to calculate the amount of O_2 consumed as a function of time and the red line represents actual experimental data using an antioxidant to calculate the rate of initiation.

A general free-radical oxidation reaction can be divided into 4 steps: initiation, chain transfer, propagation and termination (see the introduction for more details). The oxygen uptake can be used to probe the rate of elemental steps which compose the free-radical process. The rate of propagation, which corresponds to the rate at which the oxygen is consumed, is represented by the black trace in Figure 2.34. It is also possible to probe the rate of initiation (equation 3) by adding an antioxidant that will trap free-radicals formed from non-radical precursors. The rate of initiation is calculated using equation 10, where the rate of initiation is related to the concentration of antioxidant used,

the amount of free-radical trapped per molecule of antioxidant (n) and the length of the inhibition period (τ) is represented by the red curve in Figure 2.34.

$$R_i = \frac{n(antioxidant)}{\tau} \quad (10)$$

$$\nu = \frac{R_p}{R_i} \quad (11)$$

The chain length (υ) in equation 11 provides an estimate for the length of the free-radical chain. In other words, how many times the elementary step illustrated in propagation is happening when compared to the initiation step. One calculates the chain length by dividing calculated R_p by the measured value for R_i.

2.8. References

(1) Weissermel, K.; Arpe, K. J. Industrial Organic Chemistry, 4th Edition; Wiley-VCH Darmstadt, Germany, 2003.

(2) Hereijgers, B. P. C.; Weckhuysen, P. M. J. Catal. 2010, 210, 16.

(3) Xu, Y. J.; Landon, P.; Enache, D.; Carley, A. F.; Roberts, M. W.; Hutchings, G. J. Cat. Lett. 2005, 101, 175.

(4) Liu, Y.; Tsunoyama, H.; Akita, T.; Xie, S.; Tsukuda, T. ACS Catal. 2011, 1 2.

(5) Zhou, H. J.; Luo, H.; Zeng, C.; Lia, D.; Liu, Y. Cat. Lett. 2006, 108, 49.

(6) Centi, G.; Perathoner, S.; Trifiro, F. Sustainable Industrial Chemistry; Wiley-VCH: Weinheim, Germany, 2009.

(7) Zu, S.; Hang, C.; Zhang, J.; Chen, B. Korean J. Chem. Eng. 2009, 26, 1568.

(8) Woodward, A.; Mesrobian, R. B. J. Am. Chem. Soc. 1953, 75, 6189.

(9) Kamir, Y.; Beaton, S.; Lafortune, A.; Ingold, K. U. Can. J. Chem. 1963, 41, 2020.

(10) Varma, G. R.; Graydon, W. F. J. Catal. 1973, 28, 236.

(11) Richardson, W. H. J. Am. Chem. Soc. 1965, 87, 1096.

(12) Van Ham, N. H. A.; Nieuwenhuys, B. E.; Sachtler, W. M. H. J. Catal. 1971, 20, 408.

(13) Panayotava, E. N.; Dimitrov, D. I.; Petkov, A. A. J. Catal. 1976, 41, 329.

(14) Casemier, J. H. R.; Nieuwenhuys, B. E.; Sachlter, W. M. H. J. Catal. 1973, 29, 367.

(15) Lloyd, R.; Jenkins, R. L.; Piccinini, M.; He, Q.; Kiely, C. J.; Golunski, S. E.; Bethell, D.; Bartley, J. K.; Hutchings, G. J. J. Catal. 2011, 283, 161.

(16) Mitsudome, T.; Noujima, A.; Mizugaki, T.; Jitsukawa, K.; Kaneda, K. Adv. Synth. Catal. 2009, 351, 1890.

(17) Mitsudome, T.; Mikami, Y.; Funai, H.; Mizugaki, T.; Jitsukawa, K.; Kaneda, K. Angew. Chem. Int. Ed. 2008, 47, 138.

(18) Barrett, K. E.; Thomas, H. R. J. Polym. Sci. Pol. Chem. 1969, 7, 2621.

(19) Francisco, M. A. Chem. Eng. News 1993, 22, 4.

(20) Kharasch, M. S.; Fono, A.; Nudernberg, W. J. Org. Chem. 1950, 763.

(21) Kharasch, M. S.; Fono, A.; Nuderberg, W. J. Org. Chem. 1950, 748.

(22) Salukvadze, L. V.; Norikov, Y. D.; Valendo, A. Y.; Blyumberg, E. A. Russ. Chem. Bull. 1972, 7, 1478.

(23) Solomon, D. H.; Murray, H. M. Clays and Clays Miner. 1972, 20, 135.

(24) Jana, S. K.; Wub, P.; Tatsumi, T. J. Catal. 2006, 240, 268.

(25) Corma, A.; Garcia, H. Chem. Soc. Rev. 2008, 37, 2096.

(26) Naya, S.-i.; Teranishi, M.; Kimurab, K.; Tada, H. Chem. Commun. 2011, 47, 3230.

(27) Totten, G. E., MacKenzie, D.S. Handbook of Aluminum, Vol. 2, Alloy Production and Materials Maufacturing. ; CRC Press: New York, 2003.

(28) Barclay, L. R. C. J. Am. Chem. Soc. 1981, 103, 6478.

(29) Hallett-Tapley, G. L.; D'Alfonso, C.; Pacioni, N. L.; McTiernan, C. D.; González-Béjar, M.; Lanzalunga, O.; Alarcona, E. I.; Scaiano, J. C. Chem. Commun. 2013, 49, 10073.

(30) Asadirad, A. M.; Erno, Z.; Branda, N. R. Chem. Commun. 2013, 49, 5639.

(31) Gan, W.; Xu, B.; Dai, H. L. Angew. Chem. Int. Ed. 2011, 50, 6622.

(32) Navalon, S.; Martin, R.; Alvaro, M.; Garcia, H. Angew. Chem. Int. Ed. 2010, 49, 8403.

(33) Jones, A. M.; Garg, S.; He, D.; Pham, A. N.; Waite, T. D. Environ. Sci. Technol. 2011, 45, 1428.

(34) Aprile, C.; Corma, A.; Domine, M. E.; Garcia, H.; Mitchell, C. J. Catal. 2009, 264, 44.

(35) Maillard, B.; Ingold, K. U.; Scaiano, J. C. J. Am. Chem. Soc. 1983, 105, 5095.

(36) Bar-Ziv, R.; Zilbermann, I.; Zidki, T.; Cohen, H.; Meyerstein, D. J. Phys. Chem. C. 2009, 113, 3281.

(37) Howard, J. A. Advances in Free Radical Chemistry, Volume 4; Logos Press: London, England, 1972.

(38) Fillippenko, V., Oxygen Uptake Studies of Organic and Inorganics Oxidations, MSC thesis, University of Ottawa, 2010

(40) Barclay, L. R. C.; Vinqvist, M. R. Free Radic. Biol. Med. 1994, 16, 779.

(41) Frenette, M., Fluorescent Probe Design and Radically Different Antioxidants, PhD Thesis, University of Ottawa, 2009.

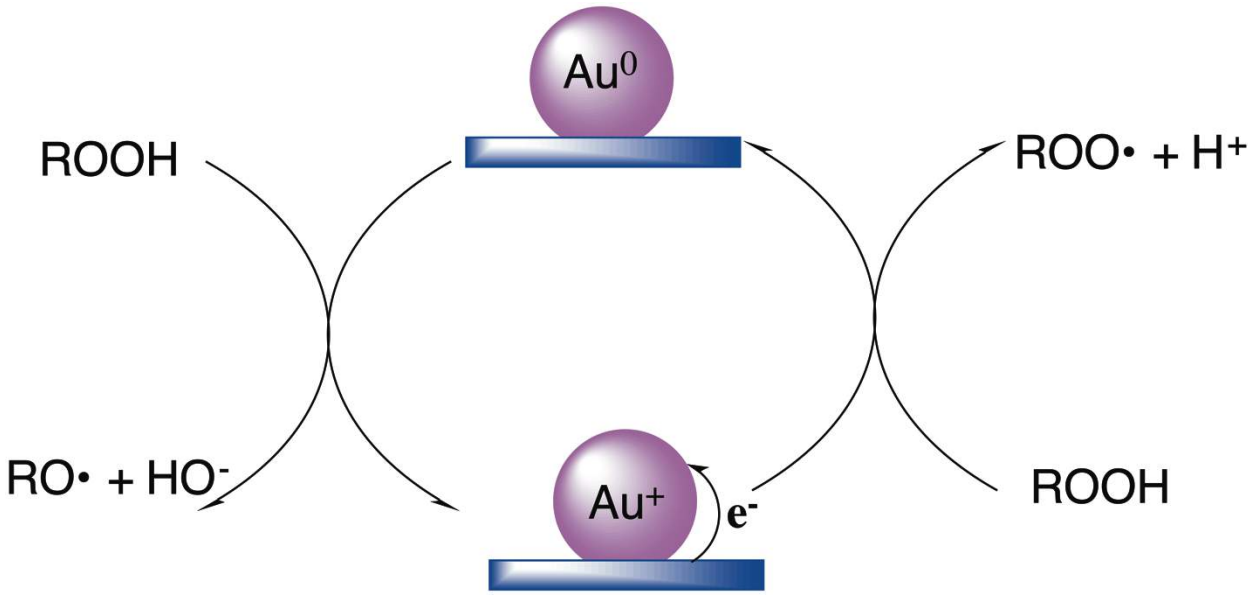

3. Insight into the role of the support in the supported AuNP catalysed-peroxidation of cumene

3.0 Table of Contents

3.1. Introduction

The role of the support in heterogeneous catalysis using supported gold nanoparticles (AuNP) has been underestimated,[1,2] since the support could play a key role in the reaction.[3,4] Recently, specific product selectivity has been reported to be influenced by support interactions.[5] A representative example of this is the carbonylation *versus* the methylation of amines, (see Scheme 3.1) where the methylated product is obtained when using AuNP@TiO_2 and carbonylation is favoured when AuNP@CeO_2 is used.[6]

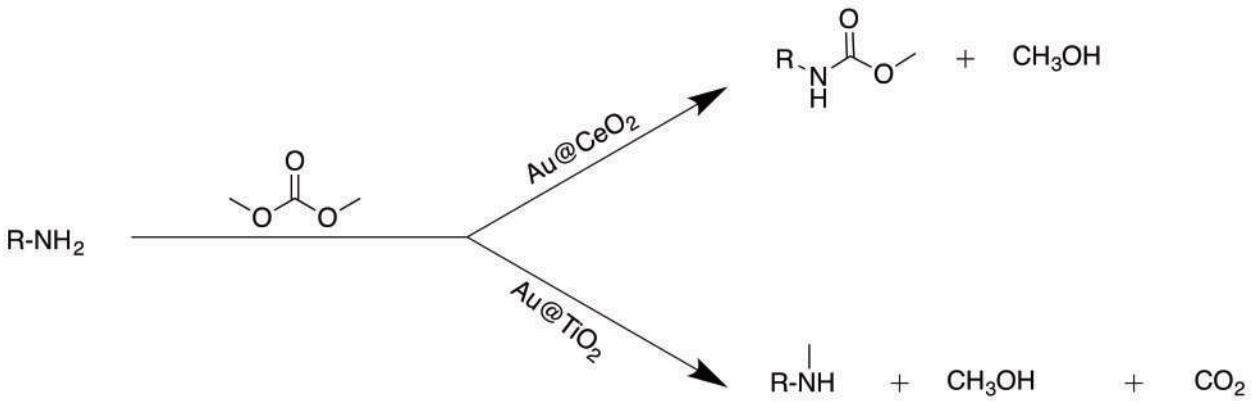

Scheme 3.1. N-carbamoylation using AuNP@CeO_2 of primary amine versus N-methylation using AuNP@TiO_2

The formation of ionic gold at the gold nanoparticle-support interface is believed to be responsible for the catalytic performance of supported AuNP on semi-conductors like TiO_2 and CeO_2.[7] Alcohol oxidation[8] and CO oxidation are two good examples of such activity.[9] As discussed in Chapter 2, the

peroxidation of cumene shows that the difference in activity between AuNP@HT and AuNP@TiO_2 could be due to the difference in the size of the nanomaterial and differences in AuNP-support interactions.

In this chapter, we present new insights into the role of the support in the peroxidation of cumene. As discussed in Chapter 2, a free-radical reaction is composed of initiation, chain transfer, propagation and termination steps. The previous study of the AuNP initiated peroxidation of cumene has shown that the initiation pathway can be largely influenced by the active nature of AuNP in Fenton-like reactions and also through the active decomposition of peroxyl radicals on the nanoparticle surface (forming alkoxyl radicals). These conclusions from Chapter 2 will be taken into account when considering the study of the role of the support in the AuNP catalyzed peroxidation process. The role of the support will be assessed by varying a set of experimental conditions, such as the quantity of catalyst used (in mg), the amount of initiator used and the temperature of the reaction. Three different supported AuNP catalysts were chosen for this study: commercially available cAuNP@TiO_2, "home-made" hAuNP@TiO_2 and "home-made"AuNP@HT.

3.2. Results

3.2.1. TEM of supported AuNP

As mentioned above, 3 different catalysts were used in this study. TEM and size analysis for commercial cAuNP@TiO_2 and AuNP@HT were presented in Chapter 2. To quickly summarize, commercial AuNP@TiO_2 had an average nanoparticle size of 2.3 ± 0.6 nm and AuNP@HT, 5.8 ± 2.7 nm (Section 2.2.1.) The TEM image of the home made hAuNP@TiO_2 nanocomposite is presented in Figure 3.1, where the average nanoparticle size was determined to be 3.5 ± 0.9 nm and was synthesised using a procedure adapted from literature.[10]

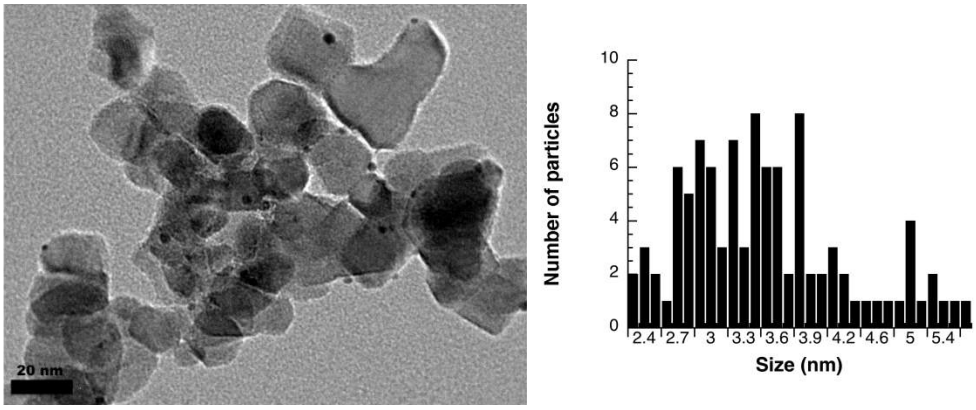

Figure 3.1. TEM (left) and size distribution histogram (right) of home made hAuNP@TiO_2

3.2.1. Varying the temperature

The reaction conditions used in this study are slightly different than those used in Chapter 2. In all cases, air is bubbled through the solution. The following

temperatures were used: room temperature, 40°C, 80°C and 110°C. Control reactions were carried out at all temperatures used in this study. The controls consisted of no catalyst (initiator only) and the two supports used in this study (TiO_2 and HT), as presented in Table 3.1. No product was obtained when the peroxidiation of cumene was carried out at room temperature or at 40°C. Traces of cumene hydroperoxide were obtained when using either HT or no catalyst at a reaction temperature of 80°C.

Table 3.1. % Conversion of cumene into cumene hydroperoxide, cumyl alcohol and acetophenone in control reactions using HT, TiO_2 and in the absence of catalyst after 240 min at various temperatures.

% Conversion	*Temperature (°C)*	*Cumene Hydroperoxide*	*Cumyl Alcohol*	*Acetophenone*
HT	RT	ND	ND	ND
HT	40	ND	ND	ND
HT	80	0.6	ND	ND
HT	110	8.0	ND	ND
TiO_2	RT	ND	ND	ND
TiO_2	40	ND	ND	ND
TiO_2	80	ND	ND	ND
TiO_2	110	1.0	0.1	ND
No Catalyst	RT	ND	ND	ND
No Catalyst	40	ND	ND	ND
No Catalyst	80	0.4	ND	ND
No Catalyst	110	4.0	ND	ND

In all cases, 0.42 mmol of TBHP in H_2O as initiator and 100 mg of the catalyst were used in 10 mL of cumene (ND= not detected)

Interestingly, significant quantities of cumene hydroperoxide were obtained when the reaction was done at 110°C: 8 % for HT, 1.0 % for TiO_2 and 4.0 % in the absence of catalyst. This surprising conversion in the absence of an active

nanoparticle catalyst is explained by the ability of CHP to easily undergo homolytic cleavage of the O-O bond at the given reaction temperature to initiate a free radical chain reaction.[11]

The amounts of cumene peroxidation products obtained after 30 minutes and 4 hours when using AuNP@HT and cAuNP@TiO_2 are shown in Table 3.2. Several general observations can be made regarding the values presented. First, cumyl alcohol is clearly the favoured product formed in the presence of both supported AuNP catalysts. Second, cAuNP@TiO_2 is a more active catalyst than AuNP@HT because of to the large difference in cumyl alcohol formation as compared at room temperature (0.8% *versus* 17.1% for AuNP@HT and cAuNP@TiO_2, respectively). Third, the results obtained using cAuNP@TiO_2 at 110°C do not follow the same trend as the others, being that the yield of cumyl alcohol increases at higher temperature. The amount of cumyl alcohol observed after 240 min is actually less at 110°C (6.5%) than at 80°C (25.6%).

Table 3.2. % Conversion of cumene into cumene hydroperoxide, 2-phenyl-2-propanol and acetophenone after 240 min at various reaction temperatures.

Catalyst	*Temperature (°C)*	*Cumene Hydroperoxide*		*Cumyl Alcohol*		*Acetophenone*	
		30 min	240 min	30 min	240 min	30 min	240 min
AuNP@HT	RT	0.5	1.4	0.2	0.8	ND	ND
AuNP@HT	40	1.0	3.5	0.8	4.0	ND	0.4
AuNP@HT	80	1.5	12.3	2.9	23.4	0.1	1.9
AuNP@HT	110	1.5	8.4	4.3	25.2	0.1	2.3
cAuNP@TiO_2	RT	0.3	1.6	4.1	17.1	0.1	0.5
cAuNP@TiO_2	40	0.8	2.6	10.2	19.2	0.4	1.0
cAuNP@TiO_2	80	2.0	8.1	10.5	25.6	1.0	2.8
cAuNP@TiO_2	110	0.3	0.8	6.1	6.5	0.5	4.3

In all cases, 0.42 mmol of TBHP in H_2O as initiator and 100 mg of the catalyst were used in 20 mL of cumene (ND= not detected)

For every reaction presented in Table 3.2, an associated kinetic plot is presented in Appendix 1 (Figures 3.7 to 3.14). The ability of each catalyst to decompose CHP into the corresponding alcohol is directly related to the observed amount of cumyl alcohol formed throughout the reaction. Figure 3.3. shows that the amount of cumyl alcohol obtained when using AuNP@HT increases in a mostly linear fashion over 30 minutes as the reaction temperature is gradually increased from room temperature to 110°C. However, when the time is extended to 240 min, the amount of cumyl alcohol obtained seems to plateau as the reaction temperature is increased from 80 to 110°C.

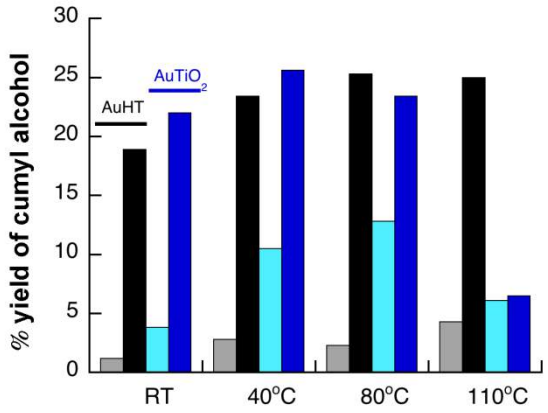

Figure 3.2. % Yield of cumyl alcohol as a function of temperature using AuNP@HT: after 30 minutes in grey; after 240 minutes in black. cAuNP@TiO_2: after 30 min, in light blue; after 240 minutes, in dark blue.

However, the trend observed when AuNP@TiO_2 is used as the reaction catalyst presents some interesting behaviour and does not appear to be linear, as was observed in the case of AuNP@HT. Specifically, the amount of cumyl alcohol obtained after 30 and 240 minutes shows a decrease as the reaction temperature is increased to 110°C (see Figure 3.2). Moreover, the reaction time seems to have very little effect on the overall conversion to cumyl alcohol, with both 30 and 240 minutes of reaction time yielding the same amount of the alcohol product, as is depicted in Figure 3.2. Further investigation into the stability of CHP at 110°C indicates that the considerable decrease in the amount of cumyl alcohol obtained when using cAuNP@TiO_2 as the catalyst can be attributed to the inability to keep the free-radical chain reaction going at this temperature due to the decomposition of the CHP by the catalyst into

cumyl alcohol and acetophenone. This behaviour will be discussed further in the upcoming sections (Section 3.4, *vide infra*). The corresponding kinetic traces for each reaction temperature over 30 and 240 minutes for each AuNP@HT and cAuNP@TiO_2 (Figures 3.7 to 3.14) are presented in Appendix 1.

The difference in the yield of cumyl alcohol obtained after 30 minutes as compared to that observed after 240 minutes can be interpreted using the kinetic traces presented in Appendix 1. A representation of these plots is shown in Figure 3.3 and shows the formation of cumyl alcohol as a function of reaction time using 100 mg of supported AuNP catalyst. The large increase in cumyl alcohol formation in the first 30 minutes of the reaction when using cAuNP@TiO_2 can be observed. However, this rapid alcohol formation is absent from the curves obtained using AuNP@HT, as was also illustrated above, with this kinetic curve showing a more gradual and linear formation of cumyl alcohol over time.

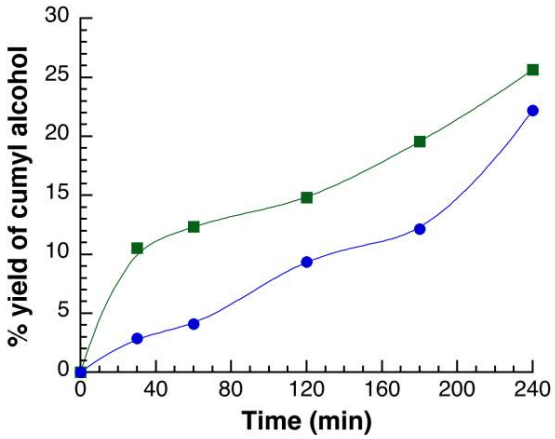

Figure 3.3. Percent yield of cumyl alcohol versus time using AuNP@HT (●) and AuNP@TiO_2 (■), at 80 °C. (Reaction conditions: 100 mg of catalyst and 0.42 mmol of *tert*-butyl hydroperoxide and 10 mL of cumene).

3.2.2. Varying the quantity of initiator

The quantity of *tert*-butyl hydroperoxide initiator was varied from 4.2 mM to 84 mM to allow for the investigation of the influence on the product yield versus the concentration of initiator. A table summarizing the product distribution of acetophenone, cumyl alcohol and CHP obtained using these initiator concentrations over 240 minutes, at 80°C, and in the presence of both AuNP@HT and cAuNP@TiO_2 is presented in Appendix 1 (figure 3.15-3.18).

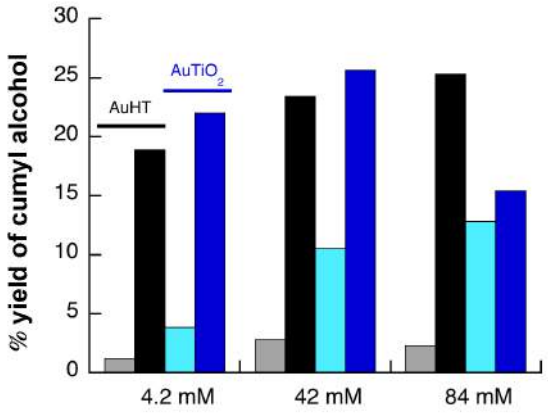

Figure 3.4. % Yield of cumyl alcohol as a function of the quantity of TBHP using: AuNP@HT: after 30 minutes in grey; after 240 minutes in black. cAuNP@TiO_2: after 30 min in light blue; after 240 minutes in dark blue.

Figure 3.4 illustrates the difference in yield obtained using different amounts of initiator. From these data, we can see that the amount of cumyl alcohol generated when using cAuNP@TiO_2 as the catalyst increases in a linear fashion over 30 minutes, but when the reaction time is increased to 240 min the yield of alcohol product decreases significantly in the presence of higher concentrations of initiator (84 mM). On the other hand, the results obtained using AuNP@HT show a linear increase on the product formation after 240 minutes.

3.2.3. Varying the quantity of catalyst

The quantity of catalyst was also varied: using 25 mg, 100 mg and 200 mg. The corresponding kinetic traces obtained at 80°C (Figures 3.19-3.22) and Table 3.5

summarizing the product distribution can be found in Appendix 1. Figure 3.5 shows the yield of cumyl alcohol obtained after 30 minutes and 240 minutes using varying amounts of the supported AuNP catalysts. The product obtained after 30 minutes using both AuNP@HT and cAuNP@TiO_2 catalysts shows a linear increase in the conversion of CHP to cumyl alcohol as the amount of catalyst is systematically increased from 25 to 200 mg. However, after 240 minutes, both catalysts show a decrease in alcohol production when the upper limit of 200 mg of catalyst is used.

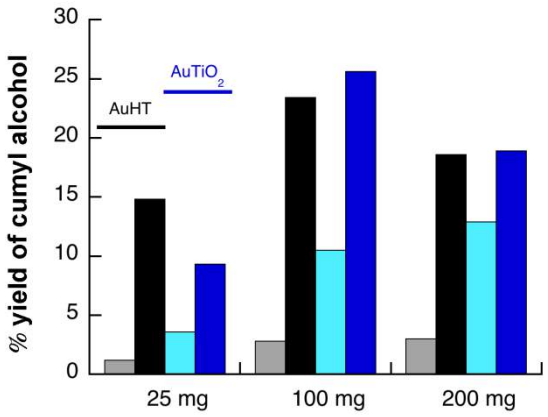

Figure 3.5. % Yield of cumyl alcohol as a function of the quantity of catalyst using: a) AuNP@HT: after 30 minutes in grey; after 240 minutes in black. b) cAuNP@TiO_2: after 30 min in light blue; after 240 minutes in dark blue.

Surprisingly, a large variation in the amount of cumyl alcohol obtained after 30 minutes was observed when the catalyst was varied from AuNP@HT to cAuNP@TiO_2. In particular, a higher yield of cumyl alcohol is clearly obtained within the first 30 minutes when using cAuNP@TiO_2. Figure 3.5 shows the time

profile of the reaction using 200 mg of catalyst and 42 mM of TBHP at 80°C which is clearly non-linear, as the majority of cumyl alcohol is obtained in the first 30 minutes. Furthermore, the reaction slows down after 180 minutes performed using cAuNP@TiO_2 (green trace). The reaction was also done using AuNP@HT (see the blue trace in figure 3.6) and in this case it shows a linear profile.

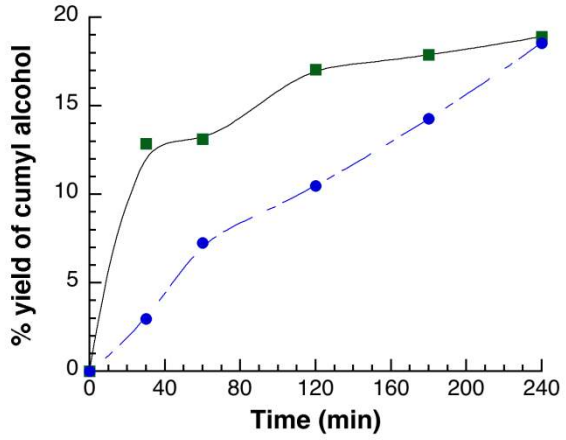

Figure 3.6. % Yield of cumyl alcohol in the peroxidation of cumene using 200 mg of catalyst and 42 mM of the initiator *tert*-butyl hydroperoxide, at 80°C, using AuNP@HT (●) and cAuNP@TiO_2 (■).

3.2.4. Using hAuNP@TiO_2 as a catalyst

When considering catalysis using supported gold nanoparticles, it is clear that the size of the gold nanoparticles plays an important role in the ability of these materials to catalyze reactions.[12] Therefore, in order to have a catalyst that was more directly comparable with the homemade AuNP@HT, a hAuNP@TiO_2 analogous to cAuNP@TiO_2 was synthesized (average NP size = 3.5 nm). The

peroxidation of cumene was attempted using the following experimental conditions: 100 mg of catalyst, 42 mM of TBHP at 80°C over 30 minutes. The resulting yields of cumyl alcohol after 30 minutes using 10 mL of cumene were comparable (see Table 3.3) to those obtained when using the cAu@TiO_2, even though the average nanoparticle size of the commercial catalyst was found to be smaller (~ 2.3 nm). These results suggest that the size of the nanoparticle is not the only factor that dictates the difference in activities of AuNP@HT *versus* AuNP@TiO_2 and that the nature of the support must also be considered.

Table 3.3. % Yield of cumyl alcohol using cAuNP@TiO_2 and hAuNP@TiO_2 after 30 minutes for the commercial versus Home made

Catalyst	*%Yield cumyl alcohol*
cAuNP@TiO_2 (commercial)	10.2
hAuNP@HT (Home made)	10.0

3.4. Discussion

When comparing the catalytic efficiency of the cAuNP@TiO_2 *versus* AuNP@HT, the former was found to be a superior catalyst with respect to cumyl alcohol formation. From the kinetic data presented in Appendix 1, a general observation would be that a more linear formation of cumyl alcohol takes place when using AuNP@HT. On the other hand, in the presence of cAuNP@TiO_2,

cumyl alcohol generation occurs more rapidly within the first 30 minutes of reaction. The faster formation of cumyl alcohol over the first 30 mintues in the presence of cAuNP@TiO_2 seems to occur, regardless of any increase in the temperature, the amount of initiator or the amount of catalyst used. Furthermore, in the presence of cAuNP@TiO_2, the amount of cumyl alcohol was found to decrease as the reaction temperature was increased to 110°C. Previous work has shown that peroxidation of organic solvents using metal ions shows an upper yield that begins to decrease once one exceeds the optimal reaction temperature.[13] The result obtained at 110°C using cAuNP@TiO_2 may be explained by the fact that, at this reaction temperature, the optimal temperature value for this system may have been exceeded which relates to the rate of initiation and termination. In other words, the rate of initiation (the rate at which the *tert*-butyl hydroperoxide is decomposed) and termination could be so fast that the reaction is not able to keep going.

As shown in table 3.3 the nanoparticle size cannot itself explain the different catalyst activity between cAuNP@TiO_2 and AuNP@HT. The reasoning behind the activity of the TiO_2 support in cumene peroxidation and, in particular, its impressive ability to produce cumyl alcohol remains largely unanswered. One major difference between the two supports employed in this work is the fact that TiO_2 is a semi-conductor, while HT is largely considered an insulator. From our previous work, Fenton chemistry was demonstrated to be partly responsible

for the decomposition of CHP into cumyl alcohol.[14] The Fenton induced formation of cumyl alcohol should dominate in the early stages of the reaction and, thus, the nature of the support should, in principle, influence this process. The fact that TiO_2 and HT, themselves, do not show any activity towards cumyl alcohol formation suggests that the difference in activities of AuNP@HT versus cAuNP@TiO_2 has to do with interaction between the support and the AuNP surface. Thus, any contribution from the support in the formation of cumyl alcohol needs to come from the synergistic interactions between supports and nanoparticles, with the role of TiO_2 most likely enhancing the Fenton activity of the AuNP. By increasing the ability of AuNP to shuttle electrons to the TiO_2 and *vice versa*. A study on the decomposition of H_2O_2 using a series of AuNP on semiconductor supports, such as WO_3, In_2O_3, TiO_2, ZnO and $SrTiO_2$ can be found in the literature and shows the difference in the Fenton activities of these different metal oxide supported AuNP.[15] The difference in the Fenton activity of these AuNP nanocomposites was attributed to the difference in the Fermi level of both the support and the AuNP and it was concluded that a more active Fenton catalyst can be obtained by maximising the mixing of the initial Fermi level of the support and the AuNP. An increase in the compatibility of the Fermi levels directly translates into a catalyst that is able to shuttle electrons from the support to the nanoparticle surface in a more efficient manner.[15]

There are two types of reaction involved in Fenton chemistry.[16,17] First, a reductive pathway, in which is an electron transfers from the AuNP@support to a molecule of hydroperoxide (left side of Scheme 3.2). Second, an oxidative pathway, in which is an electron transfers from the cumene hydroperoxide to the AuNP@support (right side of Scheme 3.2). Navalon *et al.*[18] have suggested that a similar reaction was involved in the decomposition of H_2O_2 in the presence of AuNP.

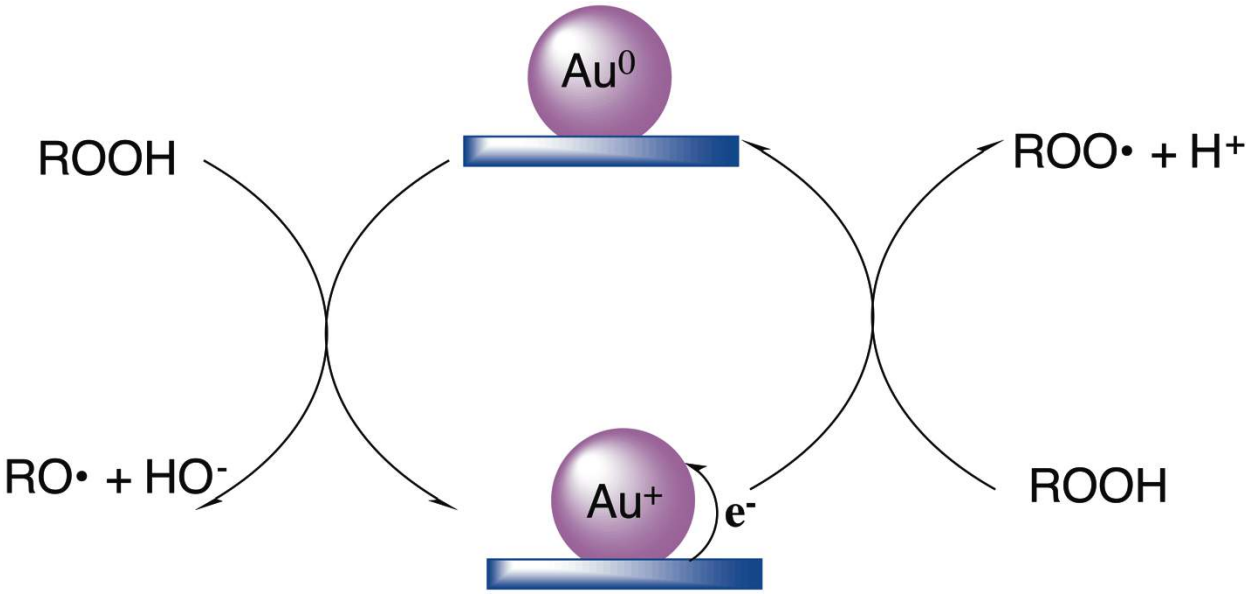

Scheme 3.2. Representation of the Haber-Weiss cycle for the AuNP catalyzed decompostion of cumene hydroperoxide

The reductive and oxidative pathways can be made more efficient by increasing the amount of electrons participating in these two pathways, achievable by participation of the support in the composite system. Such a scenario is possible with TiO_2, whereby the semiconductor support allows for the

participation of more electrons due to the Fermi level equilibration as described by Naya *et al*[15]. Given the insulator properties of HT, such an enhancement of Fenton chemisty is not possible.

3.5. Conclusion

The role of the support in the peroxidation of cumene using AuNP@HT or AuNP@TiO_2 was determined by varying the amount of initiator, the amount of catalyst and the reaction temperature. The catalytic activity of cAuNP@TiO_2 and hAuNP@TiO_2 was shown to be higher than that of AuNP@HT, especially when considering the larger conversions of CHP to cumyl alcohol over the first 30 minutes of reaction. These considerable differences in catalyst activity were attributed to the nature of the support and specifically the semiconductor, characteristics of TiO_2. In the case of the TiO_2, since it is a semiconductor allows for participation in the peroxidation mechanism *via* Fenton chemistry by permitting the shuttling of electrons within the nanocomposite.

3.6. Experimental

3.6.1. Instruments.

The size of the metallic nanoparticles was determined using a JEM-2100F FETEM transmission electron microscope from Jeol Ltd. Analysis of the reaction mixture (cumyl alcohol, acetophenone and cumene hydroperoxide) was carried out using normal phase Agilent 1100 HPLC (eluent 99:1 *n*-heptane:*iso*-propanol).

3.6.2. Synthesis of supported AuNP on hydrotalcite.

The experimental procedure for the synthesis of AuNP@HT is presented in Chapter 2 section 2.6.4.

3.6.3. Synthesis of supported AuNP on TiO_2.

The procedure was adapted from previous work from Mitsudome *et al*.[10] The same procedure was employed in the synthesis of AuNP@HT (Chapter 2, Section 2.6.4).[10] The theoretical loading was 1% and the average nanoparticle size was determined to be 3.5 nm by TEM (Figure 3.1)

3.6.4. Peroxidation of cumene under air saturated conditions.

In a 50 mL, two-neck round bottom flask, 100 mg of catalyst and 100 μL (42 mM) of a solution of *tert*-butyl hydroperoxide in water were added to 10 mL of cumene and the reaction heated to the desired temperature. An aliquot was taken from the reaction mixture at pre-determined times and the reaction was analyzed by HPLC. Air was continuously bubbled into the solution using a Teflon needle in order to prevent contamination by iron. The air flow was controlled by a flow regulator. The same general protocol was used when the quantity of catalyst or the amount of initiator was varied. Control reactions, such those performed with the support only and in the absence of the catalyst, were carried out in the same manner. The typical experiment error that was obtained using HPLC analysis is around 10% of the reported values.

3.7. Appendix 1

3.7.1. Varying the temperature

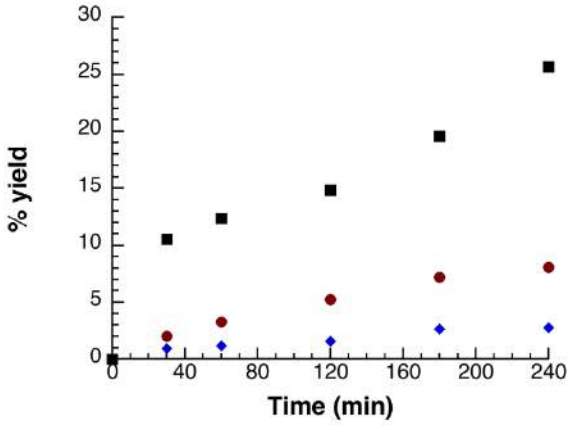

Figure 3.7. **%** Yield of cumyl alcohol (■), CHP (●) and acetophenone (◆) for the peroxidation of cumene using cAuNP@TiO_2 at 80°C, using 100 mg of catalyst and 42 mM of *tert*-butyl hydroperoxide as initiator**.**

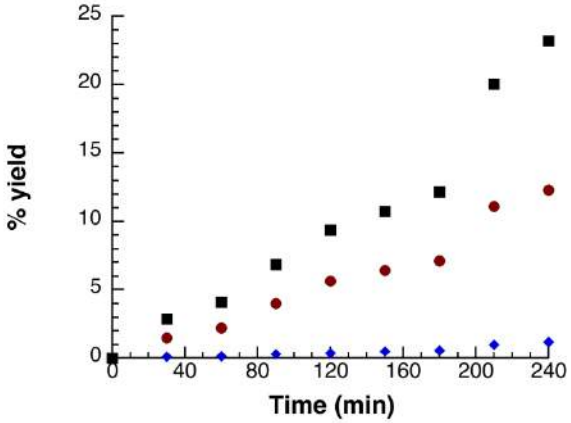

Figure 3.8. **%** Yield of cumyl alcohol (■), CHP (●) and acetophenone (◆) for the peroxidation of cumene using AuNP@HT at 80°C, using 100 mg of catalyst and 42 mM of *tert*-butyl hydroperoxide as initiator.

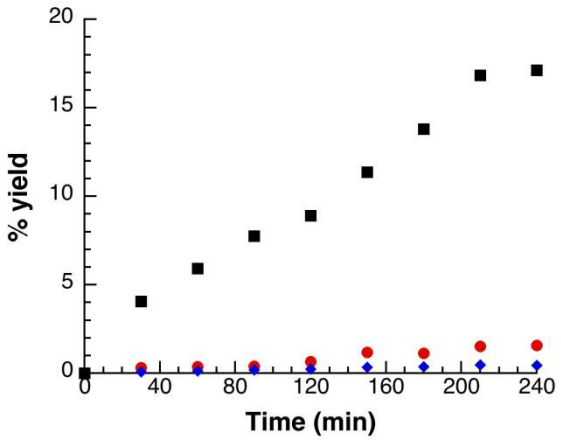

Figure 3.9. **%** Yield of cumyl alcohol (■), CHP (●) and acetophenone (◆) for the peroxidation of cumene using cAuNP@TiO_2 at room temperature, using 100 mg of catalyst and 42 mM of *tert*-butyl hydroperoxide as initiator.

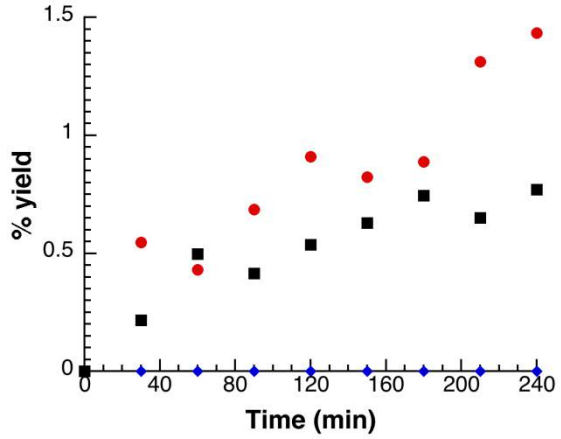

Figure 3.10. % Yield of cumyl alcohol (■), CHP (●) and acetophenone (◆) for the peroxidation of cumene using AuNP@HT at room temperature, using 100 mg of catalyst and 42 mM of *tert*-butyl hydroperoxide as initiator.

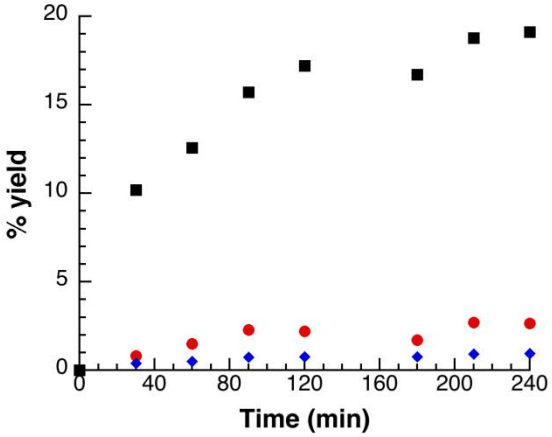

Figure 3.11. % Yield of cumyl alcohol (■), CHP (●) and acetophenone (◆) for the peroxidation of cumene using cAuNP@TiO_2 at 40°C, using 100 mg of catalyst and 42 mM of *tert* -butyl hydroperoxide as initiator.

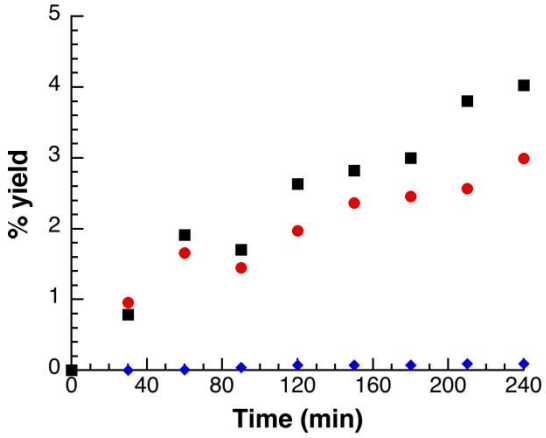

Figure 3.12. % Yield of cumyl alcohol (■), CHP (●) and acetophenone (◆) for the peroxidation of cumene using AuNP@HT at 40°C, using 100 mg of catalyst and 42 mM of *tert* -butyl hydroperoxide as initiator.

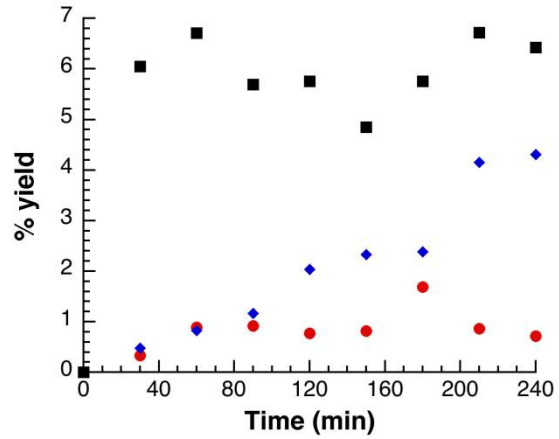

Figure 3.13. **%** Yield of cumyl alcohol (■), CHP (●) and acetophenone (◆) for the peroxidation of cumene using cAuNP@TiO_2 at 110°C, using 100 mg of catalyst and 42 mM of *tert*-butyl hydroperoxide as initiator.

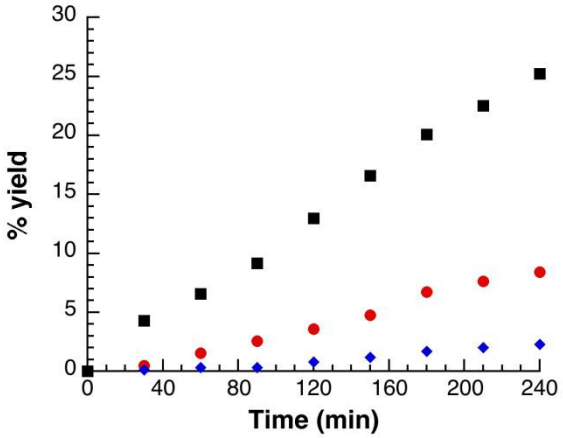

Figure 3.14. **%** Yield of cumyl alcohol (■), CHP (●) and acetophenone (◆) for the peroxidation of cumene using AuNP@HT at 110°C, using 100 mg of catalyst and 42 mM of *tert*-butyl hydroperoxide as initiator.

3.7.2. Varying the quantity of Initiator

Table 3.4. % Conversion of cumene into cumene hydroperoxide, cumyl alcohol and acetophenone using AuNP@HT and AuNP@TiO_2 as catalysts over 240 min using various concentrations of *tert*-butyl hydroperoxide.

% Conversion	*Quantity of initiator (mmol)*	*Cumene hydroperoxide*	*Cumyl Alcohol*	*Acetophenone*
cAuNP@TiO_2	4.2	8	22	4
cAuNP@TiO_2	24	8.1	25.6	2.8
cAuNP@TiO_2	84	5.2	15.4	2.4
AuNP@HT	4.2	9.2	18.9	1.6
AuNP@HT	42	12.3	23.4	1.9
AuNP@HT	84	9.4	25.3	2.3

In all cases, 100 mg of catalyst was used at a reaction temperature of 80°C using 10 mL of cumene

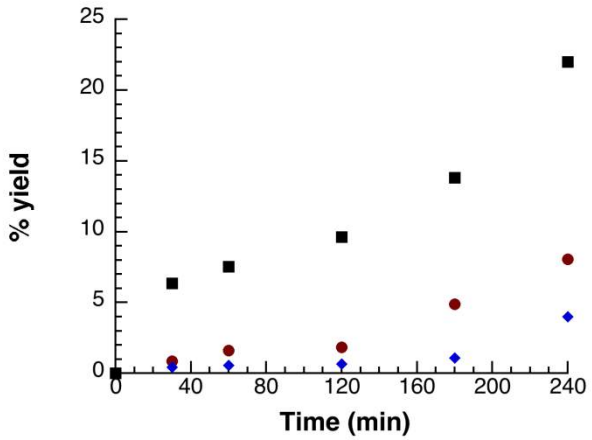

Figure 3.15. % Yield of cumyl alcohol (■), CHP (●) and acetophenone (◆) for the peroxidation of cumene using cAuNP@TiO_2 at 80°C, using 100 mg of catalyst and 4.2 mM of *tert*-butyl hydroperoxide as initiator.

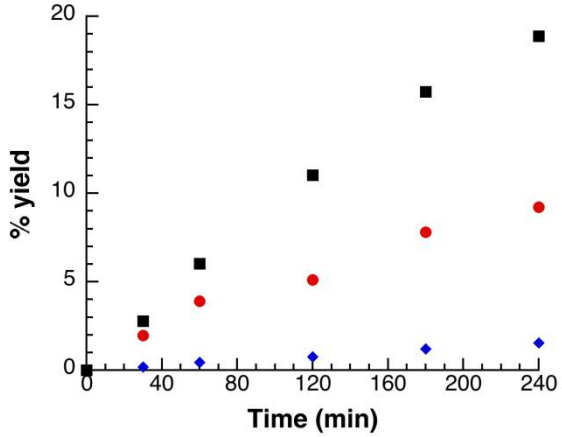

Figure 3.16. **%** Yield of cumyl alcohol (■), CHP (●) and acetophenone (◆) for the peroxidation of cumene using AuNP@HT at 80°C, using 100 mg of catalyst and 4.2 mM of *tert*-butyl hydroperoxide as initiator.

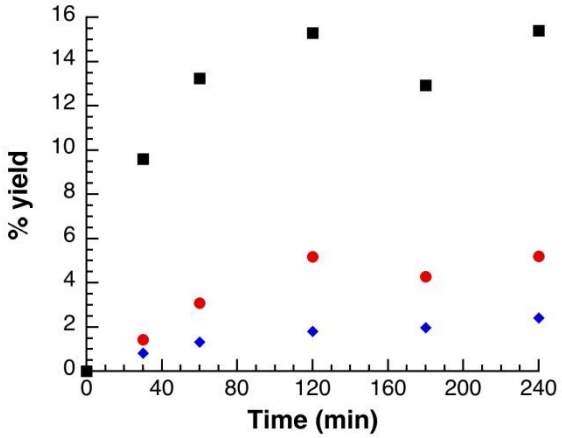

Figure 3.17. % Yield of cumyl alcohol (■), CHP (●) and acetophenone (◆) for the peroxidation of cumene using cAuNP@TiO_2 at 80°C, using 100 mg of catalyst and 84 mM of *tert*-butyl hydroperoxide as initiator.

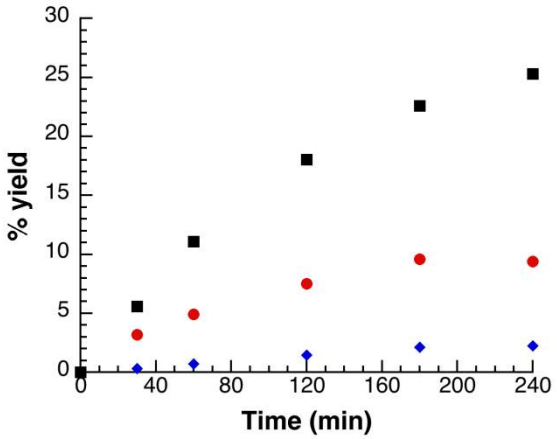

Figure 3.18. % Yield of cumyl alcohol (■), CHP (●) and acetophenone (◆) for the peroxidation of cumene using AuNP@HT at 80°C, using 100 mg of catalyst and 84 mM of *tert*-butyl hydroperoxide as initiator.

3.7.3. Varying the quantity of catalyst

Table 3.5: % yield of the peroxidation of cumene using AuNP@HT and AuNP@TiO_2 after 4 hours, when the quantity of initiator is varied

% Conversion	*Quantity of initiator (mg)*	*Cumene hydroperoxide*	*Cumyl alcohol*	*Acetophe-none*
cAuNP@TiO_2	25	7.2	9.3	0.8
cAuNP@TiO_2	100	8.1	25.6	2.8
cAuNP@TiO_2	200	3.3	18.9	4.0
AuNP@HT	25	10.2	14.8	1.0
AuNP@HT	100	12.3	23.4	1.9
AuNP@HT	200	8	18.6	1.4

In all cases, 42 mM of TBHP in H_2O was used as initiator at a reaction temperature of 80^{o}C using 10 mL of cumene

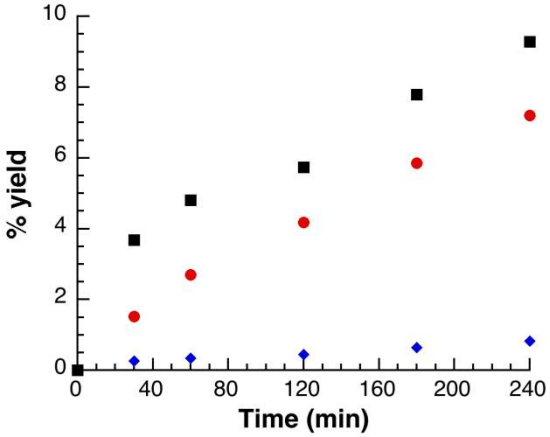

Figure 3.19. % Yield of cumyl alcohol (■), CHP (●) and acetophenone (◆) for the peroxidation of cumene using cAuNP@TiO_2 at 80°C, using 25 mg of catalyst and 42 mM of *tert*-butyl hydroperoxide as initiator.

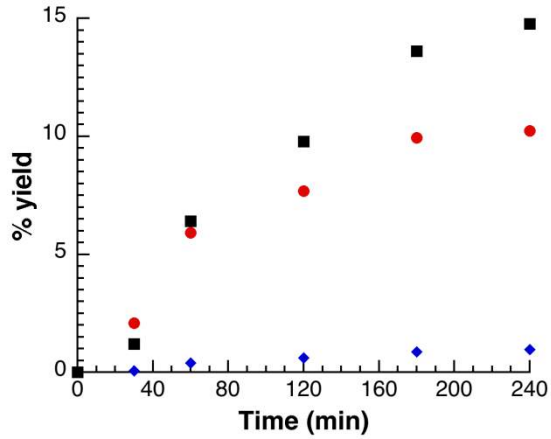

Figure 3.20. % Yield of cumyl alcohol (■), CHP (●) and acetophenone (◆) for the peroxidation of cumene using AuNP@HT at 80°C, using 25 mg of catalyst and 42 mM of *tert*-butyl hydroperoxide as initiator.

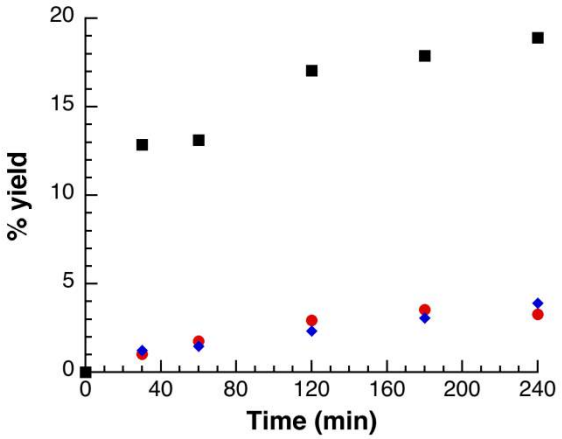

Figure 3.21. % Yield of cumyl alcohol (■), CHP (●) and acetophenone (◆) for the peroxidation of cumene using cAuNP@TiO_2 at 80°C, using 200 mg of catalyst and 42 mM of *tert*-butyl hydroperoxide as initiator.

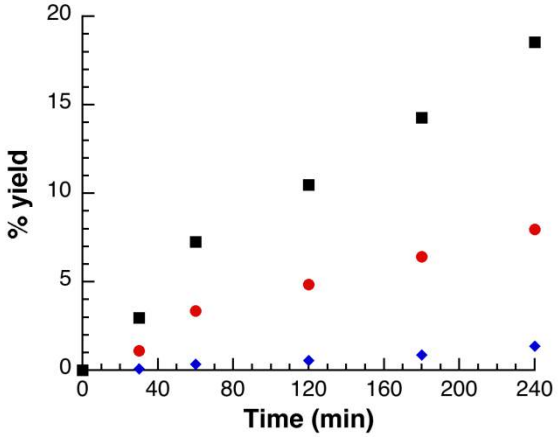

Figure 3.22. % Yield of cumyl alcohol (■), CHP (●) and acetophenone (◆) in the peroxidation of cumene using AuNP@HT at 80°C, using 200 mg of catalyst and 42 mM of *tert*-butyl hydroperoxide as initiator.

3.8. References

(1) Molina, L. M.; B., H. Phys. Rev. Lett. 2003, 90, 206102.

(2) Haruta, M. J. New Mat. Electrochem. Syst. 2004, 7, 163.

(3) Aprile, C.; Corna, A.; Domine, M. E.; Garcia, H.; Mitchell, C. J. Catal. 2009, 264, 44.

(4) Lloyd, R.; Jenkins, R. L.; Piccinini, M.; He, Q.; Kiely, C. J.; Golunski, S. E.; Bethell, D.; Bartley, J. K.; Hutchings, G. J. J. Catal. 2011, 283, 161.

(5) Aba, A.; Corma, A.; García, H. Chem. Eur. J. 2008, 14, 212.

(6) Juarez, R.; Corma, A.; Garcia, H. Pure and Appl. Chem. 2012, 84, 685.

(7) Casaletto, M. P.; Longo, A.; A., M.; Prestianni, A.; Venezia, M. A. Surf. Interface Anal. 2006, 38, 215.

(8) Aba, A.; Concepcion, P.; Corma, A. C.; Garcia, H. Angew. Chem. Int. Ed. 2005, 44, 4066.

(9) Denga, W.; Carpenter, C.; Yia, N.; Flytzani-Stephanopoulos, M. Top. Catal. 2007, 44, 199.

(10) Mitsudome, T.; Noujima, A.; Mizugaki, T.; Jitsukawa, K.; Kaneda, K. Adv. Synth. Catal.

2009, 351, 1890.

(11) Hiatt, R.; Mill, T.; Irwin, K. C.; Castleman, J. K. J. Org. Chem. 1968, 33, 1421.

(12) Tomokazu, K.; Qiliang, J.; Hisayoshi, K.; Hiroaki, T. ChemPhysChem 2009, 10, 2935.

(13) Denisoe, E. T.; Afanas'ev, I. B. Oxidation and Antioxidant in Organic Chemistry and Biology 2005.

(14) Crites, C.-O. L.; Hallett-Tapley, G. L.; Frenette, M.; González-Béjar, M.; Netto-Ferreira, J. C.; Scaiano, J. C. ACS Catal. 2013.

(15) Naya, S.-i.; Teranishi, M.; Kimurab, K.; Tada, H. Chem. Commun. 2011, 47, 3230.

(16) Koppenol, W. H. Redox Rep. 2001, 6, 229.

(17) Haber, F.; Weiss, J. Naturwissenschaften 1932, 20, 948.

(18) Navalon, S.; Martin, R.; Alvaro, M.; Garcia, H. Angew. Chem. Int. Ed. 2010, 49, 8403.

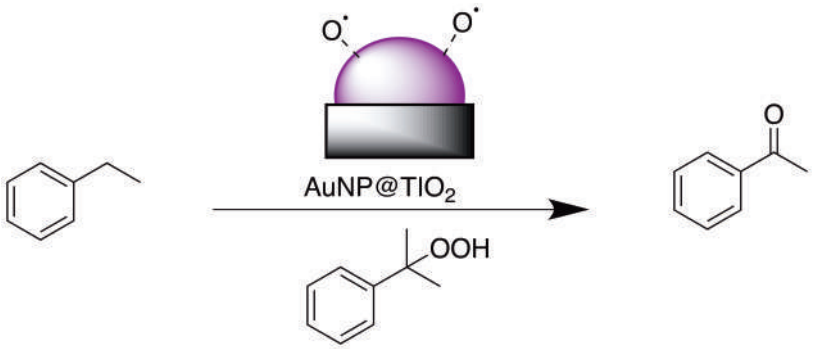

4. Catalyzed peroxidation of Ethylbenzene and n-Propylbenzene by AuNP@TiO2: exploring the Interaction between Radical Species and the Gold Nanoparticle Surface

4.0. Table of contents

4.1. Introduction

Fenton induced decomposition of H_2O_2 using AuNP as catalyst has long been recognised in the literature.[1] Moreover, AuNP have been proven to form hydroxyl radicals which can lead to the degradation of traces of phenol.[2] Likewise, the decomposition of H_2O_2 in the presence of supported AuNP has proved effective for the oxidation of alcohols to the corresponding carbonyl products.[3,4] Observations, such as those presented above, have attracted attention to the little known interactions between radical species and AuNP. Garcia *et al.*[5] have proposed that carbon centered radicals can interact with the AuNP surface. Furthermore, Bar-Ziv and co-workers[6] estimated the rate constant for the interaction between alkyl peroxyl radicals and AuNP to be on the order of 4×10^8 $M^{-1}s^{-1}$. Throughout this thesis, the focus has been on studying these radical/nanoparticle interactions, with Chapter 2 examining the role of AuNP in the peroxidation of cumene and unveiling a potential dual role of the AuNP. First, by participating in the Fenton mediated decomposition of cumene hydroperoxide (CHP) and, second, on the surface induced decomposition of peroxyl radicals to generate nanoparticle surface reactive oxygen species. The focus of Chapter 3 was more centered on the specific role of the composite support in the peroxidation mechanism. The findings from the previous two chapters will be taken into consideration when studying product formation from the supported AuNP catalyzed peroxidation of ethylbenzene.

4.2. Results

Peroxidation of ethylbenzene was performed using cumene hydroperoxide as an initiator where cumyl alcohol and acetophenone can be obtained as products (Scheme 4.1, eq. 1) followed by monitoring the product distribution formed as a result of ethylbenzene peroxidation. Scheme 4.1 illustrates the possible products from ethylbenzene peroxidation (acetophenone, *sec*-phenethyl alcohol and ethylbenzene hydroperoxide) which are dependant on the nature of the reaction conditions. This chapter will examine the effect of supported AuNP (commercial AuNP@TiO_2) on the product distribution of this peroxidation reaction.

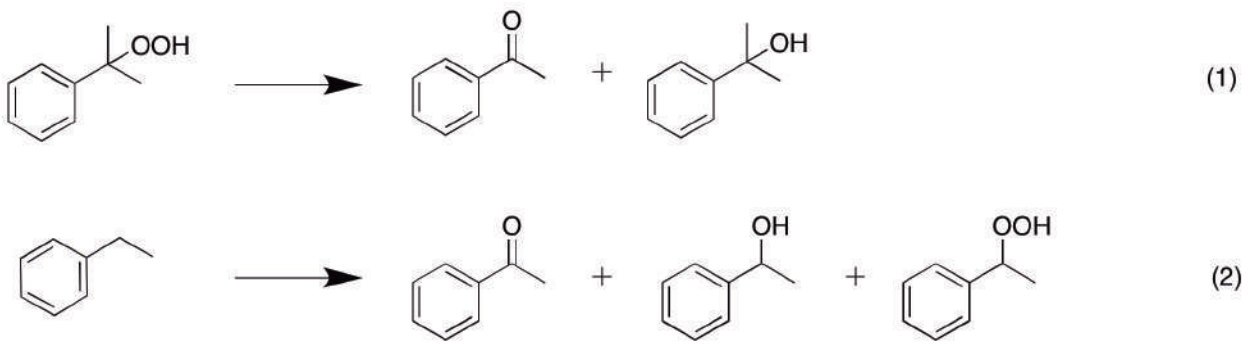

Scheme 4.1. Possible products obtained for the peroxidation of ethylbenzene: products obtained via CHP initiation (1) and directly from the peroxidation of ethylbenzene (2).

The use of CHP as an initiator in the peroxidation of ethylbenzene is not without its difficulties. Namely, acetophenone can be obtained as a product of both

CHP decomposition and ethylbenzene peroxidation. In order to determine the yield of acetophenone exclusively from the ethylbenzene process, the amount of cumyl alcohol obtained from the decomposition of CHP needs to be considered. Recall that:

$$[\text{CHP Decomposed}] = [\text{Cumyl Alcohol}] + [\text{Acetophenone CHP}] \quad (3)$$

$$[\text{Acetophenone Total}] = [\text{Acetophenone CHP}] + [\text{Acetophenone ethylbenzene}] \quad (4)$$

Equation 3 can be rearranged and substituted into equation 4 to equation 5:

$$[\text{Acetophenone ethylbenzene}] = [\text{Acetophenone Total}] - ([\text{CHP Decomposed}] - [\text{Cumyl Alcohol}]) \quad (5)$$

To further support acetophenone formation in the ethylbenzene peroxidation process, an experiment was performed using *n*-propylbenzene as the peroxidizable solvent and CHP as an initiator. In such a scenario, acetophenone would be formed exclusively from CHP degradation and propiophenone via solvent peroxidation. The purpose of this experiment was to establish the plausible formation of the carbonyl product by way of solvent peroxidation, similar to obtaining the observed acetophenone in ethylbenzene peroxidation. A more detailed discussion on this experiment can be seen in section 4.2.3 of this chapter.

4.2.1. Results for ethylbenzene at 40°C

Control reactions were performed in the presence of the support only, i.e., TiO_2 P25 and in the absence of catalyst. Neither decomposition of the CHP initiator nor peroxidation of ethylbenzene was observed. As mentioned in the introduction, the objective of using CHP as initiator in the peroxidation of ethylbenzene is to be able to monitor separately the initiation of the CHP by the AuNP and the peroxidation of ethylbenzene. However, the concern arises from the fact that acetophenone can come from both the decomposition of CHP and the peroxidation of ethylbenzene. In order to differentiate the origin of acetophenone one can use the approach presented in the introduction. Figure 4.1 shows the decomposition profile of 140 mM of CHP versus time (green circle), the formation of cumyl alcohol (black square) and the formation of acetophenone (blue triangle). The amount of acetophenone obtained from the decomposition of CHP was determined by subtracting the amount of cumyl alcohol obtained from the amount of CHP at any given time. It is important to mention that the CHP is completely decomposed after 2 hours.

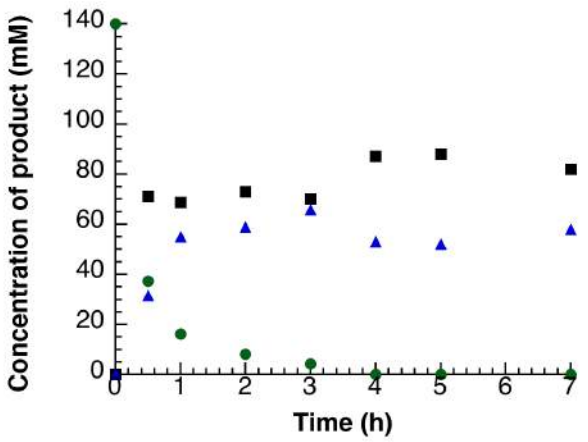

Figure 4.1. Decomposition of 140 mM of CHP over 7 hours at 40°C using commercial AuNP@TiO_2 as catalyst: CHP (●), cumyl alcohol (■), calculated amount of acetophenone formed from the decomposition of CHP (▲)

In Figure 4.2, one can see the formation of products obtained using 140 mM of CHP as initiator at 40°C. As can be seen in Figure 4.2 no significant amount of sec-phenethyl alcohol or ethylbenzene hydroperoxide is obtained but a significant quantity of acetophenone is obtained. As mentioned before, the acetophenone can be obtained via two pathways; the decomposition of CHP and the peroxidation of ethylbenzene, therefore one needs to consider this using the approach mentioned in the introduction. One can obtain the amount of acetophenone coming for the peroxidation of ethylbenzene by subtracting the total amount with the amount formed in the CHP decomposition (eq. 5).

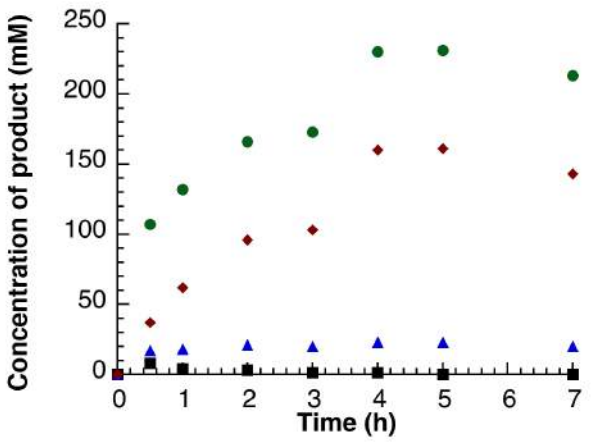

Figure 4.2. Products formed from the AuNP@TiO_2-catalyzed peroxidation of ethylbenzene using 140 mM of CHP as initiator at 40°C: total acetophenone (●),acetophenone coming from ethylbenzene peroxidation obtained by subtracting the amount formed via CHP decomposition for acetophenone total (◆), *sec*-phenethyl alcohol (▲), ethylbenzene hydroperoxide (■).

When considering the data presented in Figures 4.1 and 4.2, one can say that the peroxidation of ethylbenzene into acetophenone is still happening even if all the initiator (CHP) is gone as it completely disappeared after 2 hours.

In Figure 4.3 one can observe the decomposition of 280 mM of CHP in ethylbenzene and in this case the decomposition of CHP is not complete even after 7 hours, as was the case using 140 mM of CHP as initiator. This is most likely due to the fact that the catalyst is becoming a poor Fenton reagent. The

amount of acetophenone coming from the decomposition of CHP can be calculated before.

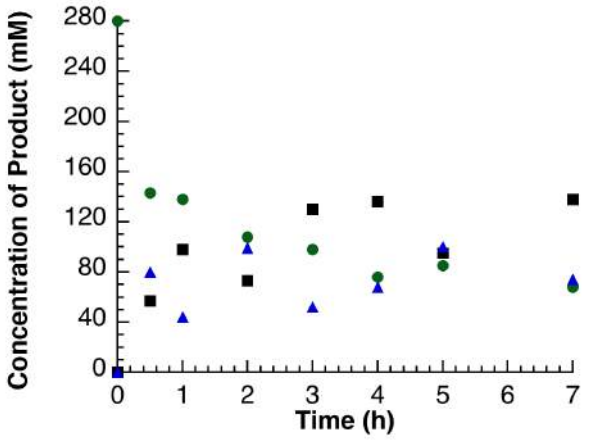

Figure 4.3. Decomposition of 280 mM of CHP over 7 hours at 40°C using commercial AuNP@TiO_2 as catalyst: CHP (●), cumyl alcohol (■), calculated amount of acetophenone formed from the decomposition of CHP (▲)

Figure 4.4 shows the formation of products from the peroxidation of ethylbenzene. As mentioned for the reaction using 140 mM of CHP, no significant amount of both *sec*-phenethyl alcohol and ethylbenzene hydroperoxide is obtained. The total amount of acetophenone and the amount formed via the peroxidation of ethylbenzene is presented in Figure 4.4. Considering that the amount of acetophenone formed via the peroxidation is determined mathematically, the error is higher because one adds it to the total amount of acetophenone and the amount of cumyl alcohol.

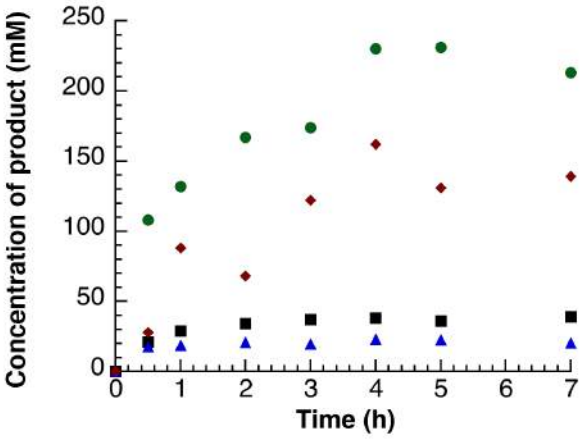

Figure 4.4. Products formed from the AuNP@TiO_2-catalyzed peroxidation of ethylbenzene using 280 mM of CHP as initiator at 40°C: total acetophenone (●), acetophenone coming from ethylbenzene peroxidation obtained by subtracting the amount formed via CHP decomposition for acetophenone total (◆), *sec*-phenethyl alcohol (▲), ethylbenzene hydroperoxide (■).

Again, the important element to mention is that the peroxidation of the ethylbenzene is still happening even after the decomposition of the CHP is slowing down significantly

4.2.2. Results for ethylbenzene at 80°C

The experiments carried out at 40°C were repeated using the same experimental procedure at 80°C in order to ascertain the influence of reaction temperature on product formation from the ethylbenzene peroxidation. In the absence of catalyst, neither decomposition of the CHP initiator nor any peroxidation of ethylbenzene was observed. Control reactions using TiO_2 P25 did

show decomposition of CHP into phenol, a pathway that was previously discussed in Chapter 2, Section 2.3.2. Nevertheless, no peroxidation products were obtained. Again two concentrations of CHP were used: 140 mM and 280 mM. The result using 140 mmol of CHP as initiator can be seen in Figure 4.5 and Figure 4.6. The decomposition of CHP, the related formation of cumyl alcohol and the calculated amount of acetophenone coming from the decomposition from CHP can be seen in Figure 4.6, where all the CHP is decomposed within the first 30 minutes. In Figure 4.6 one can see that product formation, namely the formation of acetophenone, is still increasing after all the CHP has been decomposed, meaning that the formation of peroxidation product is still happening. *Sec*-Phenethyl alcohol is obtained but plateaus after 30 minutes. Ethylbenzene hydroperoxide was also obtained in this case but is completely decomposed within the first hour.

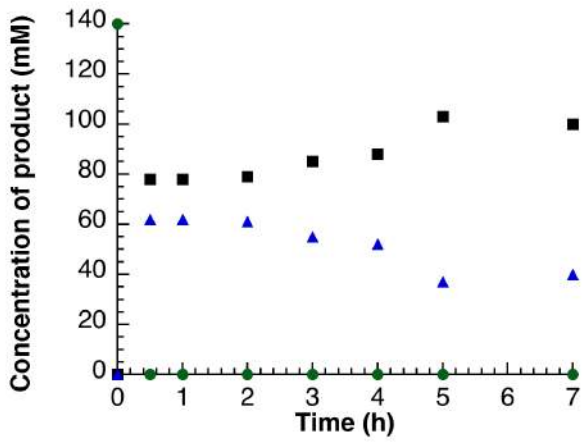

Figure 4.5. Decomposition of 140 mM of CHP over 6 hours at 80°C using commercial AuNP@TiO_2 as catalyst: CHP (●), cumyl alcohol (■), calculated amount of acetophenone formed from the decomposition of CHP (▲).

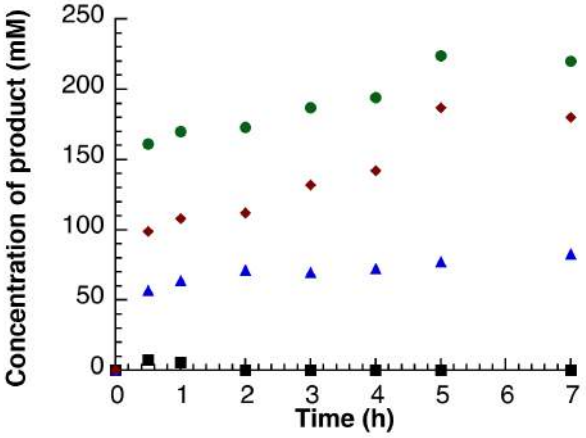

Figure 4.6. Products formed from the AuNP@TiO_2-catalyzed peroxidation of ethylbenzene using 140 mM of CHP as initiator at 80°C: total acetophenone (●), acetophenone coming from ethylbenzene peroxidation obtained by subtracting the amount formed via CHP decomposition for acetophenone total (◆),*sec*-phenethyl alcohol (▲), ethylbenzene hydroperoxide (■).

Again the decomposition of cumene hydroperoxide is shown in Figure 4.7, this time using 280 mmol of CHP as initiator where we can still see that all the cumene hydroperoxide can be decomposed within the first 30 minutes in contrast with the reaction at 40°C, when decomposition does stops. The amount of cumyl alcohol and the calculated amount of acetophenone obtained from the decomposition of CHP are presented in Figure 4.7. Figure 4.8 does show product formation and as already mentioned, the amount of acetophenone increases after all the CHP is decomposed.

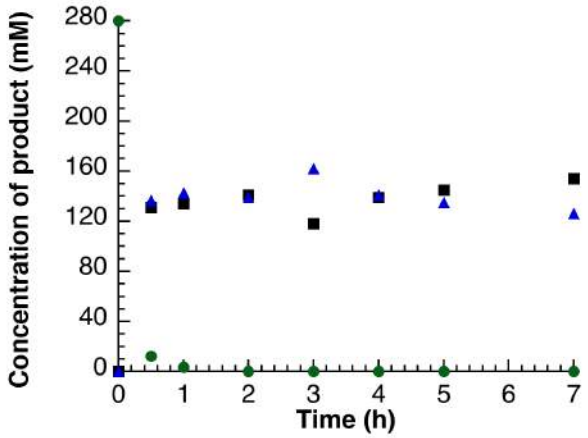

Figure 4.7. Decomposition of 280 mmM of CHP over 6 hours at 80°C using commercial AuNP@TiO_2 as catalyst: CHP (●), cumyl alcohol (■), calculated amount of acetophenone formed from the decomposition of CHP (▲)

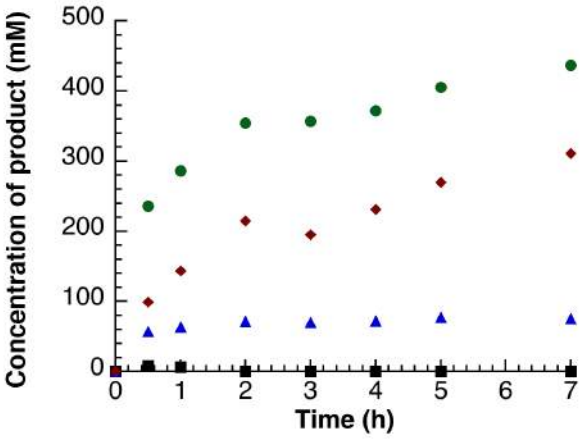

Figure 4.8. Products formed from the AuNP@TiO2-catalyzed peroxidation of ethylbenzene using 280 mM of CHP as initiator at 80°C: total acetophenone (●), acetophenone coming for ethylbenzene peroxidation obtained by subtracting the amount formed via CHP decomposition for acetophenone total (◆), sec-phenethyl alcohol (▲), ethylbenzene hydroperoxide (■).

Several general observations can be drawn from the amount of acetophenone formed with respect to initiator concentration. Importantly, after the first 30 minutes of reaction, the formation of acetophenone is not related to the decomposition of either cumene hydroperoxide or ethylbenzene hydroperoxide due to their absence in solution, thus indicating that the role of AuNPs is not simply Fenton chemistry related. This statement should not be surprising since we already stated in Chapter 2 that AuNPs were strongly implicated in the decomposition of peroxyl radicals to the corresponding alkoxyl radicals and formation of surface reactive species. Logically, after one proposed the formation of oxygen reactive species one needs to consider what kind of

reactivity these surface reactive species can have. This will be explored in the discussion section.

4.2.3. *n*-Propylbenzene peroxidation at 80°C

The peroxidation of *n*-propylbenzene using CHP as initiator was performed to independently establish if, using AuNP@TiO_2 as catalyst, propiophenone is formed as the major peroxidation product (see Scheme 4.2 for details on the products formed). The reaction conditions used were as follows: 140 mM of CHP and a reaction temperature of 80°C.

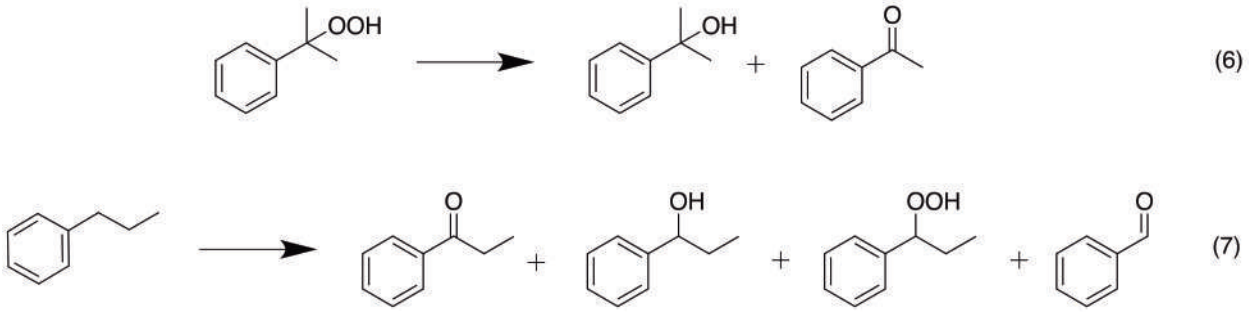

Scheme 4.2. Possible products for the peroxidation of *n*-propylbenzene obtained *via* (6) CHP initiation and (7) directly from the peroxidation of *n*-propylbenzene .

The results from Figure 4.9 depict that some acetophenone is formed from the CHP decomposition and that the major product is cumyl alcohol. The results presented in Figure 4.10 illustrate the formation of propiophenone as the major product in the peroxidation of *n*-propylbenzene, thus demonstrating that, in this case, a ketone is formed as the major product.

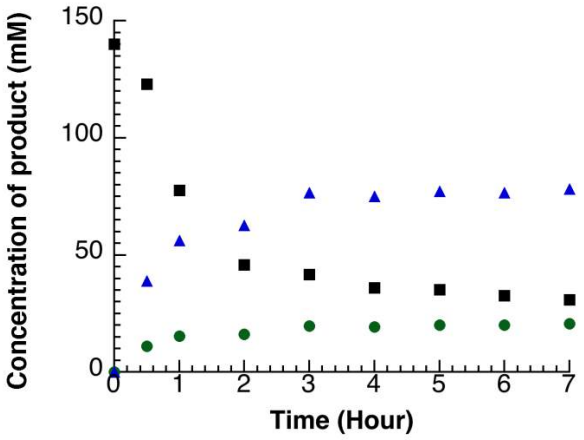

Figure 4.9. Decomposition product of CHP in the peroxidation of *n*-propylbenzene: acetophenone (●), CHP (■), cumyl alcohol (▲); conditions: at 80°C using 140 mM of CHP as initiator

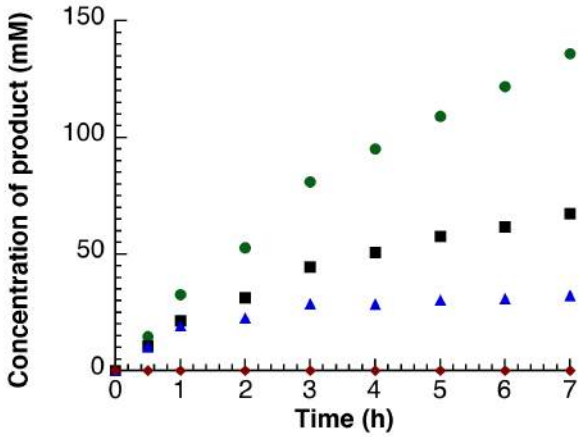

Figure 4.10. Product formation in the peroxidation of *n*-propylbenzene: propiophenone (●), 1-phenyl-1-propanol (■), benzaldehyde (▲), propylbenzene hydroperoxide (●); conditions: at 80°C, using 140 mM of CHP as initiator

The same general observation as for the ethylbenzene case can also be seen here. The formation of propiophenone can be observed after CHP stops

decomposing, which means that the formation of propiophenone is necessarily related to a pathway that does not involve the Fenton decomposition of the initiator CHP. This can be explained by considering the surface reactivity of AuNP as will be mentioned in the discussion.

4.3. Discussion

In order to identify the reactions involved in the formation of acetophenone *via* AuNP-catalyzed ethylbenzene peroxidation, it is important to consider the reactions that can happen in solution, as well as those occurring on the AuNP surface. Clearly, from the results obtained in this study, multiple pathways are involved in product formation. These pathways are also time dependant, meaning that they vary depending on which species are present in the reaction mixture. For example, CHP consumption is a very fast process when using ethylbenzene; however, even after the CHP is completely decomposed and no longer participating in the ethylbenzene peroxidation, acetophenone is formed as the reaction continues. This suggests that the oxidation capacity is localized at the AuNP at this stage.

When focusing on the reactions that occur in the first 30 minutes, one needs to consider the fast and complete decomposition of cumene hydroperoxide that occurs in every case, with exception given to the reaction performed at 40 °C using 280 mM of initiator, which is most likely due to the fact that the catalyst is

becoming a poor Fenton reagent. For these reactions where CHP is decomposed most quickly, Fenton chemistry likely leads to the formation of cumyl alkoxyl radicals (Scheme 4.3, eq. 8). Next, this alkoxyl radical abstracts a hydrogen from the ethyl benzene (Scheme 4.3, eq. 9) to form one molecule of cumyl alcohol and the ethylbenzene-derived benzyl radical. Finally, the carbon-centered radical can react with oxygen to form the ethylbenzene peroxyl radical (eq. 3).

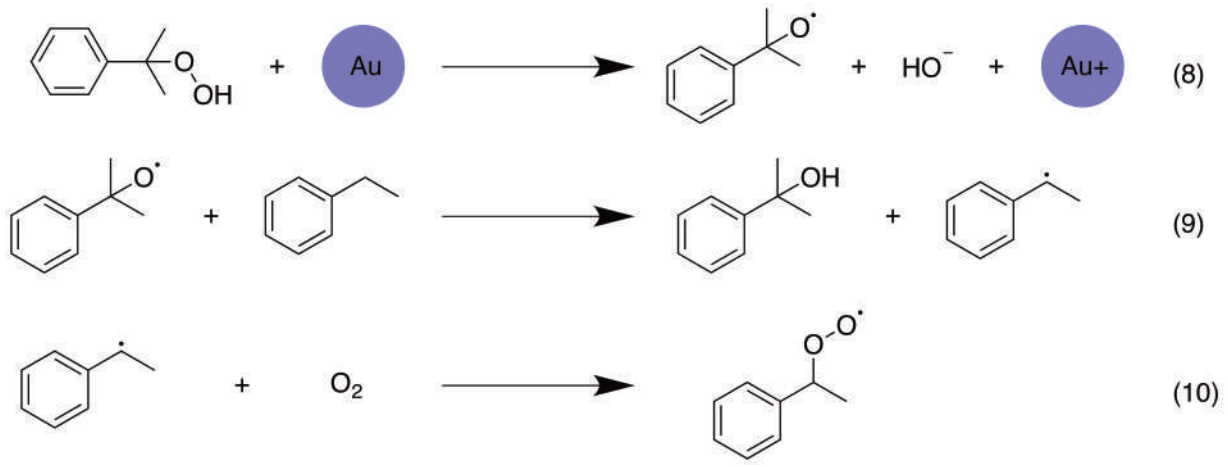

Scheme 4.3. Proposed mechanism for the formation of ethylbenzene peroxyl radicals *via* Fenton-type chemistry.

The differences in fate of the ethylbenzene peroxyl radical based on the reaction conditions stem from their ability to interact with the AuNP surface. When interaction with the nanoparticle surface is not possible, hydrogen abstraction from the solvent is favoured and results in the formation of

ethylbenzene hydroperoxide (Scheme 4.4, eq. 11). Subsequently, AuNP could lead to the formation of the ethylbenzene alkoxyl radical by interacting with ethylbenzene hydroperoxide *via* Fenton chemistry. The acetophenone would, therefore, originate from the alkoxyl radical (*vide infra*).

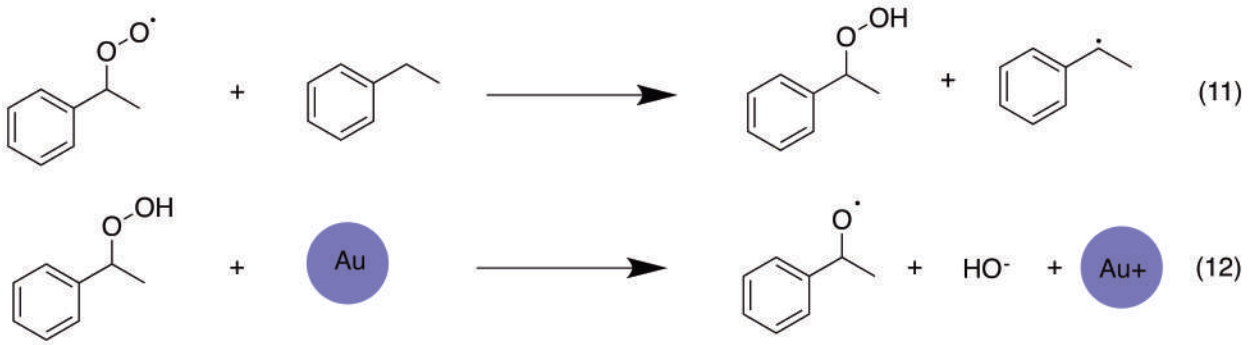

Scheme 4.4. Proposed mechanism for the formation of the ethylbenzene alkoxyl radical by way of Fenton chemistry.

On the other hand, the ethylbenzene peroxyl radical could interact and decompose at the AuNP surface (Scheme 4.5). This pathway would lead to the formation of reactive oxygen species on the nanoparticle surface, and alkoxyl radicals. This chemistry is analogous to the chemistry presented in Chapter 2.

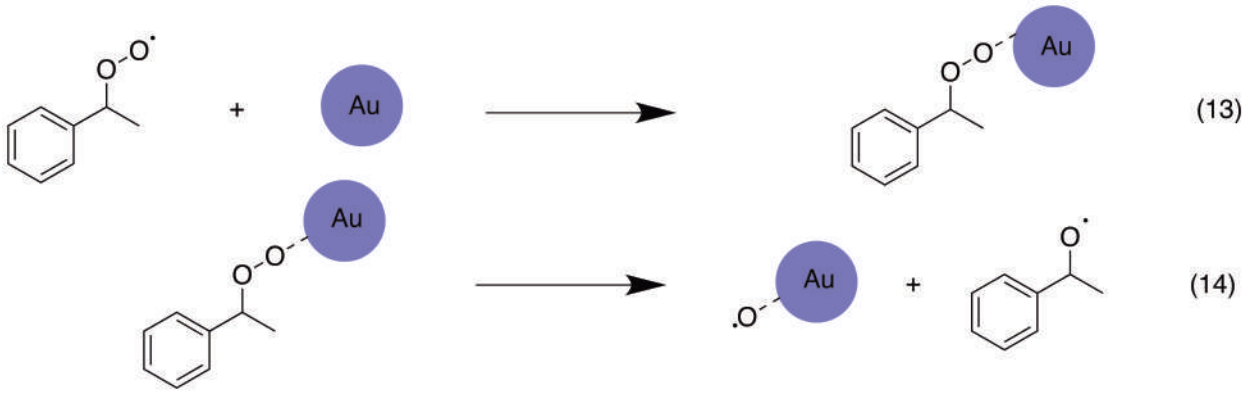

Scheme 4.5. The proposed formation of ethylbenzene alkoxyl radicals by way of AuNP surface decomposition.

Once the alkoxyl radical is formed, a hydrogen atom loss must occur in order to form acetophenone. A first possibility consists of radical disproportionation with another radical present and leading to acetophenone formation, but due to the small concentration of radicals present in solution this pathway is unfavourable. A second possibility involves the participation of AuNP in an alcohol oxidation type mechanism where the hydrogen atom is transferred to the surface of the AuNP, leading to the formation of acetophenone. A third possibility would involve the oxygen reactive species formed by the decomposition of the peroxyl radical on the AuNP surface which would abstract the hydrogen from the C-H bond of a surface bonded ethylbenzene alkoxyl radical.

After the first 30 minutes, the CHP initiator is completely decomposed in every case except when considering the 280 mmol of CHP at 40°C, where the decomposition is really slow and plateaus after 2 hours due to catalyst deactivation. The formation of acetophenone is still occurring after this time frame when 140 mM or 280 mM of CHP is used at both 40°C and 80°C. How can this be explained? Clearly, the role of the nanoparticle is not limited to the decomposition of hydroperoxide *via* Fenton chemistry. The decomposition of the peroxyl radical on the surface of the nanoparticles can lead to the formation of reactive surface oxygen species (Scheme 4.6, eq. 15 and 16). These surface oxygen species could be responsible for the abstraction of hydrogen from ethylbenzene (Scheme 4.6, eq. 17) and the resultant formation of acetophenone. The nature of the radical species on the surface of the nanoparticles is open to speculation. Nevertheless, the involvement of reactive surface oxygen species is needed in order to form acetophenone after 30 minutes. Gu *et al.*[7] have proposed the involvement of such surface species when studying the peroxidation of ethylbenzene using gold nanowires. Thus, we advance a proposed mechanism concerning the formation of acetophenone *via* ethylbenzene peroxidation in the presence of supported AuNP. Specifically, following the formation of a carbon-centered radical via intervention of the reactive surface oxygen species, the former will react with oxygen to form ethylbenzene peroxyl radical, as presented in Scheme 4.6, eq. 18.

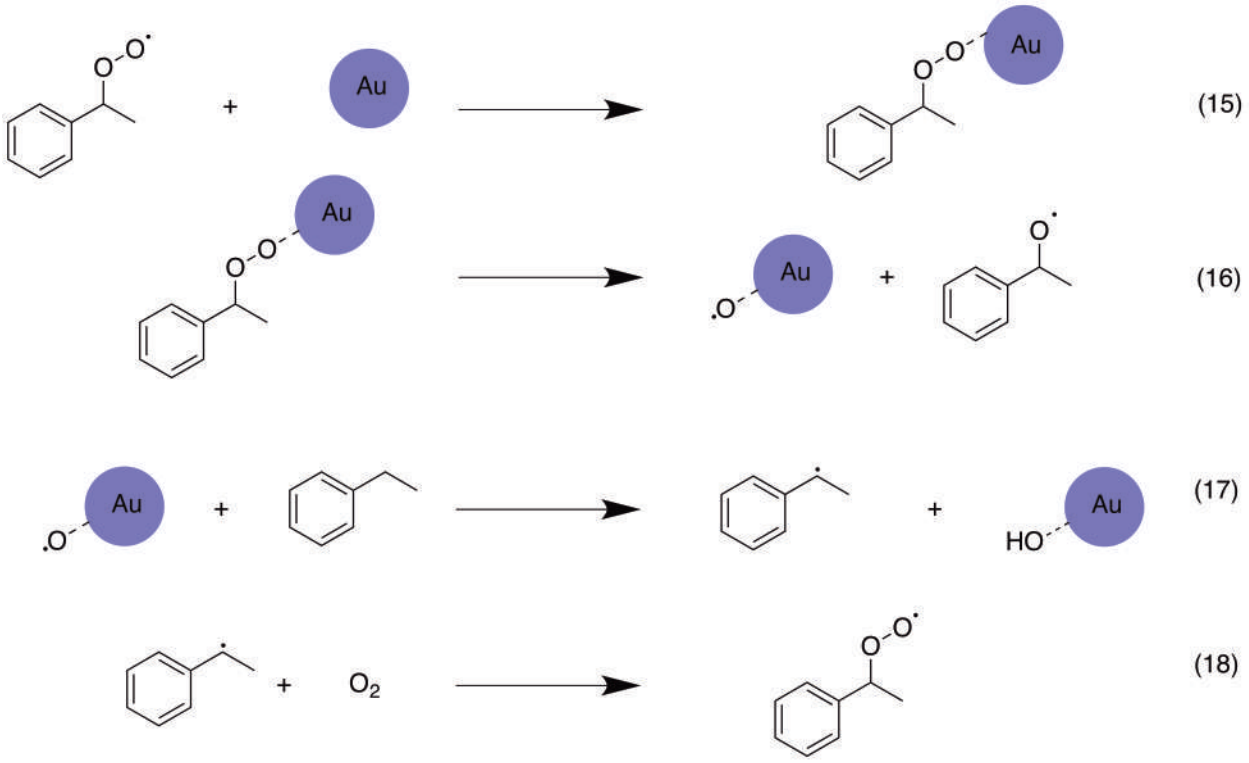

Scheme 4.6. The proposed role of the AuNP surface, leading to the formation of ethylbenzene alkoxyl radicals by way of reactive surface oxygen species.

In summary, the main reaction pathway involved in the production of acetophenone by ethylbenzene peroxidation consists of the decomposition of CHP *via* Fenton chemistry during the first 30 minutes of reaction leading to the formation of an ethylbenzene peroxyl radical which formed surface reactive species on the AuNP. After 30 minutes, acetophenone production is dictated by the participation of reactive surface oxygen reactive species.

4.4. Conclusions

Peroxidation of ethylbenzene using CHP as initiator and AuNP@TiO_2 as a catalyst was conducted by varying the quantity of initiator at 2 different temperatures. When the amount of initiator is low, acetophenone is the only product and it reaches a maximum within the first 30 minutes of reaction. When the concentration of initiator is high, acetophenone is the major compound obtained and product formation continues after the first 30 minutes. Fenton chemistry is believed to be an important part of the mechanism during the first 30 minutes, followed by the involvement of reactive oxygen species formed *via* the decomposition of ethylbenzene peroxyl radical on the AuNP surface.

4.5. Experimental

4.5.1. Reagents.

Ethylbenzene (99%), cumene hydroperoxide (80%) (CHP in cumene), cumyl alcohol (98 %; 2-phenyl-2-propanol), 1-phenyl-1-propanol, propiophenone and acetophenone (98%) were purchased from Sigma-Aldrich and used as received. n-Propylbenzene was purchased from Acros Organic. TiO_2 P25 was a gift from Evonik Degussa. AUROlite™ 1% AuNP@TiO_2 was purchased from Strem Chemicals and was ground using a mortar and pestle prior to use. Optima grade heptane and 2-propanol were purchased from Fisher Chemicals and

used as received. *Sec*-phenethyl alcohol (98%) was bought from Acros Organic and purified prior to use based on previously published methods.

4.5.2. Instruments.

The average size of the metallic AuNP was determined using a JEM-2100F FETEM transition electron microscope TEM from Jeol Ltd.

Analysis of the reaction mixtures of the peroxidation of ethylbenzene (cumyl alcohol, acetophenone, cumene hydroperoxide, *sec*-phenethyl alcohol and ethylbenzene hydroperoxide) was performed using normal phase Agilent 1100 HPLC with a 99:1 heptane/isopropanol eluent mixture. Analysis of the reaction mixtures of the peroxidation of propylbenzene (cumyl alcohol, propiophenone acetophenone, cumene hydroperoxide 1-phenyl-1-propanol and propylbenzene hydroperoxide) was performed using a normal phase Agilent 1100 HPLC with a 99:1 heptane/isopropanol eluent mixture.

4.5.3. Peroxidation of ethylbenzene under air saturated conditions

In a 50 mL, two-neck round bottom flask, 100 mg of catalyst and a quantity of cumene hydroperoxide (140 mM or 280 mM) were added to 10 mL of ethylbenzene and the reaction was heated to 40°C or 80°C. An aliquot was

taken from the reaction mixture every hour, centrifuged and subsequently analyzed by HPLC. Control reactions were carried out using the support itself and in the absence of heterogeneous materials. Air was flowed thought the solution and the flow was monitored using a Matheson flow meter. The typical experiment error that was obtained using HPLC analysis is around 10% of the reported values.

4.5.4. Peroxidation of propylbenzene under air saturated conditions

In a 50 mL, two-neck round bottom flask, 100 mg of catalyst and a quantity of cumene hydroperoxide (140 mM) were added to 10 mL of *n*-propylbenzene and the reaction was heated to 40°C or 80°C. An aliquot was taken from the reaction mixture every hour, centrifuged and subsequently analyzed by HPLC. Air was flowed thought the solution and the flow was monitored using a Matheson flow meter. The typical experiment error that was obtained using HPLC analysis is around 10% of the reported values.

4.6.1. Appendix 1: Representative HPLC trace for the peroxidation of ethylbenzene

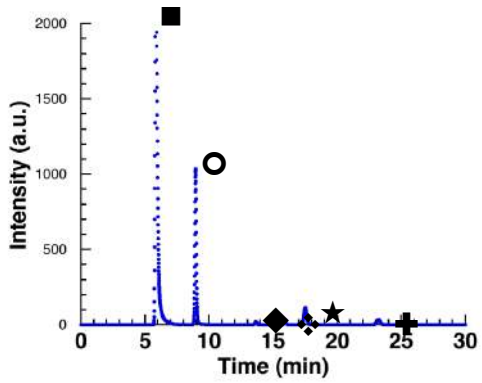

Figure 4.11. Representative HPLC trace of the peroxidation of ethylbenzene. Peak identification: Ethylbenzene and cumene (■), acetophenone (O), CHP (◆), ethylbenzene hydroperoxide (❖), cumyl alcohol (★) and *sec*-phenethyl alcohol (✚).

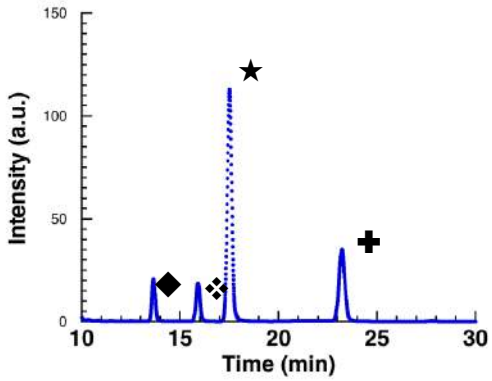

Figure 4.12. Expanded representative HPLC trace of the peroxidation of ethylbenzene. Peak identification: CHP (◆), ethylbenzene hydroperoxide (❖), cumyl alcohol (★) and *sec*-phenethyl alcohol (✚).

4.6.2. Appendix 2: Determining the calibration factor for ethylbenzene hydroperoxide

Calibration curves were used to determine the concentration of every compound involved in the reaction: cumyl alcohol, acetophenone, *sec*-phenethyl alcohol and cumene hydroperoxide. However, due to the unstable nature of the ethylbenzene hydroperoxide, isolation is not possible and therefore an alternative approach was used. The calibration factor of ethylbenzene hydroperoxide was determined by quenching the hydroperoxide using triphenyl phosphine (Scheme 4.7). Then, the concentration of *sec*-phenethyl alcohol, before and after the addition of triphenyl phosphine, was determined and the relationship between the calibration factors of the ethylbenzene hydroperoxide were compared to the calibration factors of the alcohol product.

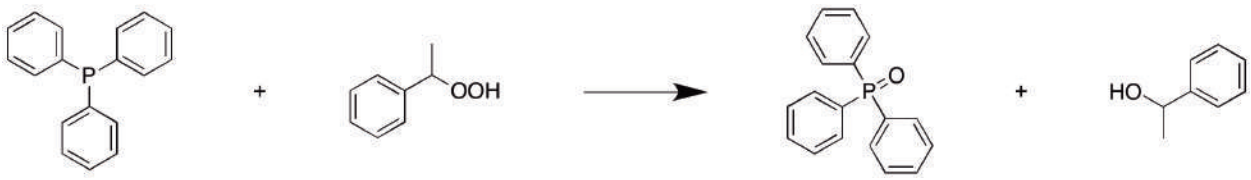

Scheme 4.7. Quenching of ethylbenzene hydroperoxide by triphenyl phosphine producing the corresponding alcohol (*sec*-phenethyl alcohol) and triphenyl phosphine oxide.[8]

4.6.3. Appendix 3: Representative HPLC trace for peroxidation of *n*-propylbenzene

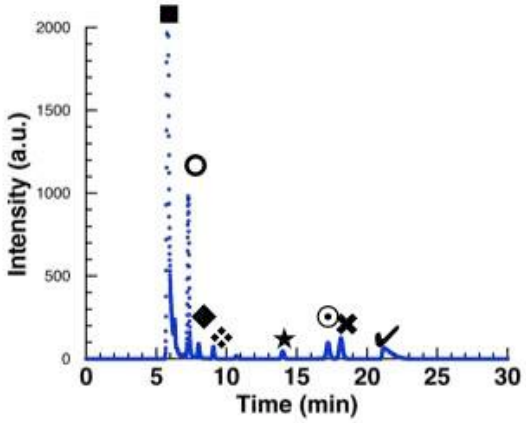

Figure 4.13. Representative HPLC trace of the peroxidation of propylbenzene. Peak identification: propylbenzene and cumene (■), propiophenone (O) benzaldehyde (◆), acetophenone (❖), cumene hydroperoxide (★), 1-phenyl-1-propanol (⊙), cumyl alcohol (✖) and *n*-propylphenol (✔)

4.7. References

(1) Navalon, S.; Martin, R.; Alvaro, M.; Garcia, H. Angew. Chem. Int. Ed. 2010, 49, 8403.

(2) Navalon, S.; Dhakshinamoorthy, A.; Alvaro, M.; Garcia, H. ChemSusChem 2011, 4, 1712.

(3) Kiyonaga, T.; Jin, Q.; Kobayashi; Tada, H. ChemPhysChem 2009, 10, 2935.

(4) Hallett-Tapley, G. L.; Silvero, M. J.; González-Béjar, M.; Grenier, M.; Netto-Ferreira, J. C.; Scaiano, J. C. J. Phys. Chem. C. 2011, 21, 10784.

(5) Alvaro, M.; Aprile, C.; Corma, A.; Ferrer, B.; Garcia, H. J. Catal. 2007, 245, 249.

(6) Bar-Ziv, R.; Zilbermann, I.; Zidki, T.; Cohen, H.; Meyerstein, D. J. J. Phys. Chem. C. 2009.

(7) Hu, L.; Cao, X.; Yang, J.; Li, M.; Haiyan, H.; Xu, Q.; Ge, J.; Wang, L.; Lu, J.; Chen, L.; Gu, H. Chem. Comm. 2011, 47, 1303

(8) Hiatt, R.; Smythea, N. D.; McColeman, C. Can. J. Chem. 1971, 49, 1707.

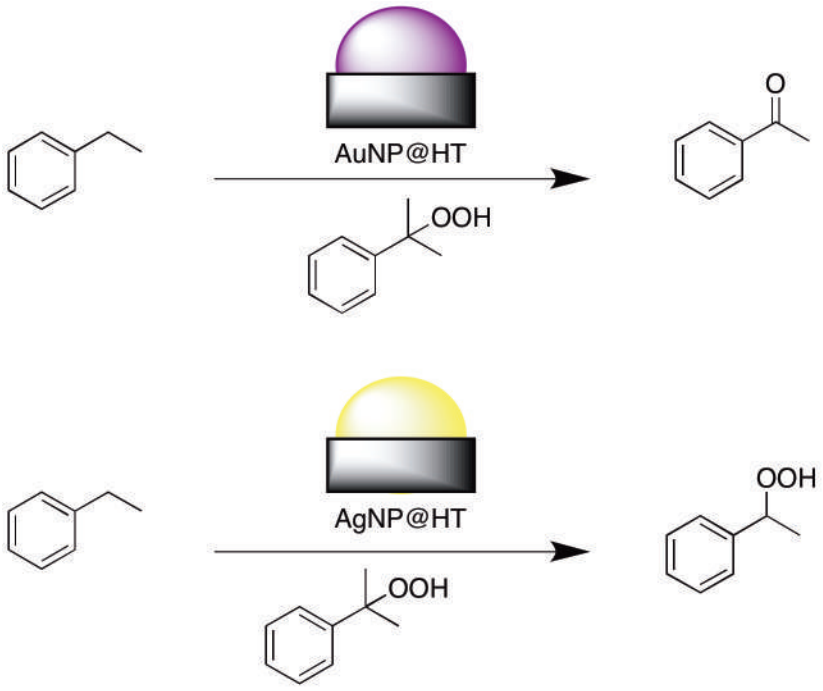

5. Surface Decomposition of Peroxyl Radicals: the Silver versus Gold Nanoparticle Surface

5.0. Table of Contents

5.1. Introduction

Free radicals are very reactive species that play a very important role in biological and chemical processes. In the context of a biological system, free radicals participate in oxidative stress, while in the context of chemical systems, free radicals are intermediates in solvent oxidations, notably cumene (Chapter 2). Interaction between free radicals and the nanoparticle surface has recently attracted considerable attention in the literature. In a report from Zidki *et al.*[1] it is noted that carbon-centered radicals react with AuNP at a rate near diffusion control. In the context of catalysis, the adducts formed by the interactions between radicals and the AuNP surface were proposed to be active species in the peroxidation of 1-decene.[2] Hutchings *et al.*[3] also proposed the involvement of AuNP surface-bound radical species in the oxidation of toluene using Au-Pd nanoparticles. The existence of free radical nanoparticle adducts have also been proposed within this thesis for the peroxidation of cumene (Chapter 2) and ethylbenzene and n-propylbenzene (Chapter 4) and were suggested to be formed *via* decomposition of peroxyl radicals on the AuNP surface. However, it is noteworthy that in the study on the peroxidation of cumene (Chapter 2) supported AgNP were unable to induce the decomposition of the suggested peroxyl radical-nanoparticle adduct and, by extension, minimized cumene hydroperoxide decomposition. As a result, the peroxyl radical-nanoparticle adduct was proposed to be reversible in the case of supported AgNP. This

chapter will aim to examine and compare, more in depth, the surface reactivity of AgNP and AuNP. In order to strengthen this study, the peroxidation of ethylbenzene and results obtained in Chapter 4 will be expanded to include the supported catalysts AuNP@HT and AgNP@HT, since they were used in the study of cumene peroxidation in Chapter 2. This will allow more reliable comparisons between the AgNP and AuNP surfaces for the previously examined peroxidation systems. Scheme 5.1 shows the products that can be obtained in the experiments that are done in this chapter.

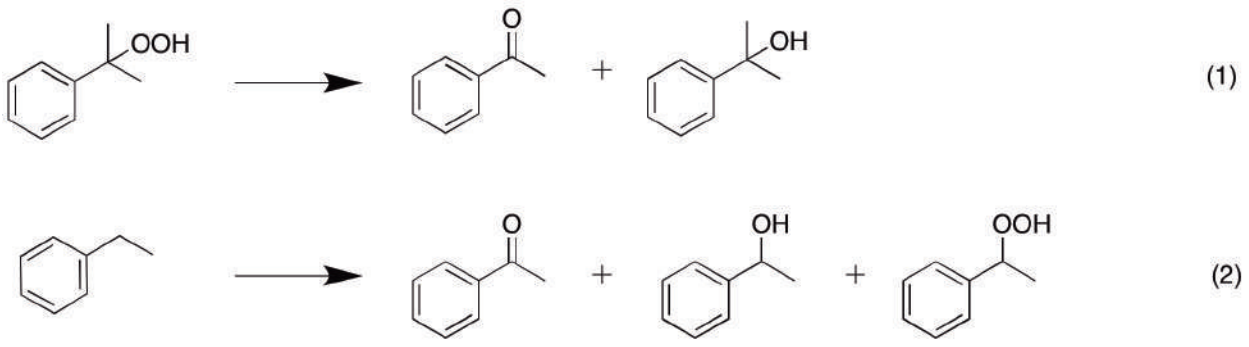

Scheme 5.1. Possible products obtained for the peroxidation of ethylbenzene: products obtained via CHP initiation (1) and directly from the peroxidation of ethylbenzene (2).

5.2. Results

5.2.1. Peroxidation of ethylbenzene using AuNP@HT and AgNP@HT.

The peroxidation of ethylbenzene has been investigated using both AuNP and AgNP supported on hydrotalcite and the same general tendencies are observed as those discussed in Chapter 4 for the supported nanoparticle catalyzed peroxidation of ethylbenzene. The control reaction using hydrotalcite yielded no significant peroxidation product. Figure 5.1 shows the disappearance of CHP as a function of time using AuNP@HT as a catalyst at 40°C and illustrates the complete decomposition of CHP within the first 2 hours of reaction. Figure 5.1 also shows the formation of cumyl alcohol and the calculated amount of acetophenone arising from the decomposition of cumyl hydroperoxide (CHP). As considered in Chapter 4, acetophenone formation is predicted to result from two distinct pathways, either CHP decomposition or peroxidation of ethylbenzene. Using the same methodology as was presented in Section 4.2, equations 1-3, one can determine the amount of acetophenone formed from ethylbenzene by examining the amount of cumyl alcohol formed by way of CHP decomposition (see Appendix 3, Chapter 4 for further details).

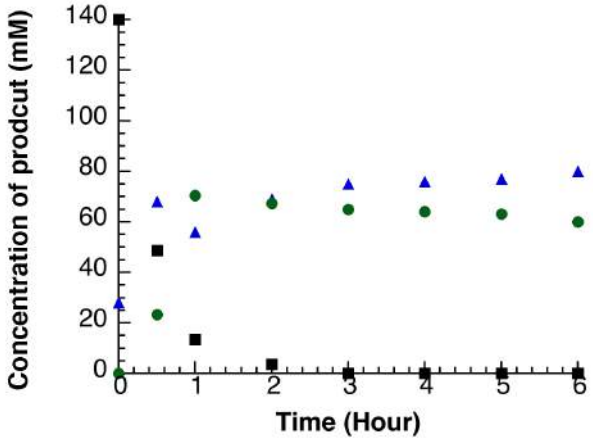

Figure 5.1 Decomposition product of CHP in the peroxidation of ethylbenzene: acetophenone (●), CHP (■), cumyl alcohol (▲); conditions: at 80°C using 140 mM of CHP as initiator.

In Figure 5.2, acetophenone is obtained as the major product when using the AuNP@HT composite at 40°C, which is in agreement with the results previously obtained for AuNP@TiO_2 (Chapter 4).

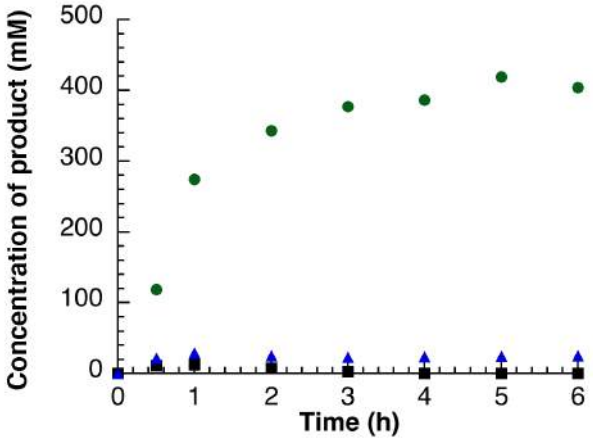

Figure 5.2. Products formed from the attempted AuNP@HT-catalyzed peroxidation of ethylbenzene using 140 mM of CHP as initiator, at 80°C: acetophenone (●),*sec*-phenethyl alcohol (▲), ethylbenzene hydroperoxide (■) (this graph has been corrected by the amount of acetophenone formed via the decomposition of CHP).

Similar experiments were performed using AgNP@HT as the peroxidation catalyst. Degradation of the CHP initiator is mostly absent when using the supported AgNP material. This experimental result is what one should expect when recalling the conclusions from Chapter 2, where the Fenton activity of AgNP@HT was determined to be lower than AuNP@HT. Figure 5.3 shows that the major product obtained from the peroxidation of ethylbenzene in the presence of AgNP@HT is ethylbenzene hydroperoxide and not acetophenone. Though acetophenone is not the major product obtained, it is observed witin the first hour of reaction with no increase in formation over the remaining course of reaction. As mentioned before, the origin of acetophenone could be either

from the peroxidation of ethylbenzene or the decomposition of CHP via β-scission of the cumyl alkoxyl radical.

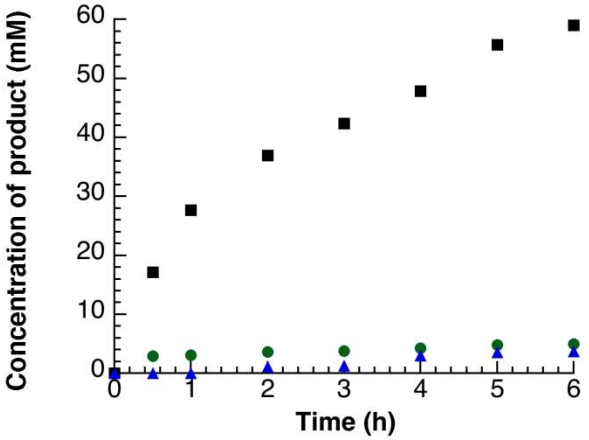

Figure 5.3. Products formed from the AgNP@HT-catalyzed peroxidation of ethylbenzene using 140 mM of CHP as initiator, at 80°C: acetophenone (●),*sec*-phenethyl alcohol (▲), ethylbenzene hydroperoxide (■).

5.3. Discussion

The results obtained using AgNP *versus* AuNP nanomaterials show a clear difference in reactivity between these two catalysts in the peroxidation of ethylbenzene. In the case of the AuNP@HT, acetophenone is obtained as the major product (Figure 5.2), while ethylbenzene hydroperoxide is favoured when AgNP@HT is used (Figure 5.4). Scheme 5.1 (eq. 3 and 4) illustrates the proposed participation of the AuNP surface with respect to the decomposition of

ethylbenzene peroxyl radicals on the nanoparticle surface, leading to the formation of reactive surface oxygen species. These species could be responsible for the hydrogen abstraction from ethylbenzene leading to the formation of a carbon-centered radical as proposed in Chapter 4. These species could also be responsible for the formation of acetophenone *via* disproportionation of the ethylbenzene alkoxyl radical at the surface of the nanoparticles (Scheme 5.2 eq. 5). Nonetheless, Scheme 5.1 takes into account the higher surface reactivity of the supported AuNP materials in the peroxidation process. When comparing the result obtained using AuNP@TiO_2 (Chapters 4) *versus* AuNP@HT, one can say that AuNP@HT is a better catalyst as the amount of product formed is higher; this could be due to the influence of the support in the Fenton chemistry *versus* the surface reactivity of this catalyst.

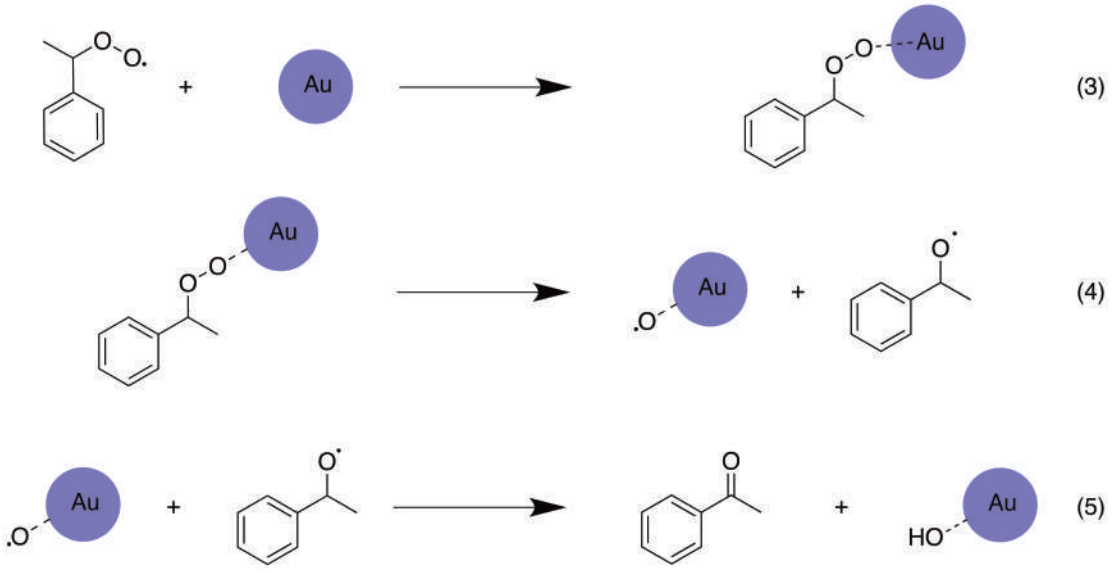

Scheme 5.2. Surface decomposition of peroxyl radicals on the AuNP surface.

Clearly, the results obtained using the supported AgNP indicate that the AgNP surface is not capable of decomposing peroxyl radicals into the corresponding alkoxyl radicals. The enhanced stability of cumene hydroperoxide and the diminished peroxidation of ethylbenzene indicate that the Fenton activity of AgNP@HT is not as efficient as for AuNP@HT. The formation of acetophenone in the first hour when using AgNP@HT as a catalyst in the peroxidation of ethylbenzene can be rationalized using two different pathways. First, the ethylbenzene alkoxyl radical is formed *via* Fenton decomposition of ethylbenzene hydroperoxide which is followed by the formation of acetophenone via an alcohol oxidation type reaction.

The second possible pathway relies on the decomposition of the ethylbenzene peroxyl radical into the corresponding alkoxyl radical on the AgNP surface, forming acetophenone. The difficulty lies in identifying which of the two aforementioned pathways is more likely, considering the decreased ability of the AgNP surface to decompose peroxyl radicals as compared to supported AuNP. Furthermore, the ability of the peroxyl radicals to interact with AgNP surface in a reversible fashion, as proposed in Chapter 2, must also be considered.

5.4. Conclusions

The peroxidation of ethylbenzene was used as a probe system in order to gain further information on the observed surface reactivity differences of AuNP@HT and AgNP@HT towards peroxyl radicals. AgNP@HT were found to be unable to decompose the ethylbenzene peroxyl radical. On the contrary, AuNP@HT rapidly degraded the ethylbenzene peroxyl radical. This observation can explain the preferred formation of acetophenone when ethylbenzene peroxidation is carried out in the presence of supported AuNP catalysts, while ethylbenzene hydroperoxide is favoured in the presence of heterogeneous AgNP materials.

5.5. Experimental

5.5.1. Reagents.

Ethylbenzene (99%), cumene hydroperoxide (80%) (CHP), cumyl alcohol (98 %; 2-phenyl-2-propanol) and acetophenone (98%) were purchased from Sigma Aldrich and used as received. Optima grade heptane and 2-propanol were purchased from Fisher Chemicals and used as received. *Sec*-phenethyl alcohol (98%) was bought from Acros Organics and purified according to standard methods. [4]

5.5.2. Instruments.

The average size of the metallic nanoparticles was determined using a JEM-2100F FETEM transmition electron microscope TEM from Jeol Ltd.

Analysis of the reaction mixtures (cumyl alcohol, acetophenone, cumene hydroperoxide, *sec*-phenethyl alcohol and ethylbenzene hydroperoxide) was performed using a normal phase Agilent 1100 HPLC with 99:1 heptane/isopropanol as the eluent mixture.

5.5.3. Synthesis of supported gold nanoparticles on hydrotalcite (AuNP@HT).

The experimental procedure concerning the synthesis of AuNP@HT is presented in Chapter 2 section 2.6.4.

5.5.4. Synthesis of supported silver nanoparticles on hydrotalcite (AgNP@HT).

The experimental procedures concerning the synthesis of AgNP@HT is presented in Chapter 2 section 2.6.5.

5.5.5. Peroxidation of ethylbenzene under air saturated conditions

In a 50 mL, two-neck round bottom flask, 100 mg of catalyst (either AuNP@HT or AgNP@HT) and 140 mM of cumene hydroperoxide were added to 10 mL of ethylbenzene and the reaction was heated to 80°C. An aliquot was taken from the reaction mixture every hour, centrifuged and subsequently analyzed by HPLC. Air was flowed through the solution and the flow was monitored using a Matheson flow meter. The typical experimental error that was obtained using HPLC analysis is approximately 10% of the reported values.

5.6. References

(1) Zidki, T.; Cohen, H.; Meyerstein, D. Phys. Chem. Chem. Phys. 2006, 8, 3552.

(2) Aprile, C.; Corma, A.; Domine, M. E.; Garcia, H.; Mitchell, C. J. Catal. 2009, 264, 44.

(3) Saiman, M. I. b.; Brett, G. L.; Tiruvalam, R.; Forde, M. M.; Sharples, K.; Thetford, A.; Jenkins, R. L.; Dimitratos, N.; Lopez-Sanchez, J. A.; Murphy, D. M.; Bethell, D.; Willock, D. J.; Taylor, S. H.; Knight, D. W.; Kiely, C. J.; Hutchings, G. J. Angew. Chem. Int. Ed. 2012, 51, 5981.

(4) Hallett-Tapley, G. L.; Silvero, M. J.; González-Béjar, M.; Grenier, M.; Netto-Ferreira, J. C.; Scaiano, J. C. J. Phys. Chem. C. 2011, 21, 10784.

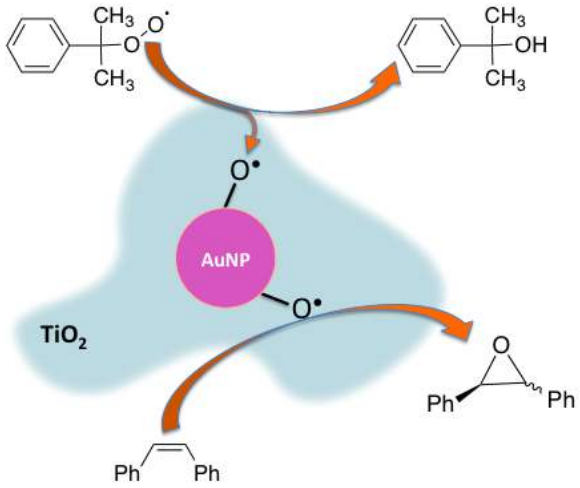

6. Epoxidation of Stilbene using Supported Gold Nanoparticles: Cumyl Peroxyl Radical Activation on the Nanoparticle Surface

6.0. Table of contents

6.1. Introduction

Epoxides are very versatile and reactive species that play an important role in organic chemistry. Epoxidation at the laboratory scale is usually done using peracids, such as *meta*-chloroperbenzoic acid (*m*-CPBA). The Sharpless epoxidation occurs in a concerted fashion using hydroperoxide and a titanium complex as reagents.[1] A heterogeneous version of the Sharpless chemistry has also been developed using a Ti-MCM-41-based catalyst with good results.[2-4] The use of supported AuNP has also been proposed as an alternative for the epoxidation of stilbene.[5] In this type of reaction, a solvent that can be easily oxidized (*e.g.,* cumene or methylcyclohexane) is used in conjunction with an initiator, such as an azo compoud[6] or, more frequently, a hydroperoxide.[7,8] The peroxyl radical formed in the peroxidation process is believed to be responsible for the epoxidation. The ability of peroxyl radicals to react with alkenes and form an epoxide was first proposed by Ingold in 1969.[9] The mechanism of nanoparticle-catalyzed epoxidation proposed by Caps,[10] illustrated in Scheme 6.1, shows that the role of the AuNP is limited to decomposition of the hydroperoxide. In order to continually propagate the free-radical chain, as illustrated in part 1 of Scheme 6.1, the peroxidation must happen as illustrated in Part 2 by using the peroxyl radical formed *via* the radical chain reaction. Therefore, the role of the AuNP in the epoxidation reaction is limited to the

peroxidation of the solvent and does not directly participate in the epoxidation itself.

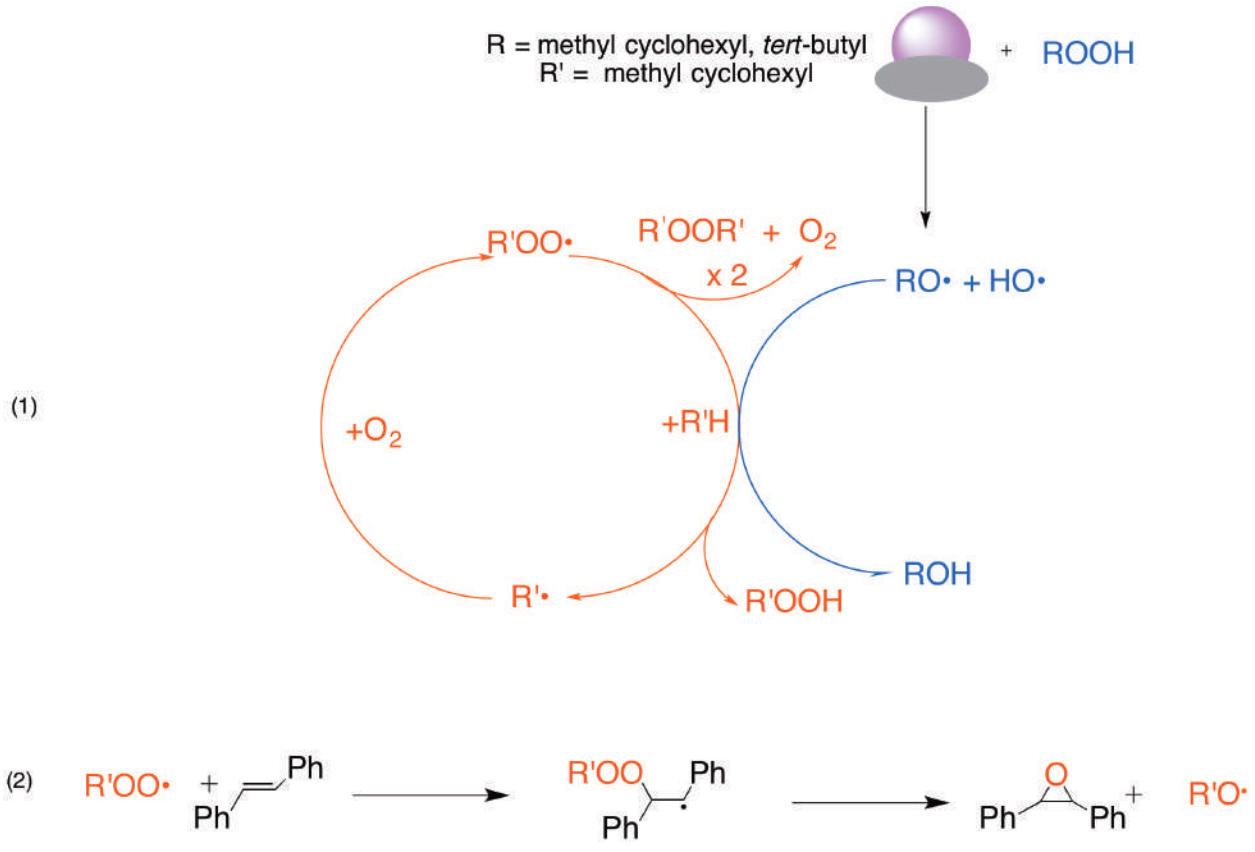

Scheme 6.1. Proposed mechanism for the epoxidation of *trans*-stilbene using a supported AuNP catalyst (adapted from Caps *et al.*[10])

As epoxidation is only a secondary process, an understanding of the primary peroxidation process is required in order to gain mechanistic information on the AuNP mediated epoxidation process. The objective of Chapter 2 was to study this primary peroxidation process. Building on this, a new mechanism for noble

metal nanoparticle epoxidation will be proposed that takes into account the findings from Chapter 2, in conjunction with the findings presented herein.

6.2. Results

6.2.1. Epoxidation of *cis*-stilbene

The catalyst used in this study is commercial AuNP@TiO_2 containing 1% AuNP loading and with an average size of 2.3±0.6 nm (see section 2.2.1 for more details). To gain some insight into the reaction mechanism of AuNP catalyzed epoxidation, *cis*-stilbene was used as the epoxidation substrate under air. In addition, the formation of *cis versus trans* epoxide can reveal information as to whether or not the reaction is concerted. The results of the epoxidation of *cis*-stilbene in the presence of commercial AuNP@TiO_2 after 24 hours are presented in Table 1. The formation of both *cis* and *trans* epoxide was observed only in the presence of the catalyst. The fact that both *cis* and *trans* epoxide were observed strongly indicates that the reaction mechanism is non-concerted, similar to what has been previously observed by Hughes *et al.* when studying stilbene epoxidation using AuNP@graphite as a catalyst.[7] When using TiO_2 as the catalyst more than 48 % of the *cis*-stilbene was converted to what was described by Caps and co-workers[6] as a decomposition product. Finally, no degradation or formation of epoxide was observed in the absence of heterogeneous materials, such as TiO_2 or AuNP@TiO_2.

Table 6.1. % Conversion of *cis*-stilbene and % yield of *trans*-stilbene oxide (TSO) and *cis*-stilbene oxide (CSO) after 24 h reaction.[a]

Catalyst	*% Conversion*	*% yield (TSO)*	*% yield (CSO)*
AuNP@TiO_2	18.7	16.3	2.6
TiO_2	48	ND	ND
No Catalyst	0	ND	ND

[a] Reaction performed at 80°C for 24 hours using cumene as the solvent. (ND= not detected) Reprint with permission from ***Chem. Commun.***, 2014,**50**, 2289 Copyright 2014 Royal Society of Chemistry

As cumene was used as the solvent for this reaction, the yield of both cumene hydroperoxide (CHP) and cumyl alcohol can also be determined for the reaction using AuNP@TiO_2, TiO_2 and in absence of catalyst. As anticipated considering the results discussed in Chapter 2, the amount of cumyl alcohol is higher than the amount of CHP (549 mM versus 89 mM) when using commercial AuNP@TiO_2 as the catalyst. When TiO_2 P25 is used as the catalyst, neither CHP nor cumyl alcohol were obtained as product; however, a trace amount of phenol is obtained, most likely arising from the ionic decomposition of CHP.[11] In the absence of catalyst, even if the conversion for the epoxidation product is zero, one still can observe some peroxidation of the solvent, with the formation of approximately 420 mM of CHP and 24 mM of cumyl alcohol.

Table 6.2. Yields of CHP and cumyl alcohol obtained in the epoxidation reaction of 50 mM *cis*-stilbene in cumene using AuNP@TiO_2.

Catalyst	*CHP(mM)*	*Cumyl Alcohol(mM)*
AuNP@TiO_2	89	549
TiO_2[a]	ND	ND
No Catalyst	420	24

[a]Phenol was obtained as the only product (ND= not detected) Reprint with permission from ***Chem. Commun.***, 2014,**50**, 2289 Copyright 2014 Royal Society of Chemistry

Important information can also be obtained by comparing the results obtained in Table 1 and Table 2. In the absence of catalyst, no epoxidation product was observed, even if 420 mM of CHP was obtained from the peroxidation of cumene. The result obtained using AuNP@TiO_2, shows that *cis*-stilbene is being epoxidized. However cumyl alcohol is the major product obtained from the peroxidation of cumene.

6.2.2 EPR results

An EPR spin-trap experiment (see Section 6.5.4 for details) was done using 5,5-Dimethyl-1-Pyrroline-N-Oxide (DMPO) as a trapping agent. Scheme 6.2 shows the reaction involved in the formation of a radical spin trap adduct between DMPO and a cumyl alkoxyl radical (eq. 1) or a peroxyl radical (eq. 2).

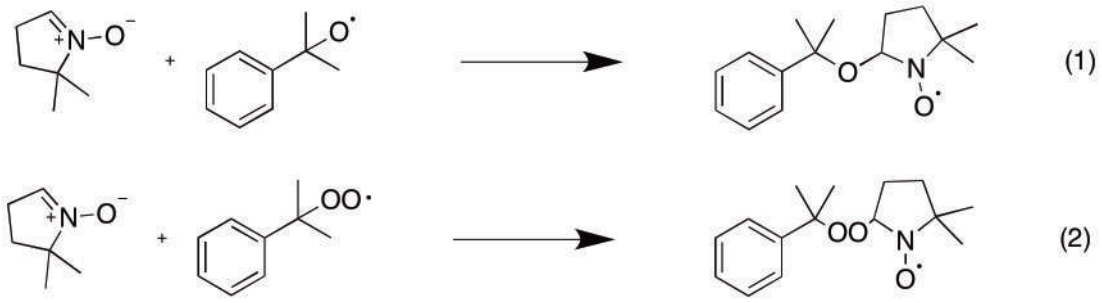

Scheme 6.2. Formation of a spin-trapped radical adducts between DMPO and a cumyl alkoxyl radical (1) or a cumyl peroxyl radical (2).

Briefly, in the absence of *cis*-stilbene, an aliquot of the reaction is added to 50 mg of DMPO the catalyst is then centrifuged out, the reaction mixture is

separated and an EPR spectra is recorded in order to observe the presence of oxygen centered-radical species in solution see Figure 6.1. The coupling constants (determined graphically) are αH = 9.8 G (N=1/2) and αN = 14.9 G (N=1). EPR measurements were collected using a Joel FA-100 X-band instrument. The specific signal identity (*i.e.,* alkoxyl radical *vs.* peroxyl radical) was not possible due to the characteristic ambiguotiy of EPR spin-trap experiments.[12] Spectra were also recorded in the presence of TiO_2 or in the absence of catalyst, and show the absence of spin trapped species (Figures 6.2 and 6.3).

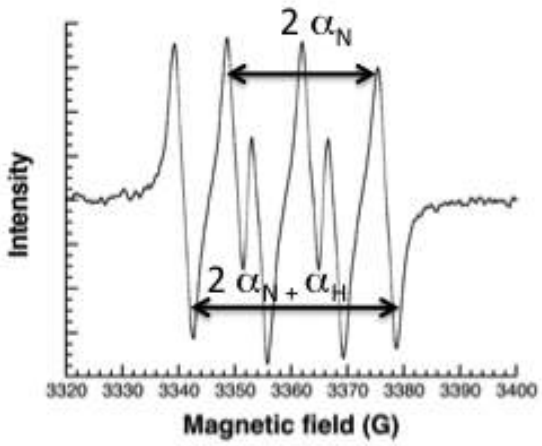

Figure 6.1. Representative EPR spectrum for the oxygen centered radical/DMPO adduct obtained in the AuNP@TiO_2-catalyzed peroxidation of cumene using 10 mL of cumene, 5.0 mM of TBHP and 50 mM DMPO. The coupling constants are αH = 9.8 G and αN = 14.9 G. Adapted t with permission from ***Chem. Commun.***, 2014,**50**, 2289 Copyright 2014 Royal Society of Chemistry

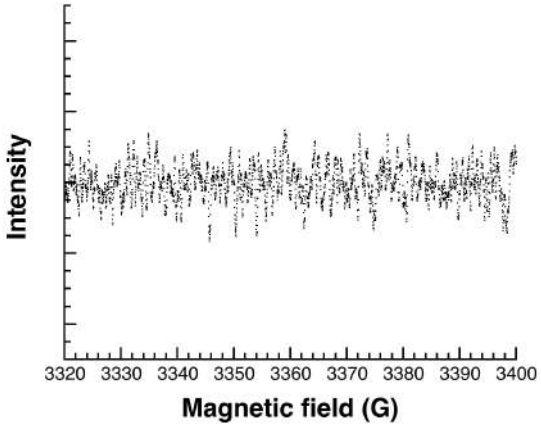

Figure 6.2. EPR spectrum recorded for the DMPO spin-trap experiment done in the absence of heterogeneous materials. Reprint with permission from ***Chem. Commun.***, 2014,**50**, 2289 Copyright 2014 Royal Society of Chemistry

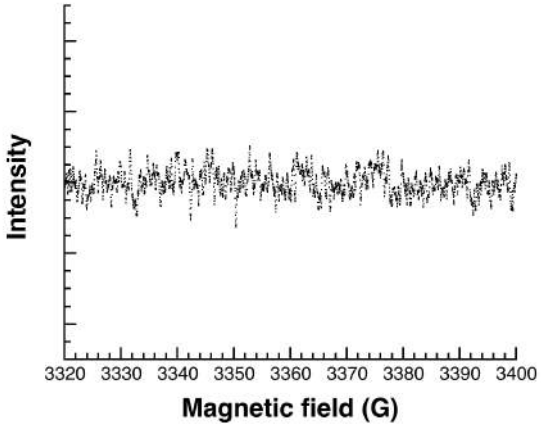

Figure 6.3. EPR spectrum for the DMPO spin-trap experiment done in the presence of TiO_2. Reprint with permission from ***Chem. Commun.***, 2014,**50**, 2289 Copyright 2014 Royal Society of Chemistry

6.3. Discussion

From the results presented herein, *cis*-stilbene epoxidation products are only obtained when using commercial AuNP@TiO_2 as the catalyst. Considering the results obtained in Chapter 2 on the investigation of the AuNP mediated peroxidation of cumene as well as the results presented in Table 2, the amount of peroxyl radical present in the solution should be low, making the peroxyl radical the unlikely species responsible for stilbene epoxidation. Unfortunately, the EPR spectrum shown in Figure 6.1 is characteristically ambiguous[12]. This is a representative EPR spectrum for the oxygen centered radical/DMPO adduct) and only indicates that an oxygen centered radical is present in the reaction mixture. This cannot confirm the presence of either the alkoxyl radical or the peroxyl radical as the dominant radical species.

Previous work from the literature has shown that direct oxygen activation can occur at the surface of small AuNP less than 2 nm in diameter which can lead to the epoxidation of styrene.[13] The propensity for AuNP to activate oxygen has been related to their size and shape using computational model as shown by Corma *et al.*[14] The results presented in Chapter 2 demonstrated the ability of supported AuNP to effectively decompose peroxyl radicals on the AuNP surface in order to form reactive surface oxygen species which could be responsible for the epoxidation reaction observed in the *cis*-stilbene case. The mechanism of the epoxidation could then involve the proposed steps presented in scheme 6.3,

where the peroxyl radical interacts with the AuNP and undergoes subsequent decomposition in order to form the reactive surface oxygen species, available for participation in the epoxidation process.

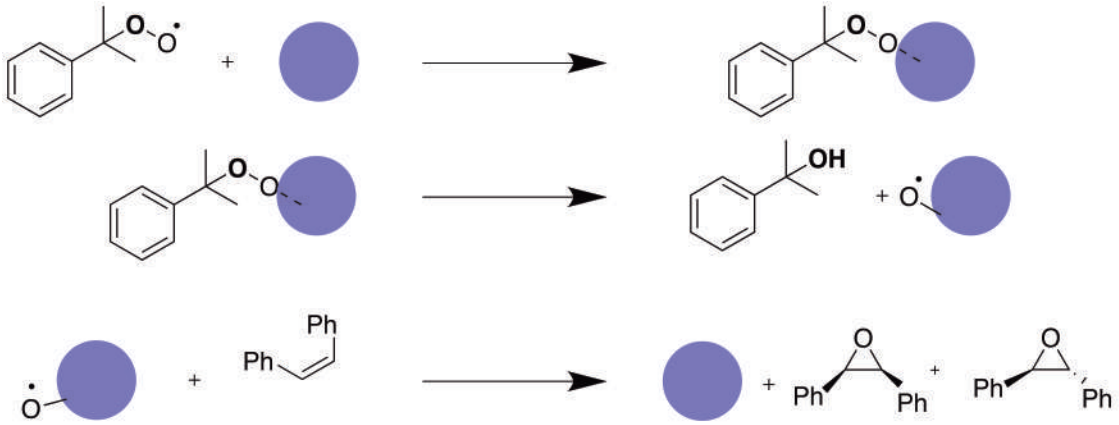

Scheme 6.3. Proposed steps for the epoxidation of *cis*-silbene involving reactive oxygen species on the AuNP surface. Reprint with permission from ***Chem. Commun.***, 2014,**50**, 2289 Copyright 2014 Royal Society of Chemistry

The exact nature of the intermediates involved in this reaction is open to speculation. Based on the previous work of Bruice and Castellino,[15] two different epoxidation pathways can be envisioned. First, a pathway where the reactive surface oxygen species directly attacks the stilbene double bond and, second, a mechanism that would involve an electron transfer. These two pathways are shown in scheme 6.4 where in pathway *a* the direct radical reaction is proposed and in pathway *b*, AuNP lead to the formation of stilbene radical cation and ionic gold that would then react together to form a radical intermediate. The isomerisation of azobenzene[16] in the presence of AuNP has also been proposed

to occur by way of electron transfer with the participation of AuNP surface. Finally, in both pathways depicted in scheme 6.4, a ring closure step can occur. In pathway *a*, the ring closure is due to a radical-radical recombination whereas in pathway *b*, the recombination step involves the oxygen species on the nanoparticle and the radical present on the stilbene backbone. In addition, in both cases the formation of *cis* and *trans*-stilbene oxide is possible due to rotation about the central stilbene C-C bond as the result of a radical mediated step.

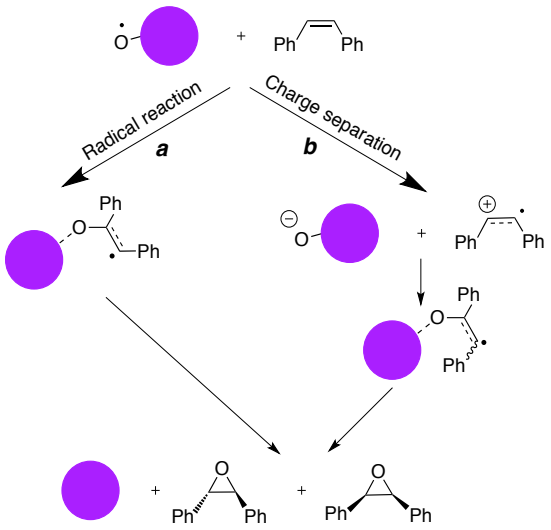

Scheme 6.4. Possible pathways for the direct reaction of the AuNP-oxygen radical adduct and *cis*-stilbene. Reprint with permission from ***Chem. Commun.***, 2014,**50**, 2289 Copyright 2014 Royal Society of Chemistry

6.4. Conclusions

A new mechanism for the epoxidation of *cis*-stibene in the presence of an oxidizable solvent (cumene), oxygen and commercial AuNP@TiO_2 is proposed. The results obtained using the EPR spin-trap experiment together with results obtained in Chapter 2, indicate that participation of the cumyl peroxyl radical in the epoxidation mechanism is unlikely due to the fact that cumyl alcohol is the major product of the peroxidation and that the most probable radical species present in solution is the alkoxyl radical. The proposed mechanism involves the formation of a reactive oxygen surface species. Two pathways are then suggested. In the first pathway, a direct reaction between the reactive oxygen species followed by ring closure is proposed, whereas the second pathway involves an electron transfer from the AuNP to form a stilbene radical cation which would then react with the negatively charged oxygen on the AuNP surface. The stereochemistry of the reaction can be explained by the fact that in both proposals the reaction goes through non-concerted type intermediates.

6.5. Experimental

6.5.1. Reagents.

Cumene, cumene hydroperoxide (CHP), (technical grade 80%, largely cumene impurity), cumyl alcohol (98 %; 2-phenyl-2-propanol), *tert*-butyl hydroperoxide solution in H_2O (80%), *trans*-stilbene, *trans*-stilbene oxide, *cis*-stilbene, *cis*-stilbene

oxide, and optima grade acetonitrile were purchased from Sigma-Aldrich and used as received. TiO_2 P25 was a gift from Evonik Degussa. AUROlite™ 1% AuNP@TiO_2 extrudates were purchased from Strem Chemicals and ground with a mortar and pestle prior to use Optima grade heptane and 2-propanol used in HPLC analysis were purchased from Fisher Chemicals and used as received.

6.5.2. Instrumentation.

The size of supported AuNP nanoparticles was determined using a JEM-2100F FETEM transmission electron microscope (TEM) from Jeol Ltd. Analysis of the reaction mixture (cumyl alcohol and cumene hydroperoxide.) was carried out using a normal phase Agilent 1100 HPLC (eluent 99:1 heptane/2-propanol). The amount of *trans*-stilbene, *trans*-stilbene oxide, *cis*-stilbene, *cis*-stilbene oxide were determined using a Waters HPLC fitted with a reverse phase C-18 silica column and employing an eluent mixture of 60:40 acetonitrile:water. EPR spectra were recorded on a Jeol FA-100 spectrometer.

6.5.3. Epoxidation of *cis*-stilbene.

In a 50 mL, two-neck round bottom flask, 0.1 g of catalyst, 94 μL (0.5 mmol) of *cis*-stilbene and 7.8 μL (0.05 mmol) of an aqueous solution of *tert*-butyl hydroperoxide were added to 10 mL of cumene. 500 μL (0.32 mmol) of *tert*-butyl benzene were added as an internal standard and the reaction heated to 80°C. After 24 hours, the reaction was analyzed using both normal and reverse

phase HPLC. Normal phase chromatography was used to assess the yields of peroxidation products (acetophenone, cumyl alcohol and cumene hydroperoxide) and reverse phase HPLC to examine the epoxidation products, that is, *cis*-stilbene oxide and *trans*-stilbene oxide. Control reactions were carried out using the support itself (TiO_2 P25) in the absence of heterogeneous materials (*tert*-butyl hydroperoxide initiator only).

6.5.4. EPR spin-trap experiments.

In a 50 mL, two-neck round bottom flask, 0.1 g of catalyst and 7.8 μL (0.05 mmol) of an aqueous solution of *tert*-butyl hydroperoxide was added to 10 mL of cumene and the reaction heated to 80°C. Aliquots of the reaction were added to a solution containing 50 mg (0.44 mmol) of DMPO spin trap. This solution was then centrifuged and the EPR spectrum recorded. Control EPR experiments performed using either TiO_2 P25 or no heterogeneous materials (Figures 6.2 and 6.3, respectively).

6.6. Appendix 1: Representative HPLC chromatography

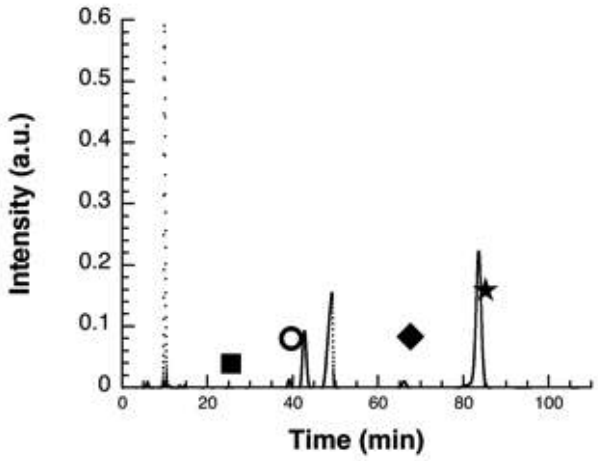

Figure 6.4. Representative normal phase HPLC spectrum of the AuNP@TiO_2-catalyzed epoxidation of *cis*-stilbene. Peak identification: *cis*-stilbene oxide(■),*trans*-stilbene oxide (O),*tert*-butyl benzene, (◆) and *cis*-stilbene (★). Reprint with permission from ***Chem. Commun.***, 2014,**50**, 2289 Copyright 2014 Royal Society of Chemistry

6.7. Appendix 2: EPR spin trap

The EPR (electron paramagnetic resonance) or ESR (electron spin resonance) is a technique that is used to study a compound or a material that has unpaired electron. Similar to NMR, the magnetic field lift the degeneracy of the electron spin state as is shown in scheme 6.5.

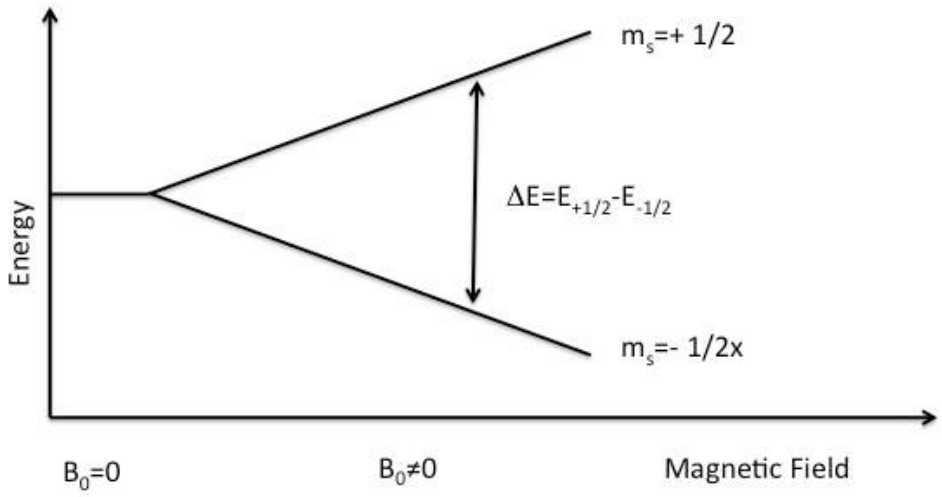

Scheme 6.5. Magnetic field splits the energy levels of the electron.

The fundamentals of EPR spectroscopy are given by the equation $h\upsilon=g_e\mu_b B_o$, where the $h\upsilon$ accounts for the microwave irradiation source, g_e the g-factor (influenced by the surrounding environment), μ_b is the Bohr magneton and B_o is the intensity of the magnetic field. There are two types of EPR, continuous wave (CW) and pulsed. The continuous wave EPR is the most common form of EPR spectroscopy and is the method used by the Scaiano group at the University of Ottawa. In continuous wave EPR, the magnetic field is varied while the microwave irradiation source is kept constant. As a result, one observes a signal once microwave wavelength and $g_e\mu_b B_o$ are in resonance. Importantly, the signal of continuous wave EPR is characteristically reported as the first derivative of absorption. Furthermore, direct observation of radical species is possible if the lifetime of the radical species is long lived, or time resolved techniques can be

used. In the case of the present study, the lifetimes of the radical species present are not long enough for their direct observation. Since time resolved EPR techniques are not available in our facilities, the use of a radical spin trap was necessary. As its name implies, spin traps will "capture" any radical species and, in the process, form a persistent radical that can be easily observed by conventional EPR spectroscopy. The resulting pattern of the radical intermediate in the EPR spectrum is attributed to interactions between the unpaired electron and the nuclear spin. This interaction will indirectly allow for identification of the radical species.

6.8. References

(1) Katsuki, T.; Sharpless, K. B. J. Am. Chem. Soc. 1980, 102, 5974.

(2) Li, K.-T.; Lin, P.-H.; Lin, S.-W. Appl. Catal. A 2006, 301, 59.

(3) Corma, A.; Domine, M.; Gaona, J. A.; Jord, J. L.; Navarro, M. T.; Rey, F.; Pérez-Pariente, J.; Tsuji, J.; McCullochd, B.; Nemethd, L. T. Chem. Commun. 1998, , 2211.

(4) Choudharya, V. R.; Patila, N. S.; Bhargavab, S. K. Catal. Lett. 2003, 89, 51.

(5) Lignier, P.; Morfin, F.; Mangematin, S.; Massin, L.; Rousset, J.-L.; Caps, V. Chem. Commun. 2007, 186.

(6) Lignier, P.; Mangematin, S.; Morfin, F.; Rousset, J.-L.; Caps, V. Catal. Today 2008, 138, 50.

(7) Hughes, M. D.; Xu, Y.-J.; Jenkins, P.; McMorn, P.; Landon, P.; Enach, D. I.; Carley, A. F.; Attard, G. A.; Hutchings, G. J.; King, F.; Stitt, E. H.; Johnston, P.; Griffin, K.; Kiely, C. J. Nature 2005, 437, 1132.

(8) Lignier, P.; Morfin, F.; Piccolo, L.; Rousset, J.-L.; Caps, V. Catal. Today 2007, 122, 284.

(9) Ingold, K. U. Acc. Chem. Res. 1969, 2, 1.

(10) Mendez, V.; Guillois, K.; Daniele, S.; Tuel, A.; Caps, V. Dalton Trans. 2010, 39, 8457.

(11) Crites, C.-O. L.; Hallett-Tapley, G. L.; Frenette, M.; González-Béjar, M.; Netto-Ferreira, J. C.; Scaiano, J. C. ACS Catal. 2013, 3, 2062.

(12) Guo, Q.; Qian, S. Y.; Mason, R. P. J. Am. Soc. Mass Spectr. 2003, 14, 862.

(13) Gao, W.; Chen, X. F.; Li, J. C.; Jiang, Q. J. Phys. Chem. C 2010, 114, 1148.

(14) Boronat, M.; Corma, A. Dalton Trans. 2010, 39, 8538.

(15) Castellino, A. J.; Bruice, T. C. J. Am. Chem. Soc. 1988, 110, 158.

(16) Hallett-Tapley, G. L.; D'Alfonso, C.; Pacioni, N. L.; D, M.; Gonzalez-Bejar, M.; Lanzalunga, O.; Alarcon, E. I.; Scaiano, J. C. Chem. Commun. 2013, 49, 10073.

7. The role of AuNP-Radical Interactions in the Peroxidation of Tetralin

7.0. Table of contents

7.1. Introduction

The peroxidation of tetralin in the presence of metal salts has been studied for several decades[1-3] and has been suggested to involve a free radical type mechanism where the metal ions act as Fenton reagents. Previous chapters in this thesis demonstrate how the interaction between free radicals and AuNP influence the peroxidation of cumene (Chapter 2), and ethylbenzene (Chapter 4). As discussed in Chapters 4 and 6, AuNP surface bound species are suggested to participate in both the peroxidation of ethylbenzene and in the epoxidation of *cis*-stilbene. The participation of nanoparticle surface bound species has also been proposed in the epoxidation of 1-decene[4] and in the peroxidation of toluene.[5] The main objective in this Chapter is to see if it is possible to extend the mechanism that has been proposed in previous chapters to the peroxidation of tetralin and, therefore, determine if our previous findings can explain the product distribution observed in the tetralin system. The possible products formed via tetralin peroxidation are presented in Scheme 7.1: α-tetralone (**1**), 1,2,3,4-tetrahydro-1-naphthol (**2**) and α-tetralin hydroperoxide (**3**). The catalyst to be used for this study will be commercial AuNP@TiO_2.

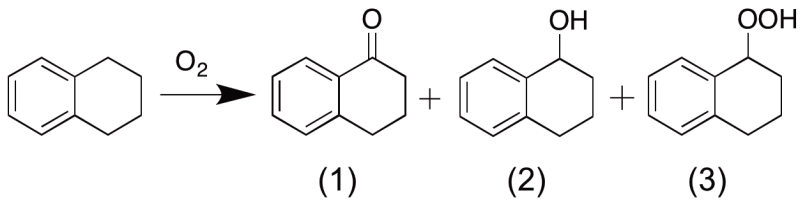

Scheme 7.1. Possible products formed by the peroxidation of tetralin: α-tetralone (1), 1,2,3,4-tetrahydro-1-naphthol (2) and α-tetralin hydroperoxide (3).

7.2. Results

7.2.1. Results at 30°C

The peroxidation of tetralin was performed over an 8 hour period under oxygen flow (see the Section 7.5.3 for further details). Tetralin is a very reactive solvent towards peroxidation and, in order to ensure our results can be reproducible, tetralin was filtered through acidic alumina immediately prior to use in order to destroy all traces of hydroperoxide present in the commercial sample . Two series of experiments were then performed. In the first one, no initiator was added to the reaction mixture and, in the second, 42 mM of *tert*-butyl hydroperoxide (TBHP) was added as an initiator. The results obtained at 30°C in the absence of *tert*-butyl hydroperoxide were done using 3 different reaction conditions. Firstly in the absence of catalyst (no heterogeneous materials) where no product formation was observed. The second set of results were obtained in the presence of TiO_2 P25, where some product formation was observed (Figure 7.1) and, finally, the peroxidation of tetralin was examined in the presence of

AuNP@TiO_2 (Figure 7.2) where 1,2,3,4-tetrahydro-1-naphthol was initially the only product obtained after an induction period of 5 hours, followed by the formation of a mixture of 1,2,3,4-tetrahydro-1-naphthol, α-tetralone and α-tetralin hydroperoxide after 6 hours reactions. Moreover, after 7 hours of reaction, the major product formed was the desired tetralin hydroperoxide. The amount of tetralin hydroperoxide further increased as the monitoring time of the reaction was extended to 24 hours (Figure 7.3).

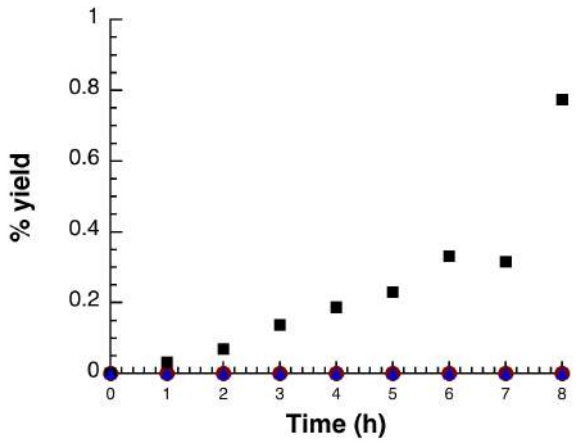

Figure 7.1. Products obtained from the peroxidation of tetralin in the absence of initiator using TiO_2 P25 as a catalyst at 30°C: α-tetralin hydroperoxide (■),α-tetralone (▲), and 1,2,3,4-tetrahydro-1-naphthol (●)

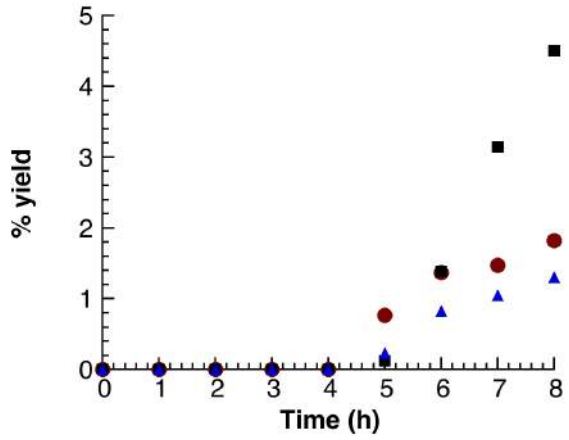

Figure 7.2. Products obtained from the peroxidation of tetralin in the absence of initiator using commercial AuNP@TiO_2 as a catalyst at 30°C: α-tetralin hydroperoxide (■),α-tetralone (▲), and 1,2,3,4-tetrahydro-1-naphthol (●).

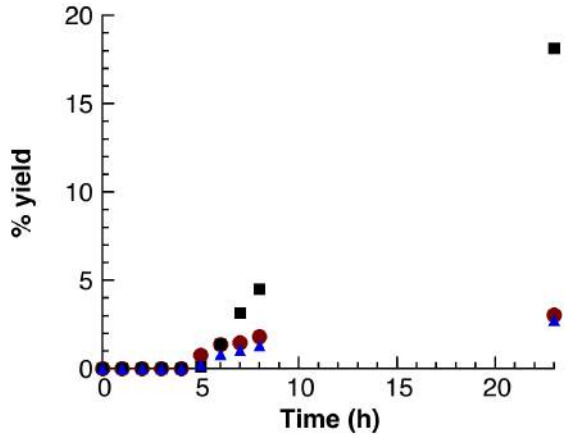

Figure 7.3. Products obtained from the peroxidation of tetralin in the absence of initiator using TiO_2 P25 as a catalyst at 30°C after 23 hours reactions: α-tetralin hydroperoxide (■),α–tetralone (▲), and 1,2,3,4-tetrahydro-1-naphthol (●).

In a second series of experiments the peroxidation of tetralin was investigated using 42 mM of tert-butyl hydroperoxide (TBHP) as initiator. Similar to the first series of experiments, the reaction was done in the absence of heterogeneous materials, in the presence of TiO_2 P25 and in the presence of commercial AuNP@TiO_2. The reaction done in the absence of catalyst, presented in Figure 7.4, shows that only a minimal quantity of α-tetralin hydroperoxide is obtained after 8 hours. The reaction done in the presence of TiO_2 P25 (Figure 7.5) also shows negligible α-tetralin hydroperoxide formation. Only in the presence of a AuNP@TiO_2 catalyst (Figure 7.6) was the generation of α-tetralin hydroperoxide favoured (14.1%), in addition to small amounts of 1,2,3,4-tetrahydro-1-naphthol and α-tetralone. The formation of the alcohol and ketone by-products occurred primarily within the first few hours of reaction. When comparing the results obtained in the absence and in the presence of TBHP (figure 7.6), an induction period was not observed when the initiator was present in the reaction mixture (Figure 7.4 to Figure 7.6).

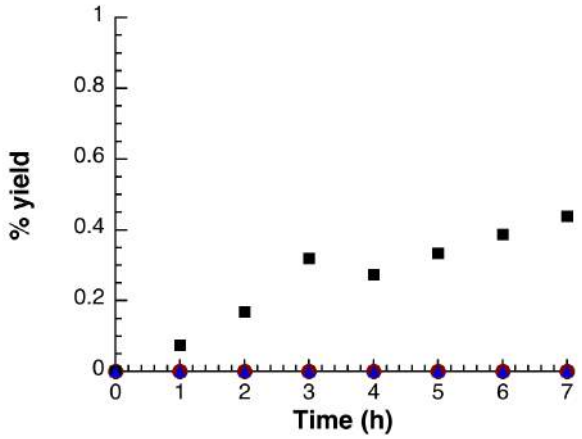

Figure 7.4. Products obtained from the peroxidation of tetralin using 42 mM of TBHP initiator in the absence of heterogeneous catalysts at 30°C: α-tetralin hydroperoxide (■),α-tetralone (▲), and 1,2,3,4-tetrahydro-1-naphthol (●).

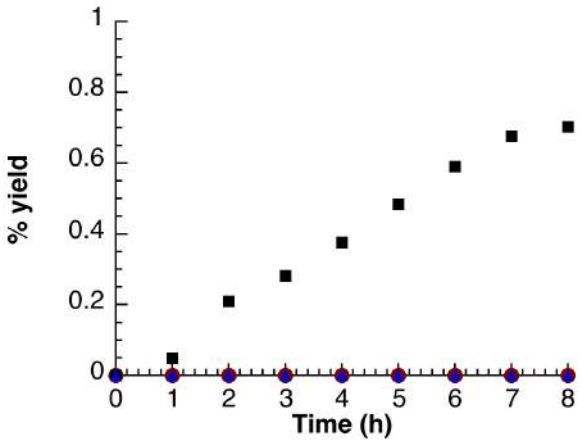

Figure 7.5. Products obtained from the peroxidation of tetralin using 42 mM of TBHP initiator and TiO_2 P25 as a catalyst at 30°C: α-tetralin hydroperoxide (■),α-tetralone (▲), and 1,2,3,4-tetrahydro-1-naphthol (●). Compare with figure 7.2

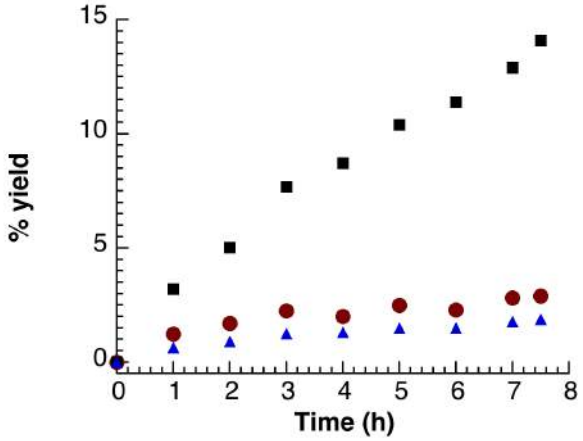

Figure 7.6. Products obtained from the peroxidation of tetralin using 42 mM of TBHP initiator and using commercial AuNP@TiO_2 as a catalyst at 30°C: α-tetralin hydroperoxide (■),α-tetralone (▲), and 1,2,3,4-tetrahydro-1-naphthol (●).

In order to put into perspective the results obtained above, a bar graph is presented in Figure 7.7 showing that some TBHP must be present in the reaction medium in order to increase the α-tetralin hydroperoxide formation Figure 7.2 versus Figure 7.4 to 7.6. Futhermore the presence of AuNP increases significantly the product when TBHP is used as initiator.

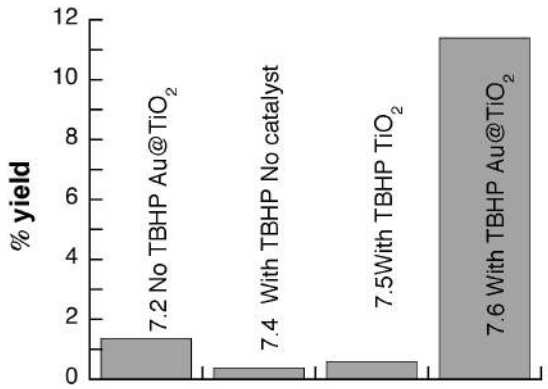

Figure 7.7. Amount of α-tetralin hydroperoxide obtained after 6 hours reaction as shown in Figure 7.2 to 7.6.

7.2.2. Results at 80°C

In order to investigate the effects of reaction temperature on the peroxidation of tetralin catalyzed by supported AuNP, the peroxidation pathway was studied again in the presence and absence of TBHP initator at 80°C. It is worth noting that the thermal decomposition of TBHP at 80°C is minimal. The product distribution for the peroxidation of tetralin in the absence of initator using no heterogeneous materials and commercial AuNP@TiO_2 as catalysts are shown in Figures 7.8 and 7.9 respectively. From Figure 7.8, only approximately 5% of α-tetralin hydroperoxide is obtained in the absence of any catalyst after 8 hours of reaction, following an initial induction period of the peroxidation reaction over 2 hours. When TiO_2 P25 was used as a catalyst no product formation was

observed likely due to the favoured acidic decompostion of α-tetralin hydroperoxide under these conditions, as discussed in Chapter 2 for the TiO_2 degradation of cumene hydroperoxide (see Section 2.3.2). When commercial AuNP@TiO_2 was employed as a catalyst (Figure 7.9), both 1,2,3,4-tetrahydro-1-naphthol and α-tetralone were obtained after an initial induction period of 3 hours. After 4 hours, formation of α-tetralin hydroperoxide was also observed and the its quantity increased over time. The final product conversions obtained after 8 hours are as follows: α-tetralin hydroperoxide (9.3 %), 1,2,3,4-tetrahydro-1-naphthol (6.9%) and α-tetralone (8.0%). Interestingly, from the values presented above, it is clear that at 80°C, formation of α-tetralin hydroperoxide is not as favoured as at 30°C with more of the alcohol and ketone products being observed in this case.

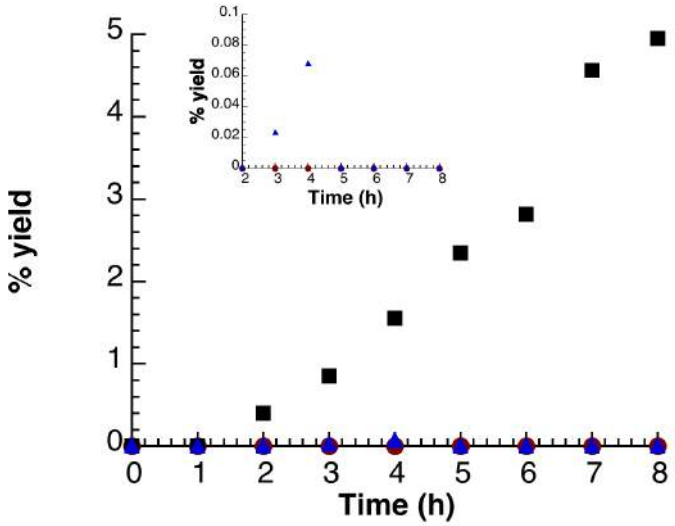

Figure 7.8. Products obtained from the peroxidation of tetralin in the absence of initiator and heterogeneous materials at 80°C: α-tetralin hydroperoxide (■),α-tetralone (▲), and 1,2,3,4-tetrahydro-1-naphthol (●).

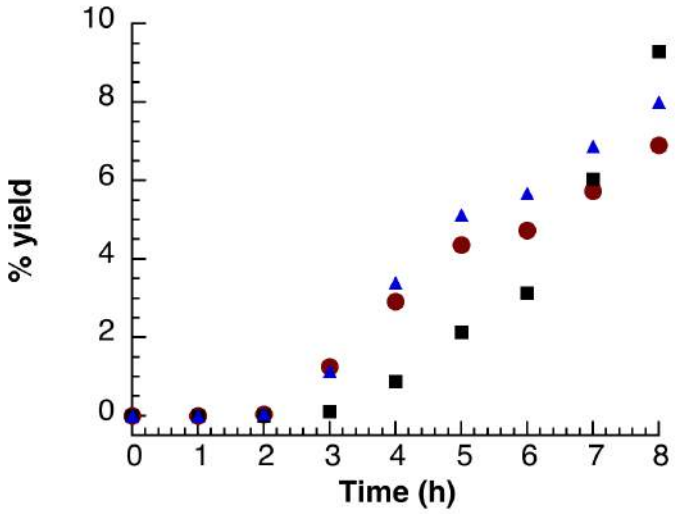

Figure 7.9. Products obtained from the peroxidation of tetralin in the absence of initiator and using commercial AuNP@TiO_2 as a catalyst at 80°C: α-tetralin hydroperoxide (■),α-tetralone (▲), and 1,2,3,4-tetrahydro-1-naphthol (●).

A second series of experiments was also performed at 80°C using TBHP as an initiator. The results obtained can be seen in Figures 7.10 to 7.12. In the absence of any catalyst (Figure 7.10), no induction period was observed (similar to the results using TBHP at 30°C) and α-tetralin hydroperoxide was obtained as the major product (15%). The results obtained using TiO_2 P25 as a catalyst (Figure 7.11) show that α-tetralin hydroperoxide is, again, the major product formed, but does so quite quickly (within the first hour of reaction) and its yield remains mostly constant throughout the 8 hours course of the reaction. Similarly, Figure 7.12 illustrates the product formation for the peroxidation of tetralin when commercial AuNP@TiO_2 is used as a catalyst. When comparing the results

obtained in the absence of TBHP (Figure 7.9), one can see that the induction period of 2 hours is no longer present. Furthermore, 1,2,3,4-tetrahydro-1-naphthol and α-tetralone are rapidly obtained within the first hour, followed by increasing formation of α-tetralin hydroperoxide. A mixture of products are observed after 8 hours, with no peroxidation product being favoured at the elevated reaction temperature in the presence of TBHP initiator: 7.7% of 1,2,3,4-tetrahydro-1-naphthol, 10.2% of α-tetralin hydroperoxide and 7.4 % of α-tetralone. Interestingly, in the presence of supported AuNP, the product distribution resulting from the peroxidation of tetralin (i.e. the final mixture) is considerably different when compared with the results obtained when using TiO_2 P25 alone was employed (exclusive formation of the hydroperoxide). Such a change may provide valuable information on the role of AuNP in the mechanism of this particular peroxidation pathway.

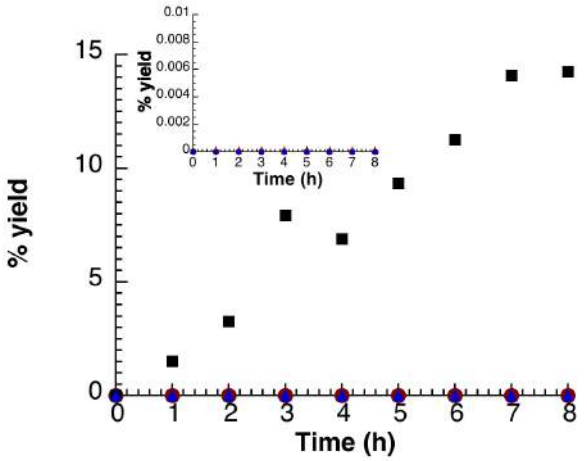

Figure 7.10. Products obtained from the peroxidation of tetralin in the absence of heterogeneous catalysts using 0.4 mmol of TBHP initiator at 80°C: α-tetralin hydroperoxide (■),α-tetralone (▲), and 1,2,3,4-tetrahydro-1-naphthol (●). The insert shows that no significant amount of either α-tetralone or 1,2,3,4-tetrahydro-1-naphthol is formed

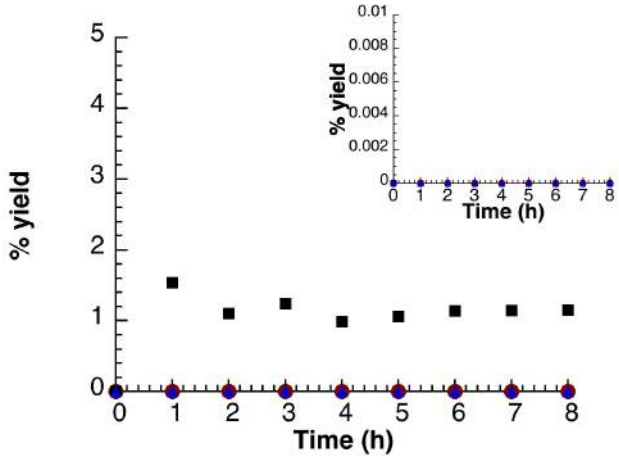

Figure 7.11. Products obtained from the peroxidation of tetralin using 42 mM of TBHP initiator and using commercial TiO_2 P25 as a catalyst at 80°C: tetralin hydroperoxide (■),α-tetralone (▲), and 1,2,3,4-tetrahydro-1-naphthol (●).α-tetralone is formed The insert shows that no significant amount of either tetralone or 1,2,3,4-tetrahydro-1-naphthol is formed

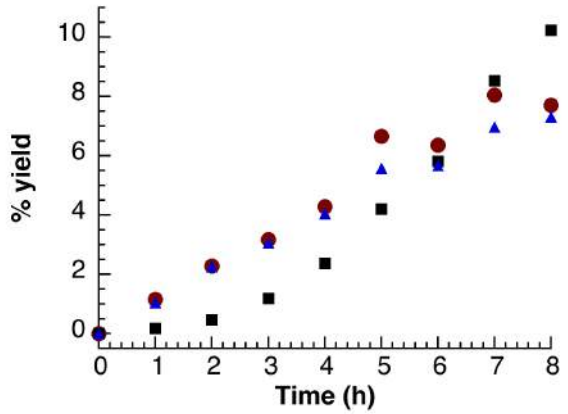

Figure 7.12. Products obtained from the peroxidation of tetralin using 42 mM of TBHP initiator and using commercial AuNP@TiO_2 as a catalyst at 80°C: α-tetralin hydroperoxide (■),α-tetralone (▲), and 1,2,3,4-tetrahydro-1-naphthol (●).

The results obtained at 30°C and 80°C show that the supported AuNP catalysts clearly enhance tetralin peroxidation product formation when compared to the amounts obtained in the absence of the catalyst. However, the most considerable difference between the two reaction temperatures lies in the nature of the product being formed when AuNP catalysts is used. At 30°C, α-tetralin hydroperoxide is the major product obtained, whereas at 80°C, a mixture of α-tetralin hydroperoxide, 1,2,3,4-tetrahydro-1-naphthol and tetralone was observed, indicating that formation of both the alcohol and ketone products is temperature dependent. A bar graph (Figure 7.13) illustrates the formation of α-tetralin hydroperoxide and the total amount of peroxidation product after 8 hours. From this plot one can see that TiO_2 is a poor catalyst at

80°C and that the presence of AuNP leads to the formation other products (α-tetralone and 1,2,3,4-tetrahydro-1-naphthol) rather than only the α-tetralin hydroperoxide as is the case in the absence of catalyst.

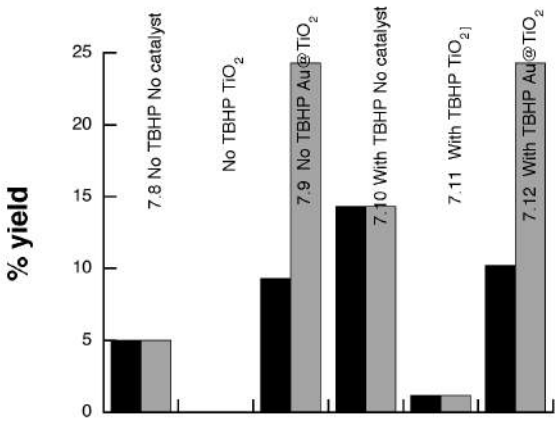

Figure 7.13. Bar graph illustrating the formation of: α-tetralin hydroperoxide (■), Total peroxidation product (■) at 80°C under different reaction condition (figure 7.8 to figure 7.12)

7.2.3. The effect of catalysts on α-tetralin hydroperoxide decomposition

To further access the stability of tetralin hydroperoxide at both 30 and 80°C, experiments analogous to those carried out in Chapter 2, Section 2.3.2 were also carried out. In brief, tetralin was allowed to be oxidized to α-tetralin hydroperoxide at 80°C in the absence of TBHP and was then diluted in toluene. The solution was then placed in contact with the desired catalyst and the

decomposition, or disappearance of the α-tetralin hydroperoxide was monitored over time using HPLC analysis (see Section 7.5.4 for more details). In the absence of any heterogeneous catalyst (Figure 7.14), the degradation of tetralin hydroperoxide is almost null at 30°C and very small at 80°C. When the same experiment was performed using TiO_2 P25 as the control catalyst (Figure 7.15) it was again demonstrated that the decomposition of the hydroperoxide at 30°C is mostly null. The more prevalent, but still minimal, hydroperoxide degradation observed at 80°C does not result in 1,2,3,4-tetrahydro-1-naphthol or α-tetralone, which is most likely due to the acidic mineralization of the hydroperoxide.[6] In the presence of supported AuNP (AuNP@TiO_2; Figure 7.16) a slow decomposition of α-tetralin hydroperoxide decomposition to 1,2,3,4-tetrahydro-1-naphthol or tetralone was observed at 30°C, showing only approximately 10% loss of the hydroperoxide over 8 hours. However, when the reaction temperature was increased to 80°C, α-tetralin hydroperoxide was completely degraded over the 8 hour time period into its free radical decomposition products, 1,2,3,4-tetrahydro-1-naphthol and α-tetralone. Closer investigation of Figure 7.14 reveals a curve that appears to be composed of two different reaction domains. In the first portion of the curve, more than 50% of the α-tetralin hydroperoxide is rapidly decomposed within the first hour of reaction. The hydroperoxide decomposition then slows down and requires much longer reaction times (up to 8 hours), giving rise to a distinct change in the

slope of the rate curve. This behaviour may be due to decreased activity of the Fenton catalyst as the reaction proceeds, as was observed in Chapter 3.

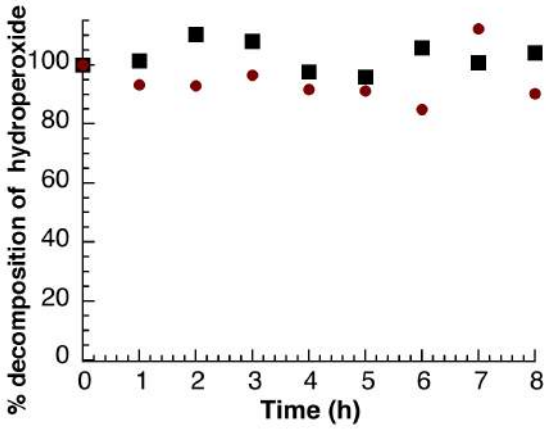

Figure 7.14. % Stability of α-tetralin hydroperoxide in the absence of catalyst at 30° C (■) and 80°C (●).

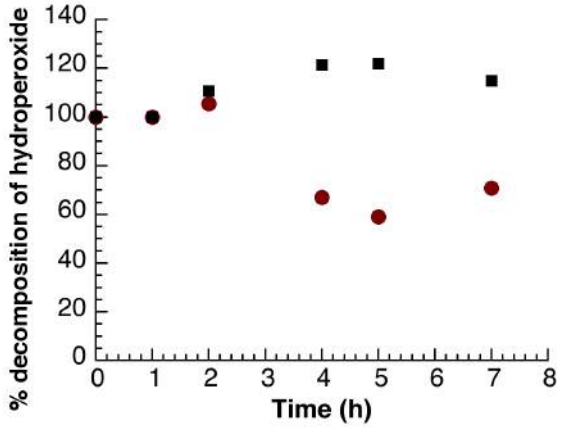

Figure 7.15. % Stability of α-tetralin hydroperoxide using TiO_2 P25 as a catalyst at 30° C (■) and 80°C (●).

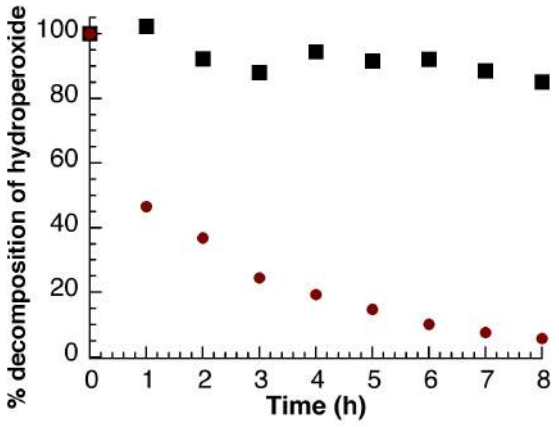

Figure 7.16. % Stability of α-tetralin hydroperoxide using commercial AuNP@TiO_2 as a catalyst at 30° C (■) and 80°C (●).

7.2.4. Lipoic acid experiments

Scheme 7.2. Chemical structure of α–Lipoic acid

In order to more closely investigate the participation of the AuNP suface in the tetralin peroxidation mechanism, lipoic acid (scheme 7.2) was used as a surface capping agent. These experiments are analogous to those discussed in Chapter 2, Section 2.3.7.2, where lipoic acid was proposed to act as protector of the AuNP surface, thus preventing the surface induced decomposition of cumyl

peroxyl radicals and stopping the peroxidation reaction. Similar experiments were carried out replacing the cumene for tetralin to determine the effect of the AuNP surface on the tetralin peroxidation mechanism. The results, presented in Figures 7.17 and 7.18, show that at both 30°C and 80°C, the addition of lipoic acid after 1 hour stops the formation of tetralin hydroperoxide as well as the alcohol and ketone peroxidation products as can be seen by the plateau in the % conversion of each of these compounds following addition of the surface protecting agent[7].

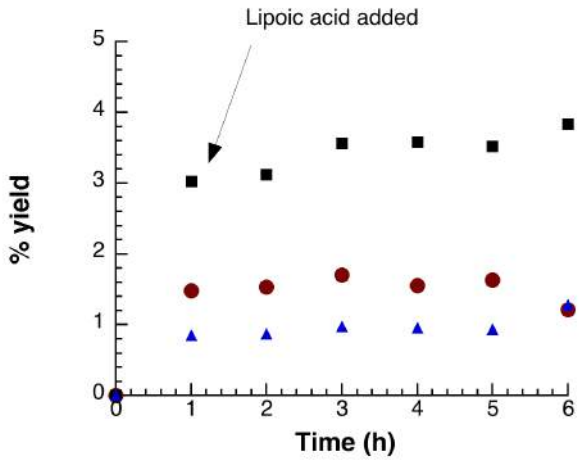

Figure 7.17. % Conversion for the tetralin peroxidation products using TBHP initiator and commercial AuNP@TiO_2 as a catalyst at 30°C with the addition of lipoic acid after 1 hour: α-tetralin hydroperoxide (■),α-tetralone (▲), and 1,2,3,4-tetrahydro-1-naphthol (●).

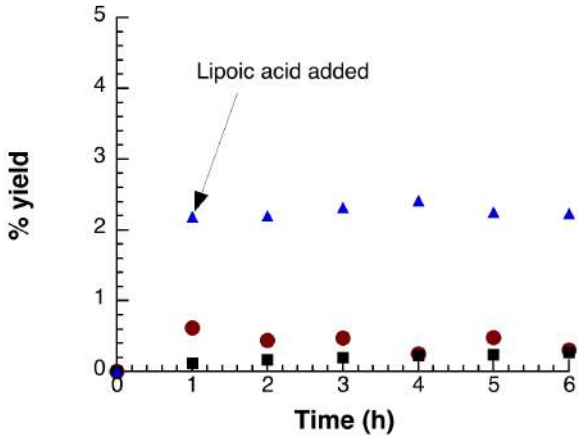

Figure 7.18. % Conversion for the tetralin peroxidation products using TBHP initiator and commercial AuNP@TiO_2 as a catalyst at 80°C with the addition of lipoic acid after 1 hour: α-tetralin hydroperoxide (■),α-tetralone (▲), and 1,2,3,4-tetrahydro-1-naphthol (●).

7.3. Discussion

From the results presented herein, several conclusions can be drawn regarding the influence of supported AuNP on the tetralin peroxidation mechanism.

1) In the presence of TBHP as initiator the formation of peroxidation products clearly occurs without an induction period for the formation of peroxidation products. Considering that TBHP is stable at 80°C within the time frame of the experiment, one can assume that the AuNP are responsible for the majority of TBHP degradation.

2) The selectivity of tetralin peroxidation is very dependent on the reaction temperature. Thus, at 30°C the product distribution was dominated by α–tetralin

hydroperoxide formation, whereas a mixture of products (α–tetralin hydroperoxide, α–tetralone and 1,2,3,4-tetrahydro-1-naphthol) was obtained at 80°C.

3) The reaction temperature also plays an important role in the stability of α–tetralin hydroperoxide, as was demonstrated by the Fenton decomposition experiments presented in Figures 7.14 to 7.16.

4) The addition of lipoic acid to the peroxidation reaction had a large impact on the product formation, with the lipoic acid acting as a surface capping agent and inhibiting the peroxidation reaction. The influence of lipoic acid on tetralin hydroperoxide decomposition emphasizes the participation of the nanoparticle surface in the reaction mechanism, even at a relatively low temperature of 30°C. In short, the reaction temperature clearly needs to be accounted for when considering and adapting the peroxidation mechanism proposed in Chapter 2 to explain the observed experimental behaviour for the tetralin peroxidation catalyzed by supported AuNP, as can be seen in Scheme 7.3.

In brief, how can reaction temperature affect both the proposed Fenton decomposition of tetralin hydroperoxide and the AuNP surface induced decomposition of the tetralin peroxyl radicals?

Thus, it is important to know how the reaction temperature can affect both the proposed Fenton decomposition of α–tetralin hydroperoxide and the AuNP surface induced decomposition of the tetralin peroxyl radicals. The discussion of results in Chapter 3 support increased Fenton activity of the catalyst with increasing reaction temperatures. This finding can be easily used to justify the observed increase of α–tetralin hydroperoxide degradation via Fenton chemistry on going from 30°C to 80°C.

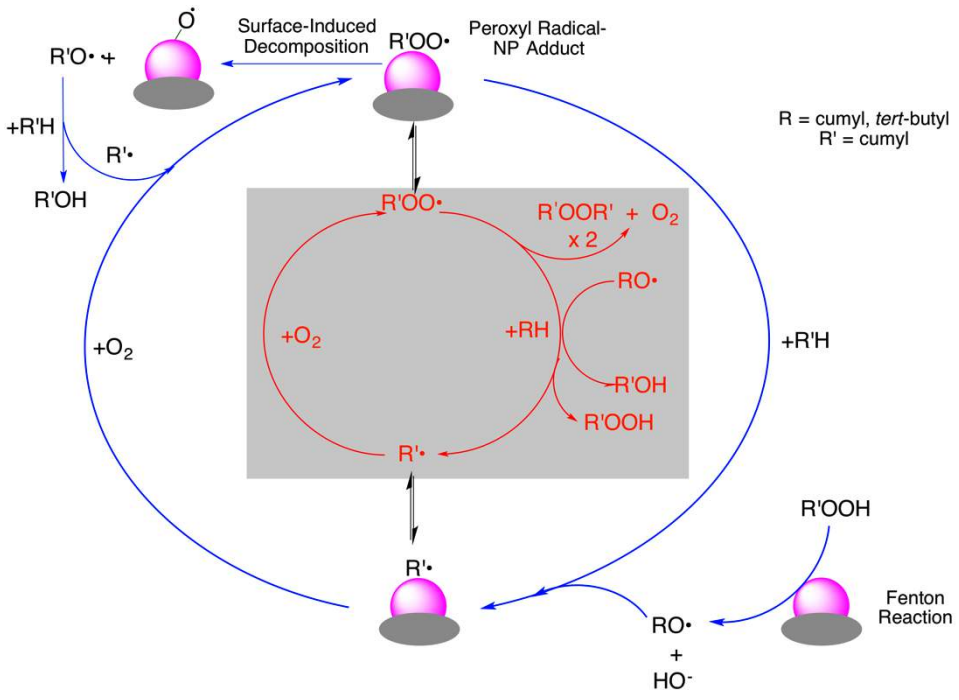

Scheme 7.3. Schematic representation of cumene peroxidation in the presence of AuNP nanoparticles. Blue arrows are representative of reactions occurring on the nanoparticle surface, while red arrows indicate pathways within the bulk solution. The red pathway enclosed in a grey box is well established in solution; such homogeneous autooxidation is a slow process at the temperatures used in this work, but this may be largely due to inefficient homogeneous initiation. The surface reactive species could further react with tetralin as shown in chapter 4.

On the other hand, Chapter 2 argues that the ability of the peroxyl radical to bind to the NP surface is reversible and plays a very large role in the decomposition of this species on the AuNP surface. Thus, the influence of temperature on this process must also be considered. The possible pathways of reaction for the peroxyl radical are schematically presented in Scheme 7.4, with the corresponding rate constants labeled, k_H, k_{GB} (constance of gold binding), k_{GB-1} and k_{SD} (constanc of suface decompsition).

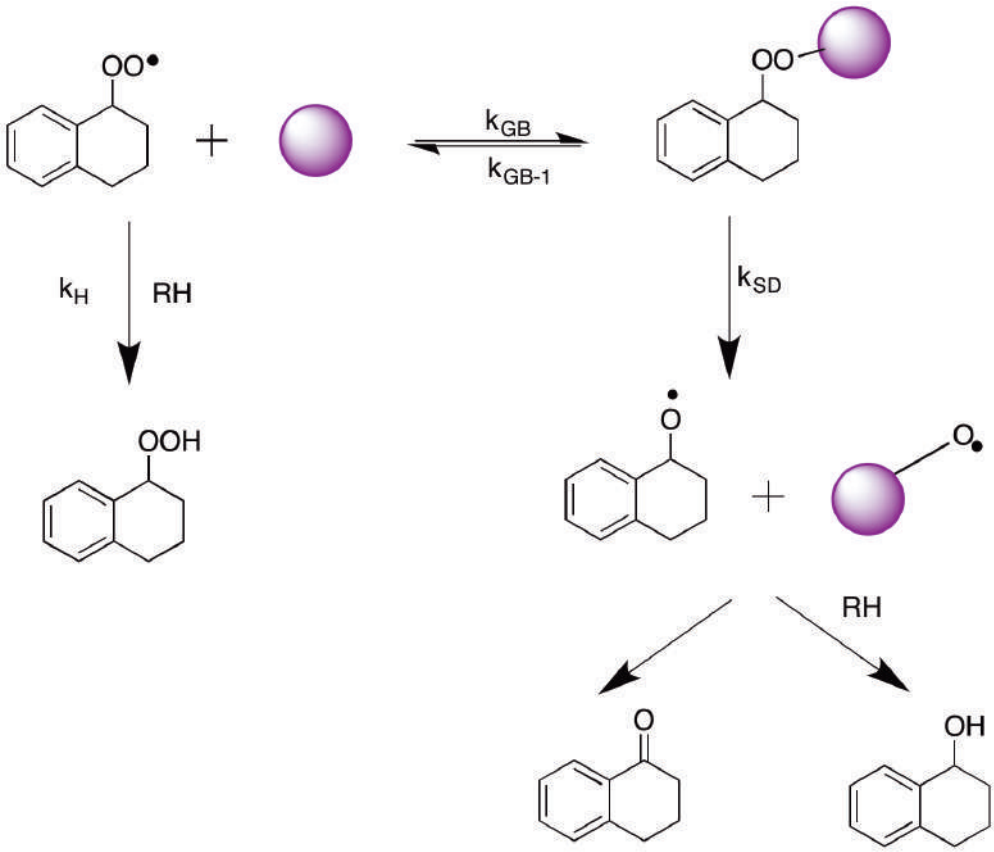

Scheme 7.4. Schematic representation of the equilibrium that occurs between the tetralin hydroperoxyl radical and the AuNP surface, as well as the reaction pathways believed to be primarily responsible for the formation of α–tetralin hydroperoxide, α–tetralone and 1,2,3,4-tetrahydro-1-naphthol.

Two rate constant parameters need to be considered when discussing the interaction between the α–tetralin peroxyl radical and the AuNP surface (k_{GB}; rate constant for gold binding) and the reverse reaction (k_{GB-1}). In principle the rate of both the interaction between the peroxyl radical and the dissociation should increase with reaction temperature. Furthermore, the influence of temperature on the nanoparticle surface-induced decomposition of the peroxyl radical (k_{SD}) and the hydrogen atom abstraction (k_H) must also be considered.

The rate constant for hydrogen atom abstraction by tetralin peroxyl radical (k_H) should increase with temperature, based solely on a logical increase in the energy available to go over the activation barrier. Clearly, k_{SD} should also increase with temperature. The suggested temperature influence on radical surface degradation is evident when the decomposition of α–tetralin hydroperoxide is done at 30°C. Under these conditions, the observed reaction rate was very low. Also, typical surface decomposition products, α–tetralone and 1,2,3,4-tetrahydro-1-naphthol, were not observed. Overall, the product distribution can be considered a competition between the rate of hydrogen abstraction by the tetralin peroxyl radical and the rate at which this radical can interact with the nanoparticle surface and undergo decomposition. Once the tetralin peroxyl radical- nanoparticle adduct is formed, decomposition is largely favoured and yields the depicted products (Scheme 7.4.; 1,2,3,4-tetrahydro-1-naphthol and α–tetralone). The α–tetralone may also be formed by way of a

reactive surface oxygen species, as discussed in Chapter 5, Section 5.3, *via* an alcohol oxidation type pathway.[8]

7.4. Conclusions

The peroxidation of tetralin was studied using supported AuNP and showed a large temperature dependence on product distribution. At a reaction temperature of 30°C, α–tetralin hydroperoxide was the major product, while at 80°C a mixture of α–tetralin hydroperoxide, α–tetralone and 1,2,3,4-tetrahydro-1-naphthol was observed. The difference in product distribution was attributed to the Fenton ability of the catalysts and the fate of the peroxyl radical-AuNP adduct. At elevated reaction temperatures, increased Fenton ability and favoured decomposition of the radical-AuNP adduct can contribute to the increased formation of both the alcohol and ketone tetralin peroxidation products

7.5. Experimental

7.5.1. Reagents.

α-Tetralone (97%), 1,2,3,4-tetrahydro-1-napthnol (97%), *tert*-Butyl hydroperoxide solution in H_2O (70%) , (±)α-lipoic acid, toluene and activated, acidic aluminium

oxide (Brockmann I) were purchased from Sigma Aldrich and used as received. Tetralin (99%) was also purchased from Sigma-Aldrich and was filtered through acidic alumina prior to use.

7.5.2. Instrumentation.

The average size of the metallic AuNPs was determined using a JEM-2100F FETEM transition electron microscope TEM from Jeol Ltd.

Analysis of the reaction mixtures (a-tetralone, 1,2,3,4-tetrahydro-1-naphthol and a-tetralin hydroperoxide) was performed using normal phase Agilent 1100 HPLC with a 99:1 heptane/isopropanol eluent mixture.

7.5.3. Peroxidation of tetralin under oxygen saturated conditions.

In a 50 mL, two-neck round bottom flask, 100 mg of catalyst (and in some cases 100 μL of TBHP, 42 mM) were added to 10 mL of tetralin and the reaction was heated to 30°C or 80°C. An aliquot was taken from the reaction mixture every hour, centrifuged and subsequently analyzed by HPLC. Control reactions were carried out using TiO_2 P25 itself and in the absence of heterogeneous materials. Air was flowed through the solution and the flow was monitored using a Matheson flow meter. The typical experiment error that was obtained using HPLC analysis is around 10% of the reported values.

7.5.4. Decomposition of a-tetralin hydroperoxide

A solution of a-tetralin hydroperoxide was obtained by oxidation of tetralin at 80°C for 24 hours in absence of either catalyst or TBHP initiator. 1 mL of this concentrated solution of a-tetralin hydroperoxide where the conversion was around 25-30% was diluted in toluene (9 mL) and used for the decomposition experiment.

In a 50 mL, two-neck round bottom flask, 100 mg of commercial AuNP@TiO_2 was added to a 10 mL solution of a-tetralin hydroperoxide in toluene and the reaction was heated to 30°C or 80°C. An aliquot was taken from the reaction mixture every hour, centrifuged and subsequently analyzed by HPLC. The typical experiment error that was obtained using HPLC analysis is around 10% of the reported values.

7.5.5. Lipoid acid experiments

In a 50 mL, two-neck round bottom flask, 100 mg of catalyst was added to 10 mL of tetralin and the reaction was heated to 30°C or 80°C. After 1 hour, 5 mg of lipoic acid was added to the solution. An aliquot was taken from the reaction mixture every hour, centrifuged and subsequently analyzed by HPLC. Control reactions were carried out using TiO_2 P25 itself and in the absence of heterogeneous materials The typical experiment error that was obtained using HPLC analysis is around 5% of the reported values.

7.6. Appendix 1: Representative HPLC chromatogram

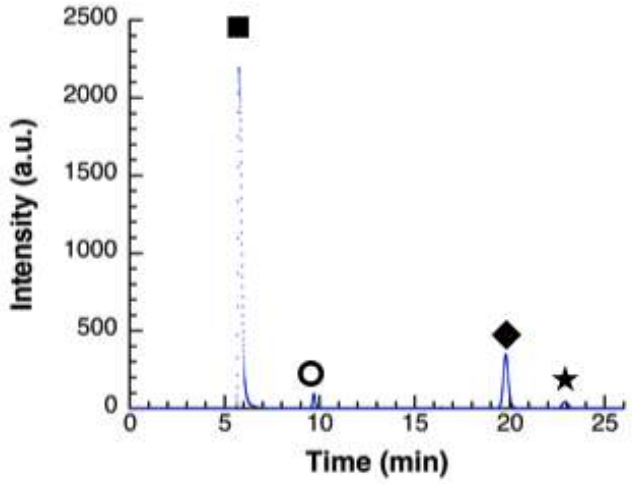

Figure 7.19. Representative normal phase HPLC chromatogram of AuNP@TiO_2-catalyzed tetralin peroxidation. Peak identification: tetralin (■), tetralone (O), tetralin hydroperoxide, (◆) and 1,2,3,4-tetrahydro-1-naphthol (★).

7.7. References

(1) Robertson, A.; Waters , K. A. J. Chem. Soc. 1948, 1578.

(2) Kamiya, Y.; Beaton, S.; Lafortune, A.; Ingold, K. U. Can. J. Chem. 1963, 41.

(3) Kamiya, Y.; Ingold, K. U. Can. J. Chem. 1964, 42, 1027.

(4) Aprile, C.; Corma, A.; Domine, M. E.; Garcia, H.; Mitchell, C. J. Catal. 2009, 264, 44.

(5) bin Saiman, M. Z.; Brett, G. L.; Tiruvalam, R.; Forde, M. M.; Sharples, K.; Thetford, A.; Jenkins, R. L.; Dimitratos, N.; Lopez-Sanchez, J. A.; Murphy, D. M.; Bethell, D.; Willock, D. J.; Taylor, S. H.; Knight, D. W.; Kiely, C. J.; Hutchings, G. J. Angew. Chem. Int. Ed. 2012, 51, 5981.

(6) Hay, J. E.; Johnstone, N. M.; Tipper, C. F. H.; Williams , R. K. J. Chem. Soc. 1954, 629.

(7) Mahmoud, A.; Zach Erno, A.; Branda, N. R. Chem. Commun. 2013, 49, 5639.

(8) Conte, M.; Miyamura, H.; Kobayashi, S.; Chechik, V. J. Am . Chem . Soc. 2009, 131, 7189.

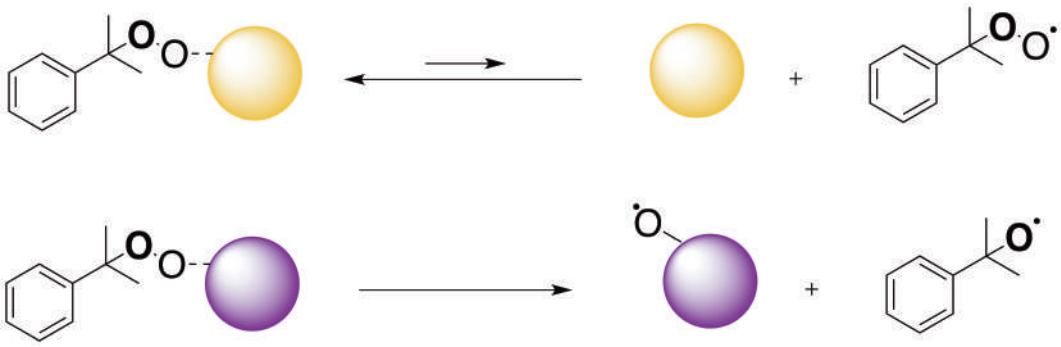

8. Conclusions and Future Directions

8.0. Table of contents

8.1. Conclusions

This thesis explored the peroxidation of several solvents, including cumene, ethylbenzene, *n*-propylbenzene and tetralin, in the presence of supported metal nanoparticles. Furthermore, the role of the TiO_2 support in AuNP catalyzed cumene peroxidation was discussed. Finally the epoxidation of *cis*-stilbene was examined using cumene as solvent and AuNP@TiO_2 as catalyst. Several relevant findings were reported within this thesis , which are summarized in the following paragraphs.

AgNP@HT was found to change the selectivity of the product distribution in cumene peroxidation. Mainly, cumene hydroperoxide was determined to be the major product, in contrast to cumyl alcohol when a AuNP-based catalyst was used. Thus, choosing the right metal and support allows for control of the dominant product formed.

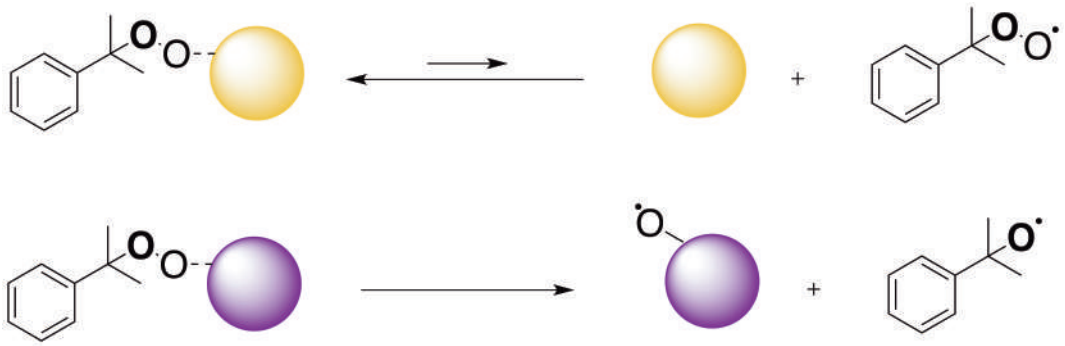

Scheme 8.1. Difference in the fate of the peroxyl radical-metal nanoparticle adduct when using supported AgNP *versus* AuNP catalysts.

This difference in the products obtained from AgNP *versus* AuNP can be attributed to a difference in the Fenton activity of these catalysts and a difference in the fate of the peroxyl radical-nanoparticle adduct (Figure 8.1). The radical-nanoparticle adduct was found to be non-reversible and was readily decomposed in the case of AuNP (Figure 8.1), while the use of AgNP promoted the formation of a reversible adduct and less peroxyl radical degradation (at 80°C). The formation of a peroxyl radical-nanoparticle adduct was corroborated by the work carried out on the AuNP and AgNP@HT catalyzed peroxidation of ethylbenzene, where the formation of acetophenone reveals the involvement of surface decomposition of ethylbenzene peroxyl radicals (as discussed in Chapter 4). The fate and the role of reactive surface oxygen species formed *via* the surface decomposition peroxyl radicals on the nanoparticle surface was also suggested to play an important role in the epoxidation of *cis*-stilbene, as presented in Chapter 6.

Furthermore, in Chapter 4, the reactive surface oxygen species were proposed to be most likely responsible for part of the successful ethylbenzene peroxidation by promoting hydrogen abstraction. These reactive surface species were also proposed to be responsible for the epoxidation of *cis*-stilbene by AuNP@TiO_2, as well as being integral participants in the supported nanoparticle catalyzed peroxidation of cumene and tetralin.

The peroxidation of tetralin was a unique study, as it demonstrated that reaction temperature, not just nanoparticle composition, can influence the product distribution obtained from supported AuNP mediated peroxidation. More specifically, when the peroxidation of tetralin was carried out at 30°C, the major product obtained was tetralin hydroperoxide, whereas at 80°C a mixture of products was obtained (tetralin hydroperoxide, α-tetralone and 1,2,3,4-tetrahydro-1-naphthol). These temperature dependent results also suggest that the association between the peroxyl radical the AuNP surface may be reversible at lower reaction temperatures and that the decomposition of the peroxyl radical on the nanoparticles surface is also surface dependent. It is also important to note that at 30°C no peroxidation is observed in the absence of catalyst.

This temperature influence was also indirectly observed in the study of AuNP catalyzed cumene peroxidation (Chatper 2). Recall that when this reaction was studied at 30°C *via* oxygen uptake experiments both cumyl alcohol and cumene hydroperoxide were obtained as products. However, when the reaction temperature was increased to 80°C, cumyl alcohol is almost the only product observed, demonstrating that the product distribution with respect to the AuNP catalyzed peroxidation of cumene is also largely influenced by the reaction temperature.

In Chapter 3, the role of the heterogeneous catalyst support in the peroxidation of cumene was more closely examined. Briefly, the support was found to play an important role by promoting more efficient electron transport and making the AuNP@TiO_2 a better Fenton reagent (Figure 8.2).

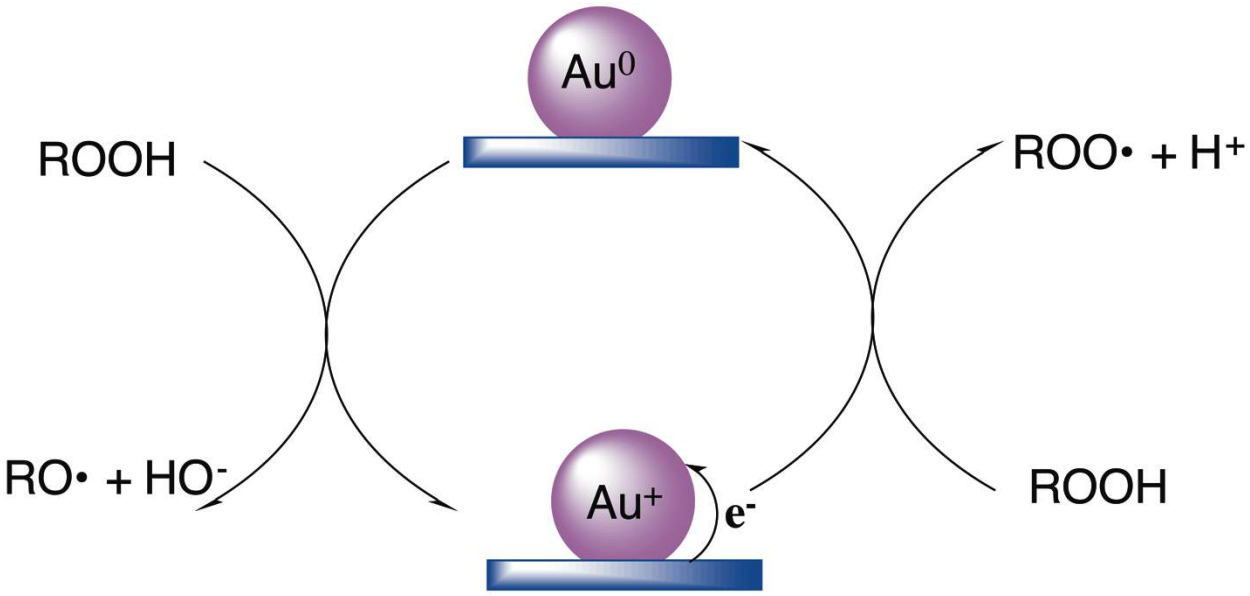

Scheme 8.2. Representation of the Haber-Weiss reactions for cumene hydroperoxide decomposition catalyzed by supported AuNP.

8.2. Future Directions

The work reported in this thesis presents a complete study on solvent peroxidation in the presence of supported AuNP and AgNP catalysts. This study could be extended to examine other solvents, notably methylcyclohexane, toluene and decalin, in an effort to gain more in-depth mechanistic insights. The

usage of other heterogeneous AuNP-based catalysts could also be considered where the nature of the support could be changed.

In the past, Keith U. Ingold[1-3] and others[4] have made use of the information derived from solvent peroxidation to learn more about the antioxidant activity of different molecules. Decades of research were needed to fully understand the role of vitamin E[1] as an antioxidant in the context of biological systems. The work in this thesis demonstrates that little is known about the actual "antioxidant" role of metal nanoparticles, such as AuNP and AgNP, and whether these materials are antioxidant[5,6] or pro-oxidant,[7,8] or simply a catalyst for hydroperoxide decomposition. Using the information presented in this thesis would be the first step to obtain more information on the nature of the antioxidant or pro-oxidant activity of AuNP and the chemical properties of AuNP in simpler chemical systems.

8.3. Claims to Original Research

(i) Study leading to the understanding of the peroxidation of cumene in the presence of AuNP@TiO_2, AuNP@HT and AgNP@HT and proposed implication of the peroxyl radical AuNP adduct and surface reactive species in the peroxidation mechanism.

(ii) Study leading to the understanding of the role of TiO_2 in the peroxidation of cumene using AuNP@TiO_2 as catalyst.

(iii) Study leading to the understanding on the peroxidation of ethylbenzene in the presence of AuNP@TiO_2, AuNP@HT and AgNP@HT, showing that the fate of the nanoparticle peroxyl adduct depends on the nature of the metal, being reversible in AgNP and non-reversible in AuNP.

(iv) A new proposed mechanism for the epoxidation of *cis*-stilbene in the presence of AuNP@TiO_2 as a catalyst and cumene as a peroxidable solvent via the involvement of the surface reactive species formed through the decomposition of the peroxyl radical nanoparticle adduct.

(v) Study leading to increased understanding of the peroxidation of tetralin in the presence of AuNP@TiO_2 as well as on the influence of temperature on the fate of the peroxyl radical nanoparticle adduct and on the product distribution.

8.4. Publications

8.4.1. Publications resulting from the work presented in this thesis.

(i) Charles-Oneil L. Crites, Geniece L. Hallett-Tapley, Mathieu Frenette, María González-Béjar, J. C. Netto-Ferreira and J. C. Scaiano. "Insights into the Mechanism of Cumene Peroxidation Using Supported Gold and Silver Nanoparticles" *ACS Catalysis*, **2013**, *3*, 2062-2071.

(ii) Charles-Oneil L. Crites, Geniece L. Hallett-Tapley, María González-Béjar, J.C. Netto-Ferreira and Juan C. Scaiano. "Epoxidation of Stilbene using

Supported Gold Nanoparticles: Cumyl Peroxyl Radical Activation at the Gold Nanoparticle Surface" *Chem. Commun.* **2014,** *50*, 2289-2291.

(iii) Oneil L. Crites,J. C. Netto-Ferreira, Geniece L. Hallet-Tapley and J. C. Scaiano. "Catalyzed Peroxidation of Ethylbenzene and *n*-Propylbenzene by AuNP@TiO_2: Exploring the Interaction between Radical Species and the Gold Nanoparticle Surface" Accepted. Invited contribution to the Journal of the Brazilian Chemical Society

(iv) Charles-Oneil L. Crites, J. C. Netto-Ferreira, Geniece L. Hallett-Tapley, and J. C. Scaiano. "Insights into the Role of the Support with Supported Gold Nanoparticle Mediated Cumene Peroxidation" *Manuscript in Preparation* ,

(v) Charles-Oneil L. Crites, J. C. Netto-Ferreira, Geniece L. Hallett-Tapley and J. C. Scaiano. "The Role of the Interaction between Radical Species and Gold Nanoparticle Surface in the Peroxidation of Tetralin" *Manuscript in Preparation*.

8.4.2. Publications resulting from work not presented in this thesis

(i) C. Díaz-Urrutia, W.-C. Chen, C.-O. Crites, J. Daccache, I. Korobkov and R. T. Baker "Towards lignin valorisation: Comparing homogeneous catalysts for the aerobic oxidation and depolymerisation of organosolv lignin",2015 RSC Advance. In press

(ii) Dimitriy Malyshev, Francisco Boscá, Charles-Oneil L. Crites, Geniece L. Hallett-Tapley, José Carlos Netto-Ferreira, Emilio I. Alarcon and Juan C. Scaiano. "Size-Controlled Photochemical Synthesis of NiobiumNanoparticles" *Dalton Trans*. **2013**, *42*, 14049-14052.

(iii) Hallett-Tapley G. L., Crites, C.-O. L., McGilvray, K. L., González-Béjar, M., Netto-Ferreira, J. C. and Scaiano, J. C. "Dry Photochemical Synthesis of Hydrotalcite, γ-Al_2O_3 and TiO_2 Supported Gold Nanoparticle Catalysts" *J. Photochem. Photobiol. A: Chem.*, **2011**, *224,* 8.

(iv) Scaiano, J. C., Netto-Ferreira, J. C., Alarcon, E., Billone, P., Alejo, C. J. B., Crites, C.-O.L., Decan, M., Fasciani, C., González-Béjar, M., Hallett-Tapley, G., Grenier, M., Mcgilvray, K. L., Pacioni, N. L., Pardoe, A., René-Boisneuf, L., Schwartz-Narbonne, R., Jazmín Silvero, M., Stamplecoskie, K. G., Wee, T.-L., "Tuning plasmon transitions and their applications in organic photochemistry" *Pure Appl. Chem.*, **2011** *83*, 913.

(v) Charles-Oneil L. Crites, Felipe Matos Lima, M. Luisa Marin, José Carlos Netto-Ferreira, Geniece L. Hallett-Tapley, Stefania Impellizzeri, Juan C. Scaiano. "Tetrahydropyranyl Protection and Deprotection of Alcohols using Niobium Phosphate as a Brønsted Acid Catalyst" Manuscript in Preparation.

(vi) Carolina G. dos Santos ,Charles-Oneil L. Crites, Daniela T. Marquez, José Carlos Netto-Ferreira, Juan C. Scaiano. "Plasmon heating mediated Friedel-Craft

alkylation of anisole using supported AuNP@Nb_2O_5 catalyst" *Manuscript in Preparation*.

8.5. References

(1) Burton, G. W.; Ingold, K. U. Ann. N. Y. Acad. Sci. 1989, 570, 7.

(2) Burton, G. W.; Hughes, L.; Ingold, K. U. J. Am. Chem. Soc. 1983, 105, 5950.

(3) Foti, M. C.; Ingold, K. U. J. Agric. Chem. 2003, 51, 2758.

(4) Burton, G. W.; Traber, M. G. Annu. Rev. Nur. 1990, 10, 357.

(5) Esumi, K.; Houdatsu, H.; Yoshimura, T. Langmuir 2004, 20, 2536.

(6) Yakimovich, N. O.; Ezhevskii, A. A.; Guseinon, D. V.; Smirnova, L. A.; Gracheva, T. A.; Klychkov, K. S. Russ. Chem. Bull. 2008, 57, 520.

(7) Navalon, S.; Dhakshinamoorthy, A.; Alvaro, M.; Garcia, H. ChemSusChem 2011, 4, 1712.

(8) Navalon, S.; Martin, R.; Alvaro, M.; Garcia, H. Angew. Chem. Int. Ed. 2010, 49, 8403.